

FAULT TOLERANT CONTROL FOR NONLINEAR SYSTEMS

New LPV and TS Fuzzy Virtual Actuator and Sensor Approaches

MARIELLA MAIA QUADROS



Graduate Program in Electrical Engineering
School of Engineering

ADVISOR: Prof. Dr. Reinaldo Martínez Palhares
CO-ADVISOR: Prof. Dr. Valter Júnior de Souza Leite

November 3, 2021

FAULT TOLERANT CONTROL FOR NONLINEAR
SYSTEMS

New LPV and TS Fuzzy Virtual Actuator and Sensor Approaches

MARIELLA MAIA QUADROS

Thesis presented to the Graduate Program in Electrical Engineering (PPGEE) of the Universidade Federal de Minas Gerais (UFMG) in partial fulfillment of the requirements to obtain the degree of Doctor in Electrical Engineering.

ADVISOR: Prof. Dr. Reinaldo Martínez Palhares
CO-ADVISOR: Prof. Dr. Valter Júnior de Souza Leite

Belo Horizonte
November 3, 2021

Q1f

Quadros, Mariella Maia.

Fault tolerant control for nonlinear systems [recurso eletrônico] : new LPV and TS fuzzy virtual actuator and sensor approaches / Mariella Maia Quadros. - 2021.

1 recurso online (x, 117 f. : il., color.) : pdf.

Orientador: Reinaldo Martinez Palhares.

Coorientador: Valter Júnior de Souza Leite.

Tese (doutorado) - Universidade Federal de Minas Gerais, Escola de Engenharia.

Apêndices: f. 100-104.

Bibliografia: f. 105-117.

Exigências do sistema: Adobe Acrobat Reader.

1. Engenharia elétrica - Teses. 2. Sistemas difusos - Teses. 3. Sensor virtual - Teses. 4. Falha de sistema (Engenharia) - Teses. I. Palhares, Reinaldo Martinez. II. Leite, Valter Júnior de Souza. III. Universidade Federal de Minas Gerais. Escola de Engenharia. IV. Título.

CDU: 621.3(043)

"Fault Tolerant Control for Nonlinear Systems: New LPV and TS Fuzzy Virtual Actuator and Sensor Approaches"

Mariella Maia Quadros

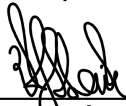
Tese de Doutorado submetida à Banca Examinadora designada pelo Colegiado do Programa de Pós-Graduação em Engenharia Elétrica da Escola de Engenharia da Universidade Federal de Minas Gerais, como requisito para obtenção do grau de Doutor em Engenharia Elétrica.

Aprovada em 03 de novembro de 2021.

Por:



Prof. Dr. Reinaldo Martínez Palhares
(UFMG) - Orientador

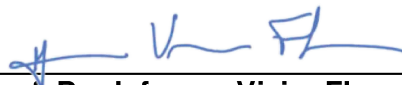


Prof. Dr. Valter Júnior de Souza Leite
(CEFET/MG) - Coorientador

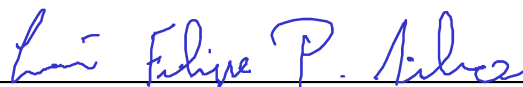


Prof. Dr. Edvaldo Assunção
(UNESP/Ilha Solteira)

Prof. Dr. Renan Landau Paiva de Medeiros
(UFAM)



Prof. Dr. Jeferson Vieira Flores
(UFRGS)



Prof. Dr. Luís Filipe Pereira Silva
(CEFET/MG)

The future belongs to those who believe in the beauty of their dreams.

— **Eleanor Roosevelt**

ACKNOWLEDGMENTS

I thank,

First God, who allowed all this to happen throughout my life and who at all times is the greatest teacher anyone can know.

My family for their ability to believe and invest in me. Mother, your care and dedication were what, at times, gave me the hope to continue. Dad, your presence meant security and certainty that I am not alone on this journey. César, for his support, patience and fun times.

My advisors, Reinaldo and Valter, for their guidance, dedication, wisdom and patience during this journey. I express my greatest thanks and respect for all that has been offered to me.

My boyfriend Víctor, for always being by my side, for all his support, companionship, understanding and patience. And for always helping me with his teachings and knowledge.

My colleagues from D!FCOM for the companionship, knowledge sharing and contribution to my PhD.

The Federal Institute of Education, Science and Technology of Minas Gerais Campus Sabará and my colleagues of the Area of Control and Industrial Processes for the time granted to me for the completion of my doctorate.

RESUMO

Ao projetar um sistema de controle para processos industriais, deseja-se que este atenda às especificações de desempenho, seja confiável, seguro e que tenha estabilidade garantida. No entanto, a ocorrência de falhas pode afetar negativamente a disponibilidade desses sistemas, implicando, em muitos casos, em perdas materiais e de funcionalidade, deterioração de desempenho, instabilidade e riscos à segurança. Portanto, é crucial que sejam implementados sistemas de controle tolerantes a falhas (FTC, do inglês *Fault Tolerant Control*), para que, mesmo na presença de falhas, seja possível garantir a estabilidade do sistema de malha fechada e assegurar um desempenho aceitável antes de uma manutenção adequada. Um dos principais métodos de projeto FTC utiliza a reconfiguração de controle quando são detectadas falhas nos sensores ou nos atuadores do processo (podendo ser simultâneas). Dessa forma, é inserido um bloco de reconfiguração entre o controlador e o sistema com falhas, composto de sensores e atuadores virtuais, com o objetivo de receber os sinais de controle e dos sensores e corrigi-los para que o mesmo controlador possa ser utilizado sem a necessidade de reprojeto. Os blocos de reconfiguração LPV (do inglês, *Linear Parameter Varying*) e *fuzzy* TS (Takagi-Sugeno) são especialmente interessantes, pois permitem representar sistemas não-lineares com não-linearidades de setor, incorporando-as nos parâmetros de escalonamento (LPV) ou variáveis premissas (TS) e usando estratégias de projeto de controle robusto. Nesta Tese, são apresentadas novas condições suficientes baseadas em LMIs (do inglês, *Linear Matrix Inequalities*) para a síntese de sensores e atuadores virtuais robustos a diferentes tipos de falhas para sistemas não-lineares descritos por modelos LPV e *fuzzy* TS. Para o caso *fuzzy* TS, as condições também permitem lidar com sistemas que possuem entrada desconhecida e cujas variáveis premissas podem não ser medidas, devido à configuração da planta ou falhas de sensores. Com o objetivo de ilustrar a eficiência dos métodos propostos, são realizados experimentos em tempo real e simulações computacionais para controle de nível em um sistema MIMO (do inglês, *Multiple-Input and Multiple-Output*) não-linear de tanques acoplados.

Palavras-chave: Reconfiguração de Controle; Sistemas LPV; Sistemas *Fuzzy* TS; Sensor Virtual; Atuador Virtual.

ABSTRACT

In order to design a control system for industrial processes, it is desired that it satisfies the performance specifications, is reliable, safe, and has guaranteed stability. However, the occurrence of faults negatively affects the availability of these systems, implying, in most cases, in material and functional losses, performance deterioration, instability, and safety risks. Therefore, it is crucial to implement Fault Tolerant Control (FTC) systems such that, even in the presence of faults, it is possible to guarantee the stability of the closed-loop system and ensure acceptable performance. One of the main methods for FTC design uses the control reconfiguration when faults are detected in process sensors or actuators. Then, a reconfiguration block is inserted between the controller and the faulty system, composed of virtual sensors and actuators, to receive the control and sensor signals and to correct them so that the current controller can be used without the need of redesign. The Linear Parameter Varying (LPV) and Takagi-Sugeno (TS) fuzzy reconfiguration blocks are especially interesting, as they allow to represent classes of nonlinear systems with sector nonlinearities, incorporating them in the scheduling parameters (for LPV) or the premise variables (for TS) and to use robust control design strategies. In this Thesis, new sufficient conditions formulated in terms of Linear Matrix Inequalities (LMIs) are presented for the synthesis of robust virtual sensors and actuators for nonlinear systems described by LPV and TS fuzzy models. For the TS fuzzy case, the conditions also allow dealing with systems that have an unknown input and whose premise variables may not be measured, due to plant configuration or sensor faults. In order to illustrate the efficiency of the proposed methods, real-time experiments and computer simulations are carried out for level-control in a nonlinear Multiple-Input and Multiple-Output (MIMO) system of coupled tanks.

Keywords: Control Reconfiguration; LPV Systems; TS Fuzzy Systems; Virtual Sensor; Virtual Actuator.

LIST OF FIGURES

Figure 1	Block diagram for the reconfigured faulty system.	3
Figure 2	Block diagram for the reconfigured faulty system.	14
Figure 3	Level-control system.	16
Figure 4	Two tank system diagram.	17
Figure 5	Actuators and nonlinear solid inserted in tank $T3$	18
Figure 6	Reconfigured system as a cascade system.	38
Figure 7	Comparative flowcharts of the proposed methodology and the one proposed in [21]	40
Figure 8	Experiments for sensor faults - Chapter 3	45
Figure 9	Performance indices for sensor faults - Chapter 3	46
Figure 10	Experiments for actuator faults - Chapter 3	47
Figure 11	Performance indices for actuator faults - Chapter 3	48
Figure 12	Experiments for sensor and actuator faults - Chapter 3	49
Figure 13	Performance indices for simultaneous actuator and sensor faults - Chapter 3	50
Figure 14	Simulations for sensor faults and disturbance for $WFTC_N$, $WFTC$, and UIO_{FTC} - Chapter 4	79
Figure 15	Simulations for sensor faults and disturbance for UIO_{FTC} and $RFTC$ - Chapter 4	81
Figure 16	Performance indices for sensor faults and disturbance - Chapter 4	82
Figure 17	Simulation for sensor faults and disturbance for UIO_{FTC} - Chapter 4	83
Figure 18	Simulations for actuator faults and disturbance for $WFTC_N$, $WFTC$, and UIO_{FTC} - Chapter 4	84
Figure 19	Simulations for actuator faults and disturbance for UIO_{FTC} and $RFTC$ - Chapter 4	85
Figure 20	Performance indices for actuator faults and disturbance - Chapter 4	86
Figure 21	Simulation for actuator faults and disturbance for UIO_{FTC} - Chapter 4	87
Figure 22	Simulations for simultaneous sensor and actuator faults and disturbance for $WFTC_N$, $WFTC$, and UIO_{FTC} - Chapter 4	89
Figure 23	Simulations for simultaneous sensor and actuator faults and disturbance for UIO_{FTC} and $RFTC$ - Chapter 4	90
Figure 24	Performance indices for simultaneous sensor and actuator faults and disturbance - Chapter 4	91

Figure 25	Simulation for simultaneous sensor and actuator faults and disturbance for UIO_{FTC} - Chapter 4	92
Figure 26	Simulations for disturbance for $WFTC_N$, UIO_{FTC} , and $RFTC$ - Chapter 4	93
Figure 27	Performance indices for disturbance - Chapter 4	94

ACRONYMS

FDI Fault Diagnosis and Isolation

FTC Fault Tolerant Control

FTC[21] FTC proposed in reference [21]

IAE Integral of Absolute Error

IOS Input-to-State Stability

ISE Integral of Square Error

ISS Input-to-State Stability

IVU Integral of Control Signal Variability

IVU1 Integral of Control Signal Variability with respect to the first actuator of the process

IVU2 Integral of Control Signal Variability with respect to the second actuator of the process

LMI Linear Matrix Inequality

LPV Linear Parameter Varying

MIMO Multiple-Input and Multiple-Output

PLC Programmable Logic Computer

RFTC Robust FTC proposed

TS Takagi-Sugeno

UIO Unknown Input Observer

UIO_{FTC} FTC based on UIO

WFTC System without any FTC strategy and with faults

WFTC_N System without any FTC strategy and without faults

CONTENTS

I	INTRODUCTION TO FAULT TOLERANT CONTROL	1
1	INTRODUCTION	2
1.1	Objectives	6
1.2	Notations	7
1.3	Structure of the document	7
2	PRELIMINARIES	9
2.1	Linear Parameter Varying Systems	9
2.2	Takagi-Sugeno Fuzzy Systems	11
2.3	Input-to-State and Input-to-Output Stability	12
2.4	H_∞ Performance of discrete-time systems	13
2.5	Fault Hiding Approach	13
2.6	Coupled Tanks Systems	15
2.6.1	Controller Design	19
2.7	Performance indices	20
2.8	Useful Lemmas	21
II	FAULT TOLERANT CONTROL FOR NONLINEAR SYSTEMS	22
3	AN LPV VIRTUAL ACTUATOR AND SENSOR APPROACH	23
3.1	Faulty Linear Parameter Varying System	23
3.2	Problem Formulation	25
3.3	LPV Virtual Sensor and Actuator	27
3.3.1	Virtual Sensor	27
3.3.2	Virtual actuator	32
3.3.3	Combination of the virtual sensor with the virtual actuator	35
3.4	Experimental Results	39
3.4.1	Controller Design	41
3.4.2	Design of Reconfiguration Blocks	41
3.4.3	Sensor faults	44
3.4.4	Actuator faults	45
3.4.5	Simultaneous sensor and actuator faults	47
4	FTC BASED ON UNKNOWN INPUT OBSERVER FOR TAKAGI-SUGENO FUZZY SYSTEMS WITH UNMEASURED PREMISE VARIABLES	51
4.1	Faulty Takagi-Sugeno Fuzzy Systems	51
4.2	Problem Formulation	53
4.2.1	Virtual Sensor	53
4.2.2	Virtual Actuator	57
4.3	Takagi-Sugeno Fuzzy Virtual Sensor and Actuator	58

4.3.1	Virtual Sensor	59
4.3.2	Virtual Actuator	61
4.3.3	Combination of the virtual sensor with the virtual actuator	65
4.4	Case Study - Coupled Tanks System	72
4.4.1	Controller Design	74
4.4.2	Reconfiguration Block Design	74
4.4.3	Sensor Faults	78
4.4.4	Actuator Faults	82
4.4.5	Simultaneous Sensor and Actuator Faults	86
4.4.6	Piecewise Constant Disturbance	90
III	FINAL DISCUSSIONS AND APPENDICES	95
5	CONCLUSIONS	96
A	CONTROLLER AND RECONFIGURATION BLOCK GAINS COMPUTED IN CHAPTER 3	100
A.1	Controller Gains	100
A.2	Virtual Sensor Gains	100
A.3	Virtual Actuator Gains	102
B	CONTROLLER AND RECONFIGURATION BLOCK GAINS COMPUTED IN CHAPTER 4	104
B.1	Controller Gains	104
B.2	TS Fuzzy Virtual Sensor Gains	104
B.3	TS Fuzzy Virtual Actuator Gains	104
	BIBLIOGRAPHY	105

Part I

INTRODUCTION TO FAULT TOLERANT
CONTROL

INTRODUCTION

The increasing complexity and automation of industrial devices and processes demand more and more reliability. However, the occurrence of faults jeopardizes the availability of these systems implying, in most cases, in material losses and risks to safety. In this context, the implementation of Fault Tolerant Control (FTC) systems is crucial to ensure the maintenance of certain system properties such as stability and performance. FTC techniques can be: passive [1–3], which deal with faults as unknown perturbations to be rejected and should be considered in the design of the controller using, for instance, robust control techniques; or active [4–8], which modify the control loop after the fault detection and diagnosis and, therefore, require information from a Fault Diagnosis and Isolation (FDI) system [9–11] beforehand. The passive approach tends to be more conservative, since in the design stage, predefined fault conditions that may affect the system are considered as well as its nominal conditions. Then, a unique closed-loop solution is provided, regardless of the occurrence of faults or the nominal behavior of the system, often resulting in poor performance. Thus, this class of approaches does not make any changes to the system when it is affected by faults and does not require real-time fault detection and isolation. On the other hand, active FTC strategies make adaptations to the closed-loop system in real-time, so that it remains stable and within certain performance conditions when faults occur. Therefore, an FDI module is extremely necessary, as these adaptations depend directly on the identification of where the failures occurred, the during period, and their intensity. The active FTC may be performed by means of fault accommodation or control reconfiguration. The first modifies the controller to mitigate the fault effects disregarding control loop changes. It uses the same sensors and actuators before of the fault occurrence. The latter modifies both the control loop and the controller that is generally redesigned to use only the healthy part of the system.

Among the control reconfiguration techniques, one that has gained prominence is the so-called fault hiding approach [12–16], that consists of adding a system, named as reconfiguration block, between the faulty plant and the controller, as shown in Figure 1. The main role of a reconfiguration block is to receive

the sensor and control signals (y_f and u_c , respectively) and to correct them so that the same controller can be used without needing a redesign. For this, the controller receives a modified output y_c , and the faulty system Σ_{P_f} has as input the control signal u_f generated by the reconfiguration block. It is important to notice that this approach allows closed-loop systems to remain stable and with satisfactory performance even in the presence of faults, without the need of modifying the structure or design of the implemented controller, being seen as a plug-in structure. In industrial processes this characteristic has great value since the control loops are often relatively complex and keep the controllers that already present satisfactory performance for the free fault system are welcome. In the literature, different applications of reconfiguration blocks are found in the case of linear systems [12], Hammerstein-Wiener models [14, 17], piecewise affine systems [18], Lur'e systems [19], Takagi-Sugeno (TS) fuzzy models [15, 20], and Linear Parameter Varying (LPV) systems [21, 22].

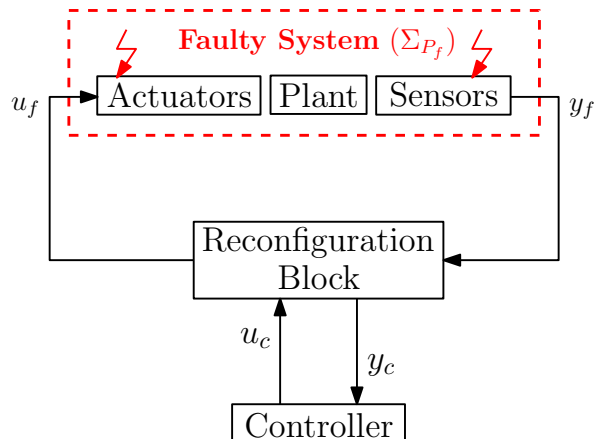


Figure 1: Block diagram for the reconfigured faulty system.

The reconfiguration blocks used for fault hiding can be virtual actuators, used in case of actuator faults, or virtual sensors, in case of sensor faults. It is shown that both virtual actuator and virtual sensor can be used in the case of simultaneous actuator and sensor faults. Furthermore, their designs are independent of each other and of the controller design due to the separation principle [12, 14]. The LPV and TS fuzzy reconfiguration blocks are especially interesting because they allow handling nonlinear systems with sector bounded nonlinearities, by embedding them into the scheduling parameters (LPV) or premise variables (TS) and using convex optimization techniques.

In particular, the LPV virtual sensors and actuators have often been used, during the last years, for fault hiding of LPV systems [21–27] and even for repelling

cyber-attacks [28]. In [21], the concept of LPV virtual sensors and actuators for FTC of LPV systems is proposed, such that the same scheduling parameters are used for both controller, plant and reconfiguration blocks. In such an approach, novel virtual actuator and sensor are designed for each fault condition that occurs. That is, for each new fault that is diagnosed by the FDI module, the reconfiguration block must be redesigned. In addition, the methodology presented in [21] does not allow the input and output matrices of the LPV model to be parameter-dependent. On the other hand, [23] allows the input and output matrices of the LPV model to be parameter-dependent, but uses different virtual actuator and sensor designs depending on whether the faults are total or partial. Another methodology is the use of a bank of reconfiguration blocks [27] that is established considering every fault scenario. The same strategy is used in [25, 26] applied to a wind turbine benchmark. Similarly, in [24], LPV virtual actuators are designed in a model reference framework integrated to a set-membership fault and in [22], a switching LPV virtual actuator is proposed for FTC of an omnidirectional mobile robot. In [29], a virtual sensor based on unknown input observer is proposed for systems described as LPV, subject to multiplicative and additive faults, but its design is developed only for sensor faults.

Regarding the use of reconfiguration blocks of the TS fuzzy type, the works [15], [20] and [30] can be highlighted. The work in [20] proposes the use of a virtual actuator for an application in a proton exchange membrane fuel cell subject to actuator faults. It uses different virtual actuator designs for partial and total (or stuck) faults. In [30], a virtual actuator design is proposed for continuous-time systems, but which is capable of handling only faults in a single actuator of the process. Moreover, [15] presents a continuous-time static reconfiguration block for sensor and actuator faults that must be designed for each new fault occurrence. A common aspect of the methodologies presented in [15], [20], and [30] is that the design of the reconfiguration block is carried out for specific faults and not for a set of faults, and [20] and [30] address only the case of actuator faults. That is, depending on the type or magnitude of the fault, different designs are carried out. Furthermore, [15, 20] do not address the inclusion of disturbances in the TS fuzzy model or in the design of the reconfiguration block, while in [30] the design is performed so that the disturbance is attenuated with a H_∞ performance. Another similarity is that these approaches consider that the premise variables of the system are measured in real-time.

It is important to emphasize that the consideration that the premise variables are measured during the entire execution time of the control algorithm may not

be applicable in many industrial processes. This is because, generally, measurements of these variables can depend directly on the values measured by the system's sensors (namely, the premise variables usually depend on the state variables). Then, if the sensors are subject to faults, the calculation of the premise variables is also affected, compromising the computation of the gains and states of the reconfiguration block and the controller (when applicable). Therefore, the behavior of the system can become unpredictable, especially in cases of more serious faults, such as, for example, with total loss of any essential measures for determining a premise variable. Currently, the FTC literature for TS fuzzy control reconfiguration does not address such an issue. Regarding the proposal of observers for systems without faults and with unmeasured premise variables, [31–35] present methodologies for state estimation and [33, 36, 37] propose unknown input observers for TS fuzzy systems (also for systems without faults). In the LPV context for reconfiguration block designs, in [21, 23, 38] it is also assumed that the time-varying parameters are available regardless of faults occurrence.

In this Thesis, novel sufficient conditions formulated in terms of Linear Matrix Inequalities (LMIs) are presented, providing an improved fault hiding approach by synthesizing robust LPV and TS fuzzy virtual actuators and sensors for dealing with faults in nonlinear systems described by LPV and TS fuzzy models.

In particular, the proposed conditions for LPV systems allow to guarantee the input-to-output stability of the closed-loop system by means of LPV reconfiguration blocks. Differently from the previous works on LPV reconfiguration blocks [21–27], this Thesis includes the various sensor and actuator fault scenarios in a polytopic representation of the faulty system. That is, the faults become time-varying parameters in the LPV model. Thus, such an approach allows to design a single LPV reconfiguration block that is able to ensure the stability for different fault scenarios even when multiple sensor and actuator faults occur simultaneously. As a consequence, it is not necessary to design different LPV reconfiguration blocks for each fault that occurs, regardless of its magnitude, or whether it is partial or total, differently from those proposed by [21, 23]. Moreover, the presented methodology makes it possible to design virtual sensors and actuators for nonlinear systems described by LPV models with parameter-dependent input and output matrices.

In the TS fuzzy context, this Thesis proposes novel sufficient conditions in terms of LMIs for the synthesis of a robust reconfiguration block based on Unknown Input Observer (UIO) considering unmeasured premise variables. These conditions guarantee H_∞ performance of the combination of the virtual sensor

with the virtual actuator for nonlinear systems described by TS fuzzy models subject to sensor and actuator faults and disturbances. The proposed fault hiding approach can ensure, in a single design, the stability and performance of the closed-loop system for different types and magnitudes of sensor and actuator faults, which can be additive or multiplicative (total or partial), and not for specific faults, as presented in [15, 20, 30]. Moreover, the design of the reconfiguration block takes into account that the TS fuzzy model may be dependent on unmeasured premise variables, including those that become unmeasured due to sensor faults, a problem that is also not addressed in the current literature [15, 20, 30]. Another contribution of the proposed approach is that the reconfiguration block structure is based on an unknown input observer, which allows the virtual sensor estimation error to be independent of the disturbance. Thus, it becomes possible for the faulty system to maintain performance close to the nominal one, even during the period of disturbance, unlike the methodologies in the literature [15, 20, 30].

1.1 OBJECTIVES

This Thesis has as main objective to develop new approaches for the design of reconfiguration blocks for discrete-time nonlinear systems. These blocks are composed of virtual sensors and actuators in order to enable the robustness of the system against sensor and actuator faults. To achieve this main objective, the system and the reconfiguration block can be described by discrete-time LPV or TS fuzzy models. Therefore, the objectives can be summarized as follows.

1. To propose novel sufficient LMI conditions for the design of virtual sensors and actuators for nonlinear systems described by LPV models with parameter-dependent input and output matrices. Thus, the results are more general than those proposed in [21] and [23].
2. To include sensor and actuator faults in a polytopic representation of the faulty LPV model.
3. To introduce a novel robust reconfiguration block composed of a virtual sensor and a virtual actuator. The design of this block is carried out for a predefined set of faults and not for a specific fault, as performed in [21]. In addition, it contemplates total and partial faults simultaneously, unlike [23].

4. To propose the synthesis of a new TS fuzzy reconfiguration block based on UIO with guaranteed H_∞ performance that is robust to different actuator and sensor faults, unlike [15, 20, 30], which present designs for specific faults. Then, with the use of a single design it is possible to deal with additive and multiplicative (partial or total) faults in both sensors and/or actuators, with distinct magnitudes.
5. To present the design of a robust TS fuzzy reconfiguration block with unmeasured premise variables, including those that may have their measurements affected by sensor faults, differently from [15, 20, 30].
6. To design a reconfiguration block based on UIO capable of maintaining the system performance close to the nominal one, even in the presence of disturbances, unlike [15, 20, 30].
7. To validate and analyze the proposed methodologies for real-time experiments and computer simulations for a Multiple-Input and Multiple-Output (MIMO) nonlinear level-control system. For this, the proposed approaches are compared with other approaches in the literature, considering different scenarios of sensor and/or actuator faults.

1.2 NOTATIONS

Throughout this Thesis, \star represents the symmetric block of a symmetric matrix and $\text{diag}\{\cdot\}$ a diagonal block matrix. I and 0 are the identity and the null matrices of appropriate dimensions, respectively, and $W > 0$ ($W \geq 0$) denotes that W is positive definite (semi-definite). Furthermore, $\mathbb{R}^{m \times n}$ denotes the set of matrices with real entries and dimensions $m \times n$. Matrix $J(\rho_k) = \sum_{i=1}^D \rho_i J_i$ is a convex combination of D matrices, with J_i denoting the vertices, where $\rho_k = [\rho_{1,k} \ \dots \ \rho_{D,k}]^T$ is the vector of time-varying parameters that belongs to the unitary simplex $\Theta_D(\rho) = \{\rho_k \in \mathbb{R}^D : \sum_{i=1}^D \rho_{i,k} = 1, \rho_{i,k} \geq 0\}, \forall i = 1, \dots, D$. $\Omega_D(J) = \{J_1, J_2, \dots, J_D\}$ denotes the polytope of D vertices of matrices J_i . A^\dagger represents the pseudoinverse of matrix A calculated as $A^\dagger = (A^T A)^{-1} A^T$.

1.3 STRUCTURE OF THE DOCUMENT

This Thesis is organized into five chapters. In Chapter 2, the main theoretical concepts for the development and understanding of this work are addressed.

Chapter 3 presents the main results of a new approach for the design of a virtual sensor and actuator for nonlinear systems described by LPV models. In addition, experimental results are presented for a nonlinear system of coupled tanks modeled as an LPV one. Chapter 4 presents a development for the proposed TS fuzzy reconfiguration block based on UIO and with unmeasured premise variables. Simulations are also carried out for the nonlinear system of coupled tanks, for different fault scenarios and disturbance. Finally, Chapter 5 presents final discussions about this Thesis.

PRELIMINARIES

This chapter presents some theoretical foundations and mathematical tools used to develop the main results of the work. Nonlinear systems described by Linear Parameter Varying (LPV) and Takagi-Sugeno (TS) fuzzy models are introduced as well as some stability concepts such as input-to-state stability (ISS), input-to-output stability (IOS) and H_∞ performance. In addition, basic principles of the fault hiding approach found in the literature as well as the performance indices used for the analysis of the simulated and implemented reconfiguration blocks are presented.

2.1 LINEAR PARAMETER VARYING SYSTEMS

Linear Parameter Varying (LPV) systems are linear dynamical systems described by differential equations (or difference equations) that depend on time-varying parameters [39, 40]. These parameters are measured and can be seen as additional or internal signals of the system that modify its internal structure over time [41].

One of the first LPV approaches was proposed in [42] in the context of gain-scheduling analysis and control of nonlinear systems, in which a nonlinear controller is designed from a set of linear controllers [41]. During the execution of the control algorithm, these controllers are combined with the use of the time-varying parameters measurement [39]. However, at the time, the theory developed did not present the adequate tools for the analysis of stability and performance of such systems. However, with the development of robust control techniques using convex optimization tools, it became possible to analyze nonlinear systems described by LPV models as well as the synthesis of controllers that satisfy certain performance and stability specifications [41]. Thus, in last years, the modeling and control of LPV systems have been widely used and studied in several applications and theoretical developments, such as robotics [43, 44], energy [45–47], aeronautics [48, 49], among others [50–54].

The polytopic framework is one of the ways to describe and analyze LPV systems, which are described by a convex combination of linear systems and

which enables the direct use of convex optimization techniques [41, 55, 56]. For this, consider the following discrete-time LPV system [40]:

$$\begin{cases} x_{k+1} &= A(\rho_k)x_k + B(\rho_k)u_k \\ y_k &= C(\rho_k)x_k + D(\rho_k)u_k, \end{cases} \quad (2.1)$$

where $x_k \in \mathbb{R}^n$ is the state vector, $u_k \in \mathbb{R}^m$ is the sequence of control input and $y_k \in \mathbb{R}^p$ is the output. The matrices $A(\rho_k) \in \mathbb{R}^{n \times n}$, $B(\rho_k) \in \mathbb{R}^{n \times m}$, $C(\rho_k) \in \mathbb{R}^{p \times n}$, and $D(\rho_k) \in \mathbb{R}^{p \times m}$ relate the dynamics, input and output of the system and are given by:

$$A(\rho_k) = \sum_{i=1}^N \rho_{i,k} A_i, \quad B(\rho_k) = \sum_{i=1}^N \rho_{i,k} B_i, \quad C(\rho_k) = \sum_{i=1}^N \rho_{i,k} C_i, \quad D(\rho_k) = \sum_{i=1}^N \rho_{i,k} D_i, \quad (2.2)$$

and $\rho_k = [\rho_{1,k} \ \dots \ \rho_{N,k}]^T$ is the vector of time-varying parameters belonging to the unitary simplex Θ_N , given by:

$$\Theta_N = \left\{ \rho_k \in \mathbb{R}^N : \sum_{i=1}^N \rho_{i,k} = 1, \rho_{i,k} \geq 0 \right\}, \quad \forall i = 1, \dots, N. \quad (2.3)$$

In addition, matrices (2.2) belong to polytopes whose vertices are known, i.e.:

$$\begin{aligned} A(\rho_k) &\in \Omega_N(A) = \{A_1, A_2, \dots, A_N\}, \\ B(\rho_k) &\in \Omega_N(B) = \{B_1, B_2, \dots, B_N\}, \\ C(\rho_k) &\in \Omega_N(C) = \{C_1, C_2, \dots, C_N\}, \\ D(\rho_k) &\in \Omega_N(D) = \{D_1, D_2, \dots, D_N\}, \end{aligned} \quad (2.4)$$

where $\Omega_N(A)$, $\Omega_N(B)$, $\Omega_N(C)$, and $\Omega_N(D)$ are, respectively, the polytopes of N vertices of matrices A_i , B_i , C_i , and D_i , with $i = 1, \dots, N$.

The scheduling parameters can be classified as exogenous, when these are independent of the states; or endogenous, when they are described as a function of system states and resulting from the LPV modeling of nonlinear systems. These systems are called quasi-LPV systems [40, 41, 57] and have a similar approach to the nonlinear systems described by TS fuzzy systems.

2.2 TAKAGI-SUGENO FUZZY SYSTEMS

The Takagi-Sugeno (TS) fuzzy systems approach was proposed by [58, 59], in which the construction of fuzzy models is able to represent nonlinear systems globally or semi-globally, from the combination of a set of linear models [60–63]. For this, the model is described by fuzzy rules which represent local linear input-output relations of a nonlinear system and the local dynamics of each rule is given by a linear model. So, the TS fuzzy model is given by the combination of the linear models [64]. A comprehensive review on TS fuzzy models and control has been recently published in [63].

Similar to quasi-LPV systems, the use of TS fuzzy models for the representation of nonlinear systems enables the analysis of these systems and the design of controllers that satisfy different specifications of stability and performance, through convex optimization tools [60, 65, 66]. Thus, the TS fuzzy modeling and control has been widely used in different areas of application in recent years, such as robotics [67–69], level control [70, 71], energy [72, 73], aeronautics [74, 75], networked systems [76], and studied in several theoretical developments, as in [77–84].

The TS fuzzy model is described from the following rules [63, 64]:

$$\begin{aligned} \text{Model Rule}_\ell : \text{IF } z_{\alpha_{1,k}} \text{ is } \Gamma_{\ell 1} \text{ and } \dots \text{ and } z_{\alpha_{q,k}} \text{ is } \Gamma_{\ell q}, \\ \text{THEN } \begin{cases} x_{k+1} = A_\ell x_k + B_\ell u_k \\ y_k = C_\ell x_k \end{cases}, \ell = 1, 2, \dots, N, \end{aligned} \quad (2.5)$$

where Rule $_\ell$ is the ℓ th fuzzy inference rule, $\Gamma_{\ell j}$, $j = 1, \dots, q$, are the fuzzy sets, N is the number of model rules, $x_k \in \mathbb{R}^n$ is the state vector, $u_k \in \mathbb{R}^m$ is the control input vector and $y_k \in \mathbb{R}^p$ is the output vector. Matrices $A_\ell \in \mathbb{R}^{n \times n}$, $B_\ell \in \mathbb{R}^{n \times m}$, and $C_\ell \in \mathbb{R}^{p \times n}$ relate the dynamics and the output of the ℓ th local model and $z_{\alpha_{1,k}}, \dots, z_{\alpha_{q,k}}$ are known premise variables that may be functions of the state variables, external disturbances, and/or time. It is assumed that

the premise variables are not functions of the input variables u_k and $z_{\alpha,k} = [z_{\alpha_1,k} \ z_{\alpha_2,k} \ \dots \ z_{\alpha_q,k}]$. Thus, the fuzzy system outputs can be defined by:

$$\left\{ \begin{array}{l} x_{k+1} = \frac{\sum_{\ell=1}^N \omega_{\ell}(z_{\alpha,k}) \{A_{\ell}x_k + B_{\ell}u_k\}}{\sum_{\ell=1}^N \omega_{\ell}(z_{\alpha,k})} = \sum_{\ell=1}^N \alpha_{\ell}(z_{\alpha,k}) \{A_{\ell}x_k + B_{\ell}u_k\} \\ \quad \triangleq A(\alpha_k)x_k + B(\alpha_k)u_k \\ y_k = \frac{\sum_{\ell=1}^N \omega_{\ell}(z_{\alpha,k}) C_{\ell}x_k}{\sum_{\ell=1}^N \omega_{\ell}(z_{\alpha,k})} = \sum_{\ell=1}^N \alpha_{\ell}(z_{\alpha,k}) C_{\ell}x_k \triangleq C(\alpha_k)x_k, \end{array} \right. \quad (2.6)$$

where the normalized membership function $\alpha_{\ell}(z_{\alpha,k})$ is given by:

$$\alpha_{\ell}(z_{\alpha,k}) = \frac{\omega_{\ell}(z_{\alpha,k})}{\sum_{\ell=1}^N \omega_{\ell}(z_{\alpha,k})}, \quad (2.7)$$

with,

$$\omega_{\ell}(z_{\alpha,k}) = \prod_{j=1}^q \psi_{\ell_j}(z_{j,k}). \quad (2.8)$$

where the term $\psi_{\ell_j}(z_{j,k})$ is the grade of membership of $z_{j,k}$ in Γ_{ℓ_j} and $\alpha_{\ell}(z_{\alpha,k})$ satisfies the convex sum properties, given by:

$$\sum_{\ell=1}^N \alpha_{\ell}(z_{\alpha,k}) = 1, \quad \alpha_{\ell}(z_{\alpha,k}) \geq 0, \quad \ell = 1, \dots, N. \quad (2.9)$$

2.3 INPUT-TO-STATE AND INPUT-TO-OUTPUT STABILITY

Throughout this Thesis, the concepts of Input-to-State Stability (ISS) and Input-to-Output Stability (IOS) are used for stability analysis and synthesis of the proposed reconfiguration blocks, as presented in the following definitions.

Definition 2.1 *Consider a nonlinear system with dynamics given by $x_{k+1} = f(x_k, v_k)$, where $x_k \in \mathbb{R}^n$ is the state and $v_k \in \mathbb{R}^d$ is the disturbance. The system is called input-to-state stable with respect to the input v_k , if for each initial condition $x_0 \in \mathbb{R}^n$ and a bounded v_k , the corresponding trajectories are bounded and, if v_k is null, the trajectories go asymptotically to the origin.*

Definition 2.2 Consider the same nonlinear system as described in Definition 2.1 with the output given by $y_k = h(x_k)$, $y_k \in \mathbb{R}^p$. The system is called input-to-output stable with respect to the disturbance v_k , if for each initial condition $x_0 \in \mathbb{R}^n$ and a bounded v_k , the output is bounded, and, if v_k is null, the output converges to zero. In addition, the output is bounded proportionally by to the initial condition of the output $y_0 \in \mathbb{R}^p$.

For more details about input-to-state stability and input-to-output stability see [21, 85–90] and references therein.

2.4 H_∞ PERFORMANCE OF DISCRETE-TIME SYSTEMS

The definition of the H_∞ performance is presented below. The idea is to obtain, along this Thesis, conditions for the synthesis of a TS fuzzy reconfiguration block with H_∞ performance.

Consider the discrete-time TS fuzzy system given by:

$$\begin{cases} x_{k+1} &= A(\alpha_k)x_k + E(\alpha_k)w_k, \\ z_k &= C(\alpha_k)x_k + F(\alpha_k)w_k, \end{cases} \quad (2.10)$$

where $x_k \in \mathbb{R}^n$ is the state vector, $w_k \in \mathbb{R}^d$ the disturbance, $z_k \in \mathbb{R}^p$ the system output, and $A(\alpha_k) \in \mathbb{R}^{n \times n}$, $E(\alpha_k) \in \mathbb{R}^{n \times d}$, $C(\alpha_k) \in \mathbb{R}^{p \times n}$, and $F(\alpha_k) \in \mathbb{R}^{p \times d}$. Then, considering zero initial conditions, the H_∞ performance of the system (2.10) is defined as the ℓ_2 induced gain [91, 92]:

$$\|H\|_\infty = \sup_{\|w_k\|_2 \neq 0} \frac{\|z_k\|_2}{\|w_k\|_2} < \eta, \quad (2.11)$$

with an upper bound given by a positive scalar η . Notice that $w_k \in \ell_2^d$ and $z_k \in \ell_2^p$. Based on the Bounded Real Lemma, and considering zero initial conditions, one can write in function of a Lyapunov candidate function $V(z_k)$ the inequality:

$$V(z_{k+1}) - V(z_k) + z_k^T z_k - \eta^2 w_k^T w_k < 0. \quad (2.12)$$

2.5 FAULT HIDING APPROACH

Among the existing FTC strategies in the literature, one that stands out is the control reconfiguration with the approach of fault hiding [15, 21, 23, 93] addressed

in this Thesis. This is due to the fact that it is an efficient methodology that allows the system to remain stable and with reasonable performance even with the fault of sensors and actuators of the process, without having to modify the designed and implemented controller. For this, a reconfiguration block is inserted between the faulty system and the controller designed for the nominal system. This block is composed of a virtual sensor and a virtual actuator, which generate alternative output (y_c) and control signals (u_f) responsible for hiding the faults of the controller, as illustrated in Figure 2, from the system output y_f and the nominal control signal u_c . As the main objective of this work is to propose FTC solutions for nonlinear systems, reconfiguration blocks and systems described by LPV and TS fuzzy are considered.

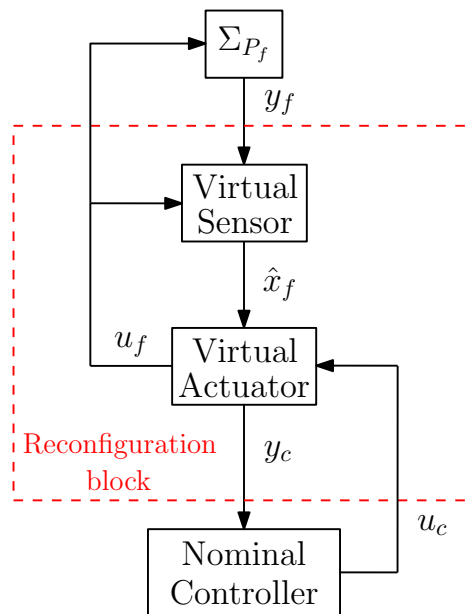


Figure 2: Block diagram for the reconfigured faulty system.

Thus, the faulty system (Σ_{P_f}) can be represented as shown in Figure 2. For the reconfiguration to be satisfactory, information about the sensor and actuator fault indications is necessary, such as where they occurred (in which sensors and/or actuators), when, and with what intensity. Then, it is necessary to use an FDI module, which provides such data in real-time, so that the faulty model is updated, allowing an adequate action of the reconfiguration block. For more details on fault detection and isolation, see [94–97]. From this, the following assumption is presented.

Assumption 2.1 *The FDI module provides accurate information about sensor and actuator faults, such as the period of the fault occurrence, its intensity and*

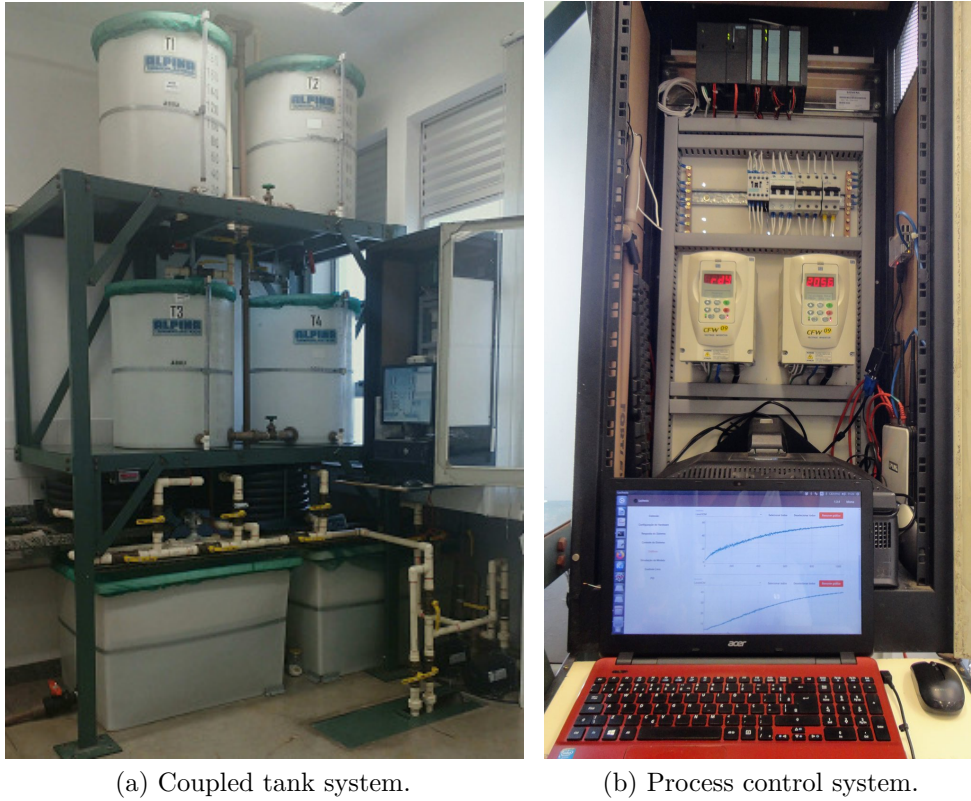
which component of the system is affected, regardless of whether the fault is multiplicative and/or additive.

Considering the assumption above, it can be said that the reconfiguration block supplies the controller with a measurement signal y_c similar to that which would be generated by the nominal system, and the control signal u_f applied in the faulty system is also adjusted by the reconfiguration block, in order to compensate the actuator faults. As the faults are hidden from the controller, it continues to control the nominal system (in its view) and, therefore, does not need to be redesigned in case of faults. In addition, as the controller is not affected by the faults, its design can be carried out taking into account only the model of the nominal system and may already be implemented before the inclusion of the reconfiguration block, regardless of its structure. Thus, the virtual sensor and the actuator can be seen as a plug-in of the system, capable of making the system satisfy conditions of stability and performance, even in the presence of faults.

Remark 2.1 *According to the fault hiding paradigm [12–14, 98], it is possible to insert a reconfiguration block into the system so that faults do not affect the response of the designed controller. Therefore, in this Thesis, as in [21], it is assumed that there is a controller designed for the nominal system, called nominal controller, which has as input the reference sequence r_k and as output the control sequence $u_{c,k}$, with appropriate dimensions. Moreover, the obtained closed-loop system is input-to-output stable with respect to the inputs (r_k, d_k) and the outputs $(u_{c,k}, x_k)$ before the insertion of the reconfiguration block, where x_k is the state vector of the nominal system.*

2.6 COUPLED TANKS SYSTEMS

The increasing complexity and automation of industrial devices and processes demand more and more reliability. In this context, the design and implementation of control (or FTC) systems are crucial to guarantee the stability, robustness and performance of the system as a whole. Among the most important industrial processes, is the level and flow control in tanks or reservoirs [99], since it is used in several application areas, such as nuclear power generation [100], mining [101], chemical [102], petrochemical [103], pharmaceutical processing [104], boilers [105], among others. Thus, different methodologies are proposed for the



(a) Coupled tank system.

(b) Process control system.

Figure 3: Level-control system.

modeling and design of control systems for this type of process, such as, for example, sliding mode [106], backstepping [107], predictive [108], hybrid [109], LPV [23] and TS fuzzy [70] approaches.

In addition, as the main objective of this Thesis is the development of reconfiguration block designs for nonlinear systems subject to faults, the set-up of a nonlinear coupled tank system, as depicted in Figure 3a, is used to illustrate the effectiveness of the methodologies proposed both for LVP and TS fuzzy models. The coupled tank system is present at the Signals and Systems Laboratory of CEFET-MG Campus Divinópolis and is inspired in the proposal in [110] and consists of four tanks ($T1$, $T2$, $T3$, $T4$) with a capacity of 200 liters each one and two reservoirs with a capacity of 400 liters each one, located at the bottom of the plant.

Only tanks $T3$ and $T4$ (bottom tanks of Figure 3a) are used in the experiments, and they are shown in the representative diagram in Figure 4 (with the respective dimensions). Moreover, a nonlinear solid [111], depicted in Figure 5b, constructed from expanded polystyrene is introduced into tank $T3$. The solid has a circular section of diameter varying between 23.3 cm and 59.8 cm. The inser-

tion of this nonlinearity allows the system to be described as an LPV or TS fuzzy model, enabling the design and implementation of LPV and TS fuzzy reconfiguration blocks. The algorithms used for the system control run on a Raspberry Pi 3 Model B through a notebook using an open-source Python-based interface [112] that communicates with a Programmable Logic Computer (PLC), as depicted in Figure 3b. The PLC is responsible for sending the control signal that commands the speed of two 1 hp hydraulic induction pumps, model CAM-W6 from Dancor, presented in Figure 5a. The coupled tanks system is configured so that the two pumps have their flow directed to the tank $T3$. Pump speeds are controlled using two frequency inverters model CFW09 manufactured by WEG, as shown in Figure 3b. Also, the level measures are stored in the PLC memory, which is accessed by the notebook's interface. The levels of the two tanks are measured using two differential pressure sensors of the model 26PCBFA6D from manufacturer Honeywell. In addition, to avoid overflowing, the process has a security system that shuts down the entire system (PLC, frequency inverters and other devices) when the level of any of the tanks exceeds the level of 70 cm.

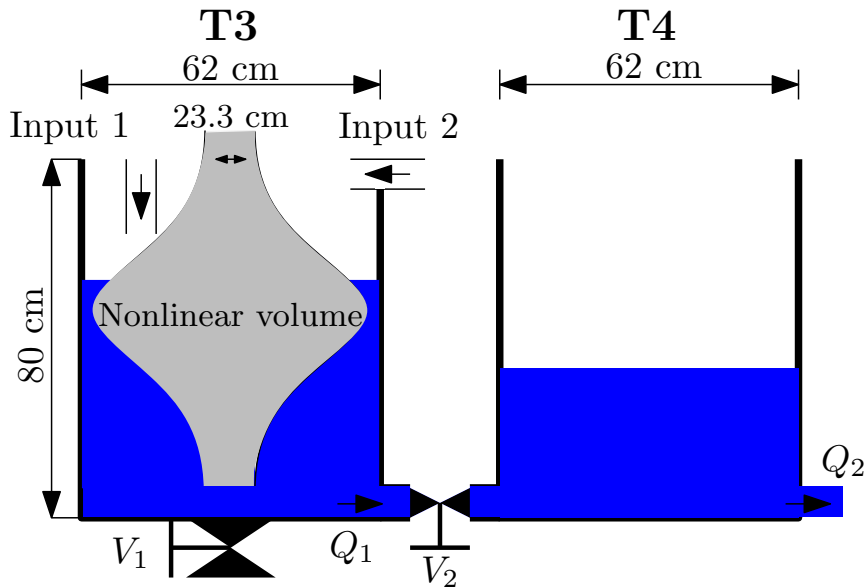


Figure 4: Two tank system diagram.

During the experiments, valve V_1 is kept closed, and valve V_2 is kept with a fixed opening, as depicted in Figure 4 (notice also from Figure 4 how the solid

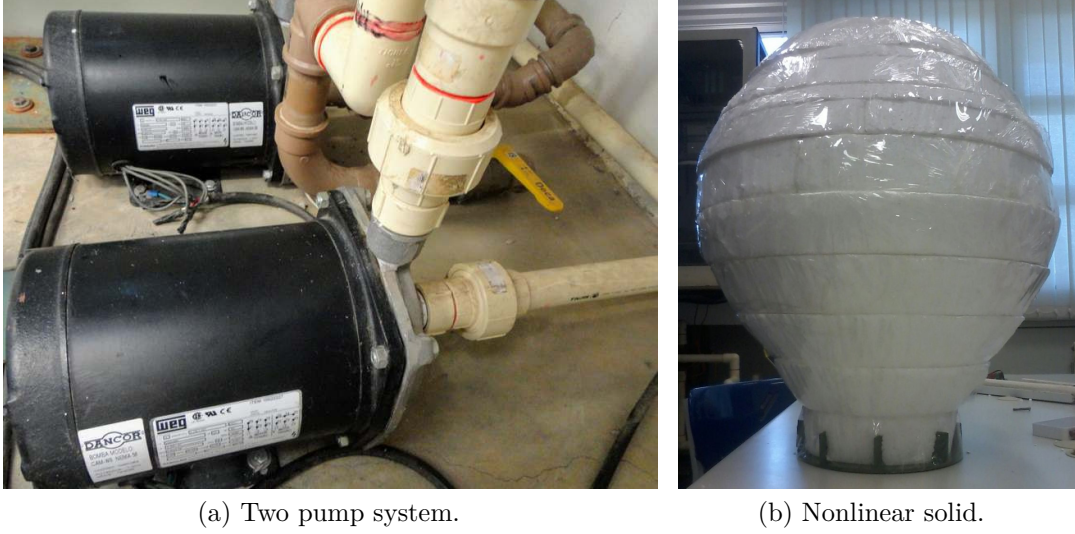


Figure 5: Actuators and nonlinear solid inserted in tank $T3$.

depicted in Figure 5b is introduced in tank $T3$). Thus, using mass balance, the following dynamic equations of the system described above are obtained:

$$\begin{aligned} \dot{h}_1(t) &= \frac{-h_1(t) + h_2(t)}{S_1(h_1(t))R_{12}(h_1(t),h_2(t))} + \frac{q_{i_1}(u_1(t))}{S_1(h_1(t))} + \frac{q_{i_2}(u_2(t))}{S_1(h_1(t))} \\ \dot{h}_2(t) &= \frac{h_1(t) - h_2(t)}{R_{12}(h_1(t),h_2(t))S_2} - \frac{q_o(h_2(t))}{S_2} \end{aligned} \quad (2.13)$$

where $h_1(t)$ and $h_2(t)$ are the levels of tanks $T3$ and $T4$, respectively, $q_{i_1}(u_1(t))$ and $q_{i_2}(u_2(t))$ are the input flows, with u_1 and u_2 being the control signals, $q_o(h_2(t))$ is the outflow of the second tank, and $R_{12}(h_1(t),h_2(t))$ is the flow resistance between the two tanks and adjusted by means of valve V_2 . The functions of $q_{i_1}(u_1(t))$, $q_{i_2}(u_2(t))$, $q_o(h_2(t))$ and $R_{12}(h_1(t),h_2(t))$ are identified by experimental essays with application of least squares. Moreover, S_2 is the area of the circular section of tank T_4 , being defined as $S_2 = 3019 \text{ cm}^2$ for the LPV approach experiments of Chapter 3 and as $S_2 = 0.3019 \text{ m}^2$ for the computer simulations of the TS fuzzy approach of Chapter 4. $S_1(h_1(t))$ is the nonlinear area of the circular section of tank T_3 , calculated as:

$$\begin{aligned} S_1(h_1(t)) &= \frac{3r}{5} \left(2.7r - \frac{\cos(2.5\pi((h_1(t) - \omega_1) \times 10^{-2} - \mu))}{\sigma\sqrt{2\pi}} \right. \\ &\quad \left. \times e^{-\frac{((h_1(t) - \omega_1) \times 10^{-2} - \mu)^2}{2\sigma^2}} \right) \times \omega_2, \end{aligned} \quad (2.14)$$

where $r = 0.31$ m is the radius of the tank, $\sigma = 0.55$ and $\mu = 0.40$. For the LPV case, $\omega_1 = 8$ cm, $\omega_2 = 10^4$, the area S_1 is given in cm^2 , the levels are in the range $0 \leq (h_1(t), h_2(t)) \leq 80$ cm and the control signals are in the range $0 \leq (u_1(t), u_2(t)) \leq 100\%$. For the TS fuzzy case, $\omega_1 = 0.08$ m, $\omega_2 = 1$, the area S_1 is given in m^2 , the levels are in the range $0 \leq (h_1(t), h_2(t)) \leq 0.80$ m and the control signals are in the range $0 \leq (u_1(t), u_2(t)) \leq 1$.

Experimental results of the implementation of LPV reconfiguration blocks proposed in this work and by other methodologies are presented in Section 3.4, considering faults of sensors and actuators. In Section 4.4, the nonlinear model of the coupled tanks system is used for computer simulations of the implementation of the TS fuzzy reconfiguration block proposed in Chapter 4 and it is also compared to the approach presented in Chapter 3 and without any FTC strategy, for different fault scenarios and with disturbance.

2.6.1 Controller Design

For controlling the process, it is established that tank $T3$ level must track a piecewise constant reference (r_k). For that, an integrator is inserted in the closed-loop system such that the error $e_{c,k} = r_k - h_{1,k}$ is null in steady state. Therefore, the system matrices must be augmented to include the dynamics of e_c and are given by:

$$A_{a_i} = \begin{bmatrix} A_i & 0 \\ -T_s C_{h_1} & 1 \end{bmatrix}; \quad B_{a_i} = \begin{bmatrix} B_i \\ 0 \end{bmatrix}; \quad \forall i = 1, \dots, \tilde{N}, \quad (2.15)$$

where A_i and B_i , are the vertices of the dynamics and input matrices of the system, respectively, with $i = 1, \dots, \tilde{N}$, $C_{h_1} = [1 \ 0]$, and T_s is the sampling time. Thus, a gain-scheduled/TS fuzzy controller is designed, with the following resulting control signal:

$$u_{c,k} = K(\alpha_k) x_{a,k}, \quad (2.16)$$

where $K(\alpha_k) \in \mathbb{R}^{m \times (n+1)}$, with $K(\alpha_k) = \sum_{i=1}^{\tilde{N}} \alpha_{i,k} K_i$, and $x_{a,k} \in \mathbb{R}^{n+1}$ is the state vector augmented, with $x_{a,k} = [h_{1,k} \ h_{2,k} \ \sum T_s e_{c,k}]^T$. To determine the gain matrices K_i for $i = 1, \dots, \tilde{N}$, the methodology proposed in [113, Theorem 2] is used, with matrices A_i and B_i in [113, Eq. (8)] replaced by the augmented matrices A_{a_i} and B_{a_i} given in (2.15).

2.7 PERFORMANCE INDICES

The control theory assumes that the designer can quantitatively specify the required performance for a closed-loop system. Thus, a certain performance index can be calculated and used to measure that performance and it is chosen for the closed-loop system evaluation so that the most relevant control specifications are emphasized.

Generally, a performance index to be useful must always be a positive or a null number. The better configuration for the system is defined as the one that minimizes a given index. Thus, to compare different closed-loop systems, it is necessary to calculate indices that ensure quantitatively which one of them has the best performance.

Very classic indices ([114]) are the ones related to the integral of the error and are usually used to compute the performance of the closed-loop systems as: integral of the absolute error (IAE), integral of the square error (ISE), integral of the time multiplied by the absolute value of the error (ITAE) and integral of the time multiplied by the square of the error (ITSE). In this work, the indices IAE and ISE are used. Furthermore, the standard deviation of the control signal (IVU), which takes into account the variability of the analyzed variable and allows an evaluation of the performance through the control signal, is used as well.

The indices IAE and ISE are given by:

$$\text{IAE} = \frac{1}{N_A} \sum_{k=1}^{N_A} |e_k|, \quad (2.17)$$

and

$$\text{ISE} = \frac{1}{N_A} \sum_{k=1}^{N_A} e_k^2, \quad (2.18)$$

where $e_k = r_k - y_k$ is the tracking error of the system output in relation to the reference signal and N_A is the total number of samples of the evaluated time period.

The variability of the manipulated variable u_k around the mean value \bar{u} is estimated by the standard deviation:

$$\text{IVU} = \sqrt{\frac{1}{N_A} \sum_{k=1}^{N_A} |u_k - \bar{u}|^2}, \quad (2.19)$$

where N_A is the total number of samples used to calculate the variability.

2.8 USEFUL LEMMAS

For a better understanding of the methodology proposed in Chapter 4, the following lemmas are presented.

Lemma 2.1 [32] *For $y \in \mathbb{R}^n$ and $\sigma > 0$, the following inequalities are equivalent:*

$$y^T y - \sigma < 0 \Leftrightarrow yy^T - \sigma I < 0. \quad (2.20)$$

Lemma 2.2 [32] *The following inequality holds:*

$$X^T Y + Y^T X \leq \mu X^T X + \mu^{-1} Y^T Y, \quad (2.21)$$

where X and Y are matrices of appropriate dimensions and μ is a positive scalar.

Lemma 2.3 *Differential Mean Value Theorem [32]: Consider $f(z) : \mathbb{R}^n \rightarrow \mathbb{R}$. If $f(z)$ is a differentiable function on $[a, b]$, with $a, b \in \mathbb{R}^n$, there exists a vector $c \in \mathbb{R}^n$ with $c_i \in]a_i, b_i[$, with $]a_i, b_i[$ an open interval between a_i and b_i and $i = 1, \dots, n$, so that:*

$$f(b) - f(a) = \nabla f(c)(b - a) \quad (2.22)$$

with $\nabla f(c) = \frac{\partial f(c)}{\partial z}$.

Part II

FAULT TOLERANT CONTROL FOR NONLINEAR
SYSTEMS

3

A LINEAR PARAMETER VARYING VIRTUAL ACTUATOR AND SENSOR APPROACH

In this chapter, novel sufficient conditions based on LMIs are proposed for the synthesis of virtual sensor and actuator for nonlinear systems described by discrete-time LPV models, ensuring the ISS of the reconfiguration block. This new methodology allows the system to be robust to different types of sensor and actuator faults with the use of a single reconfiguration block design, unlike the proposals in [21, 23]. In addition, experimental results are presented for different approaches and scenarios of faults implemented in the nonlinear system of coupled tanks presented in Section 2.6. The approach proposed in this chapter has been published in [38].

3.1 FAULTY LINEAR PARAMETER VARYING SYSTEM

Consider the discrete-time LPV system, adapted from [21], described by:

$$\Sigma_P = \begin{cases} x_{k+1} &= A(\alpha_k)x_k + B(\alpha_k)u_k + B_d d_k, \\ y_k &= C(\alpha_k)x_k, \end{cases} \quad (3.1)$$

where $x_k \in \mathbb{R}^n$ represents the state vector, $u_k \in \mathbb{R}^m$ is the sequence of control input, $y_k \in \mathbb{R}^p$ is the output, and $d_k \in \mathbb{R}^d$ denotes a disturbance sequence. The matrices $A(\alpha_k) \in \mathbb{R}^{n \times n}$, $B(\alpha_k) \in \mathbb{R}^{n \times m}$, and $C(\alpha_k) \in \mathbb{R}^{p \times n}$ relate the dynamics and the output of the system and belong to polytopes whose vertices are known as follows $A(\alpha_k) \in \Omega_N(A)$, $B(\alpha_k) \in \Omega_N(B)$, and $C(\alpha_k) \in \Omega_N(C)$. The disturbance matrix $B_d \in \mathbb{R}^{n \times d}$ is precisely known.

In this chapter the faulty model, denoted by Σ_{P_f} , is considered to be the same as the plant nominally represented by Σ_P in (3.1), but with the fault indications in the input and output matrices (which has been adapted from [23]). Then, the faulty model is:

$$\Sigma_{P_f} = \begin{cases} x_{f,k+1} &= A(\alpha_k)x_{f,k} + B_f(\alpha_k, \phi_k)u_{f,k} + B_d d_k, \\ y_{f,k} &= C_f(\alpha_k, \gamma_k)x_{f,k}, \end{cases} \quad (3.2)$$

Specifically in (3.2) the faults are represented by means of multiplicative notation such that $\phi_k \in \mathbb{R}^m$ and $\gamma_k \in \mathbb{R}^p$ are, respectively, the vectors of actuator and sensor fault indications verifying $\gamma_{j,k}, \phi_{i,k} \in [0,1] \forall i,j$. Defining the diagonal matrices $\hat{\phi} = \text{diag}(\phi_k)$ and $\hat{\gamma} = \text{diag}(\gamma_k)$ (as in [23]), the input control and output matrices of the faulty system are given by, respectively:

$$B_f(\alpha_k, \phi_k) = B(\alpha_k)\hat{\phi}, \quad (3.3)$$

and

$$C_f(\alpha_k, \gamma_k) = \hat{\gamma}C(\alpha_k). \quad (3.4)$$

As a consequence, matrices $\hat{\phi}$ and $\hat{\gamma}$ belong to polytopic domains, that is, $\hat{\phi} \in \Omega_{2^m}(\hat{\phi}_k)$ and $\hat{\gamma} \in \Omega_{2^p}(\hat{\gamma}_k)$, encompassing all possible actuator and sensor fault scenarios. Therefore, the faulty system matrices are enclosed into the new polytope $\Omega_{\bar{N}}([A, B_f, C_f^T])$, given by:

$$\Omega_{\bar{N}} = \Omega_N([A, B_f, C_f^T]) \times \Omega_{2^m}(\hat{\phi}_k) \times \Omega_{2^p}(\hat{\gamma}_k), \quad (3.5)$$

with $\bar{N} = N2^{m+p}$. Additionally, it is convenient to represent the faulty system Σ_{P_f} using a single vector of time-varying parameters which incorporates the time-varying parameters α_k , ϕ_k and γ_k . Such parameter vector is denominated $\theta_k \in \Theta_{\bar{N}}(\theta)$. In this sense, Σ_{P_f} in (3.2) with matrices belonging to the polytope described in (3.5) can be also represented by:

$$\Sigma_{P_f} = \begin{cases} x_{f,k+1} &= A(\theta_k)x_{f,k} + B_f(\theta_k)u_{f,k} + B_d d_k, \\ y_{f,k} &= C_f(\theta_k)x_{f,k}. \end{cases} \quad (3.6)$$

The following example illustrates how a faulty system is described using the notation presented in this chapter.

Example 3.1. Consider the nominal LPV system in (3.1) with the matrices:

$$A(\alpha_k) = \begin{bmatrix} 0.8 & 1 \\ 0 & \alpha_{1,k} \end{bmatrix}, B = \begin{bmatrix} 1 \\ 0 \end{bmatrix}, B_d = \begin{bmatrix} 0 \\ 1 \end{bmatrix}, C = \begin{bmatrix} 0 & 1 \end{bmatrix}, \quad (3.7)$$

where $\underline{\alpha}_{1,k} \leq \alpha_{1,k} \leq \bar{\alpha}_{1,k}$, with $\underline{\alpha}_{1,k} = 0.6$ and $\bar{\alpha}_{1,k} = 0.9$ and, consequently, $N = 2$ vertices.

Assuming the system is subject to sensor and actuator faults in the ranges $\underline{\phi}_{1,k} \leq \phi_{1,k} \leq \bar{\phi}_{1,k}$ and $\underline{\gamma}_{1,k} \leq \gamma_{1,k} \leq \bar{\gamma}_{1,k}$, with $\underline{\phi}_{1,k} = 0.1$, $\bar{\phi}_{1,k} = 1$, $\underline{\gamma}_{1,k} = 0.1$,

and $\bar{\gamma}_{1,k} = 1$, the input and output matrices of the faulty system (3.2) are given by:

$$\begin{aligned} B_f(\phi_k) &= B\phi_{1,k}, \\ C_f(\gamma_k) &= \gamma_{1,k}C, \end{aligned} \quad (3.8)$$

as shown in (3.3) and (3.4). Therefore, according to (3.5), the number of vertices of the faulty system becomes $\bar{N} = 8$, being described by (3.6), with the following matrices:

$$\begin{aligned} A_1 = A_2 = A_3 = A_4 &= \begin{bmatrix} 0.8 & 1 \\ 0 & \bar{\alpha}_{1,k} \end{bmatrix}, & A_5 = A_6 = A_7 = A_8 &= \begin{bmatrix} 0.8 & 1 \\ 0 & \underline{\alpha}_{1,k} \end{bmatrix}, \\ B_{f_1} = B_{f_2} = B_{f_5} = B_{f_6} &= \begin{bmatrix} \bar{\phi}_{1,k} \\ 0 \end{bmatrix}, & B_{f_3} = B_{f_4} = B_{f_7} = B_{f_8} &= \begin{bmatrix} \underline{\phi}_{1,k} \\ 0 \end{bmatrix}, \\ C_{f_1} = C_{f_3} = C_{f_5} = C_{f_7} &= \begin{bmatrix} 0 & \bar{\gamma}_{1,k} \end{bmatrix}, & C_{f_2} = C_{f_4} = C_{f_6} = C_{f_8} &= \begin{bmatrix} 0 & \underline{\gamma}_{1,k} \end{bmatrix}. \end{aligned} \quad (3.9)$$

The following assumption is considered throughout this chapter.

Assumption 3.1 *The vector of time-varying parameters θ_k in (3.6) is measured independently from the occurrence of faults.*

It is important to note that the time-varying parameters related to sensor and actuator fault indications are provided by the FDI module, as presented in Assumption 2.1.

3.2 PROBLEM FORMULATION

The fault hiding approach proposed in this chapter is composed of a virtual sensor and a virtual actuator to masking the sensor and actuator faults, as shown in Figure 2 of Section 2.5. Thus, alternative signals (y_c and u_f) are generated by the reconfiguration block so that it is not necessary to perform any change in the controller designed for the nominal system (3.1).

As proposed by [21], the virtual sensor is described by the following equation:

$$\hat{x}_{f,k+1} = A_\delta(\theta_k)\hat{x}_{f,k} + B_f(\theta_k)u_{f,k} - L(\theta_k)y_{f,k}, \quad (3.10)$$

where $\hat{x}_{f,k} \in \mathbb{R}^n$ is the estimated state by the virtual sensor of the faulty system, $u_{f,k} \in \mathbb{R}^m$ is the control sequence computed by the virtual actuator defined latter in this section, $A_\delta(\theta_k) = A(\theta_k) + L(\theta_k)C_f(\theta_k)$, and $L(\theta_k) \in \mathbb{R}^{n \times p}$ is the virtual sensor matrix gain given by:

$$L(\theta_k) = \sum_{i=1}^{\bar{N}} \theta_{i,k} L_i. \quad (3.11)$$

From this, the error between the estimated state ($\hat{x}_{f,k}$) and the faulty system state ($x_{f,k}$) can be calculated as $e_k = \hat{x}_{f,k} - x_{f,k}$ and has as dynamics:

$$e_{k+1} = A_\delta(\theta_k)e_k + v_k \quad (3.12)$$

where $v_k = -B_d d_k$.

Similarly, as presented in [21], the virtual actuator is defined by:

$$\begin{cases} \tilde{x}_{k+1} &= A(\theta_k)\tilde{x}_k + B(\theta_k)u_{c,k}, \\ u_{f,k} &= -M(\theta_k)x_{\Delta,k} - R(\theta_k)u_{c,k}, \\ y_{c,k} &= C(\theta_k)\tilde{x}_k, \end{cases} \quad (3.13)$$

where $\tilde{x}_k \in \mathbb{R}^n$ is the reference state generated by the virtual actuator and based on the nominal system (3.1), $u_{c,k} \in \mathbb{R}^m$ is the control sequence calculated by the nominal controller, $x_{\Delta,k} = \tilde{x}_k - \hat{x}_{f,k}$ is the difference state and $R(\theta_k) \in \mathbb{R}^{m \times m}$ is a static gain matrix. Moreover, $y_{c,k} \in \mathbb{R}^p$ is an alternative output generated by the virtual actuator that becomes the nominal controller input in the presence of faults. Finally, $M(\theta_k) \in \mathbb{R}^{m \times n}$ is the virtual actuator gain matrix described by:

$$M(\theta_k) = \sum_{i=1}^{\bar{N}} \theta_{i,k} M_i, \quad (3.14)$$

and the dynamics of the difference state is given as follows:

$$x_{\Delta,k+1} = (A(\theta_k) + B_f(\theta_k)M(\theta_k))x_{\Delta,k} + w_k, \quad (3.15)$$

where $w_k = -L(\theta_k)C_f(\theta_k)e_k + B_\Delta u_{c,k}$, with $B_\Delta = B(\theta_k) + B_f(\theta_k)R(\theta_k)$. Then, the gain matrix $R(\theta_k)$ can be designed so that the norm of the second term of w_k is as small as possible.

Thus, the main problem to be addressed in this chapter is stated.

Problem 3.1 Determine the gains $L(\theta_k)$ and $M(\theta_k)$ for the virtual sensor (3.10) and the virtual actuator (3.13) for the faulty LPV system (3.6) so that the reconfigured system composed by the virtual sensor (3.10), the virtual actuator (3.13), the faulty plant (3.6) and the nominal controller is input-to-output stable with respect to the input (r_k, d_k) , and, in addition, it is robust to a given set of sensor and actuator faults.

3.3 LPV VIRTUAL SENSOR AND ACTUATOR

In the following, the main contributions in this chapter concerning the design of robust virtual sensors and actuators are presented.

3.3.1 Virtual Sensor

Theorem 3.1 Consider the faulty LPV system in (3.6). If there exist symmetric definite positive matrices $P_i \in \mathbb{R}^{n \times n}$, matrices $G_i \in \mathbb{R}^{n \times n}$, $U_i \in \mathbb{R}^{n \times p}$, $Y_i \in \mathbb{R}^{p \times n}$, $Z_i \in \mathbb{R}^{p \times p}$, $i = 1, \dots, \bar{N}$, and a scalar $\sigma_d \geq 1$ such that the following LMIs are feasible:

$$\begin{bmatrix} P_i - G_i - G_i^T & 0 & G_i A_i & G_i & U_i \\ \star & -I & I & 0 & 0 \\ \star & \star & -P_j + C_{f_i}^T Y_j + Y_j^T C_{f_i} & 0 & -Y_j^T + C_{f_i}^T Z_j \\ \star & \star & \star & -\sigma_d I & 0 \\ \star & \star & \star & \star & -Z_j - Z_j^T \end{bmatrix} < 0, \quad (3.16)$$

$\forall i, j = 1, \dots, \bar{N}$, then, the estimation error (3.12) is input-to-state stable with respect to the disturbance d_k with ISS gain calculated by $\|B_d\| \|d\|_\infty \sigma_d$. Moreover, the LPV virtual sensor gain in (3.11) is given by:

$$L_i = G_i^{-1} U_i. \quad (3.17)$$

Proof. Consider:

$$V(e_k) = e_k^T P(\theta_{k-1}) e_k \quad (3.18)$$

where $P(\theta_{k-1}) = \sum_{j=1}^{\bar{N}} \theta_{j,k-1} P_j$, as an ISS Lyapunov candidate function.

Because $P_i > 0$, the first term of the diagonal in (3.16) implies that G_i is nonsingular. Now, define $U_i = G_i L_i$ and use in (3.16) the fact that $G_i P_i^{-1} G_i^T \geq G_i + G_i^T - P_i$, in order to obtain:

$$\begin{bmatrix} -G_i P_i^{-1} G_i^T & 0 & G_i A_i & G_i & G_i L_i \\ \star & -I & I & 0 & 0 \\ \star & \star & -P_j + C_{f_i}^T Y_j + Y_j^T C_{f_i} & 0 & -Y_j^T + C_{f_i}^T Z_j \\ \star & \star & \star & -\sigma_d I & 0 \\ \star & \star & \star & \star & -Z_j - Z_j^T \end{bmatrix} < 0. \quad (3.19)$$

The resulting inequality (3.19) is pre- and post-multiplied by $\text{diag}\{G_i^{-1}, I, I, I, I\}$ and its transpose, respectively, resulting in:

$$\begin{bmatrix} -P_i^{-1} & 0 & A_i & I & L_i \\ \star & -I & I & 0 & 0 \\ \star & \star & -P_j + C_{f_i}^T Y_j + Y_j^T C_{f_i} & 0 & -Y_j^T + C_{f_i}^T Z_j \\ \star & \star & \star & -\sigma_d I & 0 \\ \star & \star & \star & \star & -Z_j - Z_j^T \end{bmatrix} < 0. \quad (3.20)$$

The last term of the diagonal in (3.16) implies the nonsingularity of Z_i . Then, in (3.20), define $Q_i = P_i^{-1}$, $H_i = Z_i^{-T}$, and $F_i = Q_i Y_i^T H_i$, to obtain:

$$\begin{bmatrix} -Q_i & 0 & A_i & I & L_i \\ \star & -I & I & 0 & 0 \\ \star & \star & -Q_j^{-1} + \Phi_1 & 0 & -Q_j^{-1} F_j H_j^{-1} + C_{f_i}^T H_j^{-T} \\ \star & \star & \star & -\sigma_d I & 0 \\ \star & \star & \star & \star & -H_j^{-T} - H_j^{-1} \end{bmatrix} < 0, \quad (3.21)$$

$$\Phi_1 = C_{f_i}^T H_j^{-T} F_j^T Q_j^{-1} + Q_j^{-1} F_j H_j^{-1} C_{f_i}.$$

Thereafter, multiplying (3.21) on the left by:

$$S_1 = \begin{bmatrix} I & 0 & 0 & 0 & 0 \\ 0 & I & 0 & 0 & 0 \\ 0 & 0 & 0 & 0 & H_j \\ 0 & 0 & 0 & I & 0 \\ 0 & 0 & Q_j & 0 & -F_j \end{bmatrix}, \quad (3.22)$$

and on the right by its transpose, respectively, results in:

$$\begin{bmatrix} -Q_i & 0 & L_i H_j^T & I & A_i Q_j - L_i F_j^T \\ \star & -I & 0 & 0 & Q_j \\ \star & \star & -H_j - H_j^T & 0 & C_{f_i} Q_j + F_j^T \\ \star & \star & \star & -\sigma_d I & 0 \\ \star & \star & \star & \star & -Q_j \end{bmatrix} < 0. \quad (3.23)$$

Subsequently, multiply the inequality (3.23) by $\theta_{i,k}$ and $\theta_{j,k-1}$ and summing it up for all $i, j = 1, \dots, \overline{N}$, one obtains:

$$\begin{bmatrix} -Q(\theta_k) & 0 & L(\theta_k) H(\theta_{k-1})^T & I & \Phi_2 \\ \star & -I & 0 & 0 & Q(\theta_{k-1}) \\ \star & \star & -H(\theta_{k-1}) - H(\theta_{k-1})^T & 0 & \Phi_3 \\ \star & \star & \star & -\sigma_d I & 0 \\ \star & \star & \star & \star & -Q(\theta_{k-1}) \end{bmatrix} < 0, \quad (3.24)$$

$$\Phi_2 = A(\theta_k) Q(\theta_{k-1}) - L(\theta_k) F(\theta_{k-1})^T,$$

$$\Phi_3 = C_f(\theta_k) Q(\theta_{k-1}) + F(\theta_{k-1})^T.$$

Then, pre- and post-multiplying the resulting inequality (3.24) by:

$$S_2 = \begin{bmatrix} I & 0 & L(\theta_k) & 0 & 0 \\ 0 & I & 0 & 0 & 0 \\ 0 & 0 & 0 & 0 & Q(\theta_{k-1})^{-1} \\ 0 & 0 & 0 & I & 0 \end{bmatrix}, \quad (3.25)$$

and its transpose, respectively, one obtains:

$$\begin{bmatrix} -P(\theta_k)^{-1} & 0 & A_\delta(\theta_k) & I \\ \star & -I & I & 0 \\ \star & \star & -P(\theta_{k-1}) & 0 \\ \star & \star & \star & -\sigma_d I \end{bmatrix} < 0. \quad (3.26)$$

Applying the Schur complement in (3.26), gives:

$$\begin{bmatrix} A_\delta(\theta_k)^T P(\theta_k) A_\delta(\theta_k) - P(\theta_{k-1}) + I & A_\delta(\theta_k)^T P(\theta_k) \\ P(\theta_k) A_\delta(\theta_k) & -\sigma_d I + P(\theta_k) \end{bmatrix} < 0. \quad (3.27)$$

Then multiplying the inequality (3.27) on the left and right by $\begin{bmatrix} e_k^T & v_k^T \end{bmatrix}$ and its transpose, respectively, it yields:

$$(e_{k+1})^T P(\theta_k) (e_{k+1}) - e_k^T P(\theta_{k-1}) e_k \leq -e_k^T e_k + \sigma_d v_k^T v_k, \quad (3.28)$$

which can be described as:

$$V(e_{k+1}) - V(e_k) \leq -\|e_k\|^2 + \sigma_d \|v_k\|^2. \quad (3.29)$$

Moreover, if (3.26) is satisfied and rearranging the terms, then:

$$\begin{bmatrix} -I & I \\ \star & -P(\theta_{k-1}) \end{bmatrix} < 0 \quad \text{and} \quad \begin{bmatrix} -P(\theta_k)^{-1} & I \\ \star & -\sigma_d I \end{bmatrix} < 0. \quad (3.30)$$

By Schur complement, $P(\theta_{k-1}) > I$ and $P(\theta_k) < \sigma_d I$. Then,

$$\|e_k\|^2 \leq V(e_k) \leq \sigma_d \|e_k\|^2. \quad (3.31)$$

Thus, by (3.29) and (3.31), $V(e_k)$ is an ISS Lyapunov function for the estimation error (3.12), and, therefore, the system is input-to-state stable with respect to $v_k = -B_d d_k$.

In order to calculate the ISS gain of the system, a procedure similar to that of [21, Appendix A.1] is performed. From (3.29), $-||e_k||^2 \leq -(1/\sigma_d)V(e_k)$. Combining this with equation (3.31) gives:

$$V(e_{k+1}) \leq V(e_k) \left(1 - \frac{1}{\sigma_d}\right) + \sigma_d \|v_k\|^2. \quad (3.32)$$

Calculating (3.32) recursively, the solution of the discrete-time equation can be obtained as:

$$\begin{aligned} V(e_k) &\leq V(e_0) \left(1 - \frac{1}{\sigma_d}\right)^k + \sigma_d \sum_{l=0}^{k-1} \left(1 - \frac{1}{\sigma_d}\right)^{k-1-l} \|v_l\|^2 \\ &\leq V(e_0) \left(1 - \frac{1}{\sigma_d}\right)^k + \sigma_d \|v\|_\infty^2 \sum_{l=0}^{k-1} \left(1 - \frac{1}{\sigma_d}\right)^{k-1-l}. \end{aligned} \quad (3.33)$$

The term $\sum_{l=0}^{k-1} \left(1 - \frac{1}{\sigma_d}\right)^{k-1-l}$ in (3.33) can be written as $\sum_{\ell=-k-1}^0 \left(1 - \frac{1}{\sigma_d}\right)^{k-1+\ell}$ with $l = -\ell$ and $\ell \in [-(k-1), 0]$, which, in turn, can be written as $\sum_{\tilde{l}=0}^{k-1} \left(1 - \frac{1}{\sigma_d}\right)^{\tilde{l}}$ with $\ell = \tilde{l} - (k-1)$ and $\tilde{l} \in [0, (k-1)]$. Since the last sum is a geometric series and $\sigma_d \geq 1$, then:

$$\sum_{\tilde{l}=0}^{k-1} \left(1 - \frac{1}{\sigma_d}\right)^{\tilde{l}} = \sigma_d - \sigma_d \left(1 - \frac{1}{\sigma_d}\right)^k \leq \sigma_d. \quad (3.34)$$

Thus, (3.33) can be calculated by:

$$V(e_k) \leq V(e_0) \left(1 - \frac{1}{\sigma_d}\right)^k + \sigma_d^2 \|v\|_\infty^2. \quad (3.35)$$

From (3.31), equation (3.35) can be rewritten as:

$$V(e_k) \leq \sigma_d \|e_0\|^2 \left(1 - \frac{1}{\sigma_d}\right)^k + \sigma_d^2 \|v\|_\infty^2. \quad (3.36)$$

Also from (3.31), (3.36) results in:

$$\|e_k\| \leq \sqrt{\sigma_d} \|e_0\| \left(1 - \frac{1}{\sigma_d}\right)^{k/2} + \sigma_d \|v\|_\infty. \quad (3.37)$$

Therefore, the system is input-to-state stable with respect to v_k with the ISS gain given by $\sigma_d \|v\|_\infty$, and that the ISS gain with respect to d_k is calculated by $\sigma_d \|B_d\| \|d_k\|_\infty$. This concludes the proof. \square

3.3.2 Virtual actuator

Theorem 3.2 Consider the faulty LPV system (3.6) and that there exist symmetric positive definite matrices $\tilde{Q}_i \in \mathbb{R}^{n \times n}$, matrices $X_i \in \mathbb{R}^{p \times n}$, $Z_i \in \mathbb{R}^{p \times p}$, $i = 1, \dots, N$, and a scalar $\sigma_a \geq 1$ such that the following LMIs are feasible:

$$\begin{bmatrix} -\tilde{Q}_j + B_{f_i} X_j + X_j^T B_{f_i}^T & \star & \star & \star & \star \\ 0 & -I & \star & \star & \star \\ \tilde{Q}_i A_i^T & \tilde{Q}_i & -\tilde{Q}_i & \star & \star \\ I & 0 & 0 & -\sigma_a I & \star \\ -X_j + Z_j^T B_{f_i}^T & 0 & Y_i & 0 & -Z_j - Z_j^T \end{bmatrix} < 0 \quad (3.38)$$

$\forall i, j = 1, \dots, \bar{N}$. Then, the difference state (3.15) is input-to-state stable with respect to the input $(u_{c,k}, e_k)$ with ISS gain calculated by $\max(\sigma_a \max_{1 \leq i \leq \bar{N}} \|L_i\| \times \max_{1 \leq j \leq \bar{N}} \|C_{f_j}\|, \sigma_a \|B_\Delta\|)$. Moreover, the virtual LPV actuator gain in (3.14) is given by:

$$M_i = Y_i \tilde{Q}_i^{-1}. \quad (3.39)$$

Proof. Consider:

$$\tilde{V}(x_{\Delta,k}) = x_{\Delta,k}^T \tilde{P}(\theta_k) x_{\Delta,k}, \quad (3.40)$$

where $\tilde{P}(\theta_k) = \sum_{i=1}^{\bar{N}} \theta_{i,k} \tilde{P}_i$ with $\tilde{P}_i = \tilde{Q}_i^{-1}$, as an ISS Lyapunov candidate function for the difference state (3.15). Furthermore, $\tilde{P}(\theta_{k+1}) = \sum_{j=1}^{\bar{N}} \theta_{j,k+1} \tilde{P}_j$.

Notice that \tilde{Q}_i and Z_i are nonsingular. Defining $Y_i = M_i \tilde{Q}_i$ in (3.38) and pre- and post-multiplying the resulting matrix by $\text{diag}\{I, I, \tilde{Q}_i^{-1}, I, I\}$ and its transpose, respectively, results in:

$$\begin{bmatrix} -\tilde{Q}_j + B_{f_i} X_j + X_j^T B_{f_i}^T & 0 & A_i & I & -X_j + B_{f_i} Z_j \\ \star & -I & I & 0 & 0 \\ \star & \star & -\tilde{Q}_i^{-1} & 0 & M_i^T \\ \star & \star & \star & -\sigma_a I & 0 \\ \star & \star & \star & \star & -Z_j - Z_j^T \end{bmatrix} < 0. \quad (3.41)$$

In inequality (3.41) define $\tilde{P}_i = \tilde{Q}_i^{-1}$, $H_i = Z_i^{-T}$ and $F_i = \tilde{P}_i X_i^T H_i$, and one gets:

$$\begin{bmatrix} -\tilde{P}_j^{-1} + \Phi_4 & 0 & A_i & I & -\tilde{P}_j F_j H_j^{-1} + B_{f_i} H_j^{-T} \\ \star & -I & I & 0 & 0 \\ \star & \star & -\tilde{P}_i & 0 & M_i^T \\ \star & \star & \star & -\sigma_a I & 0 \\ \star & \star & \star & \star & -H_j^{-T} - H_j^{-1} \end{bmatrix} < 0, \quad (3.42)$$

$$\Phi_4 = B_{f_i} H_j^{-T} F_j^T \tilde{P}_j^{-1} + \tilde{P}_j^{-1} F_j H_j^{-1} B_{f_i}^T.$$

Then, (3.42) is multiplied on the left by:

$$S_3 = \begin{bmatrix} 0 & 0 & 0 & 0 & H_j \\ 0 & I & 0 & 0 & 0 \\ 0 & 0 & I & 0 & 0 \\ 0 & 0 & 0 & I & 0 \\ \tilde{P}_j & 0 & 0 & 0 & -F_j \end{bmatrix}, \quad (3.43)$$

and on the right by its transpose, respectively, yielding:

$$\begin{bmatrix} -H_j - H_j^T & 0 & H_j M_i & 0 & B_{f_i}^T \tilde{P}_j + F_j^T \\ \star & -I & I & 0 & 0 \\ \star & \star & -\tilde{P}_i & 0 & A_i^T \tilde{P}_j - M_i^T F_j^T \\ \star & \star & \star & -\sigma_a I & \tilde{P}_j \\ \star & \star & \star & \star & -\tilde{P}_j \end{bmatrix} < 0. \quad (3.44)$$

Thereafter, multiply the inequality (3.44) by $\theta_{i,k}$ and $\theta_{j,k+1}$ and summing it up for all $i, j = 1, \dots, \bar{N}$, results in:

$$\begin{bmatrix} -H(\theta_{k+1}) - H(\theta_{k+1})^T & 0 & H(\theta_{k+1})M(\theta_k) & 0 & \Phi_5 \\ \star & -I & I & 0 & 0 \\ \star & \star & -\tilde{P}(\theta_k) & 0 & \Phi_6 \\ \star & \star & \star & -\sigma_a I & \tilde{P}(\theta_{k+1}) \\ \star & \star & \star & \star & -\tilde{P}(\theta_{k+1}) \end{bmatrix} < 0, \quad (3.45)$$

$$\begin{aligned} \Phi_5 &= B_f(\theta_k)^T \tilde{P}(\theta_{k+1}) + F(\theta_{k+1})^T, \\ \Phi_6 &= A(\theta_k)^T \tilde{P}(\theta_{k+1}) - M(\theta_k)^T F(\theta_{k+1})^T. \end{aligned}$$

Then, pre- and post-multiplying (3.45) on the left by:

$$S_4 = \begin{bmatrix} 0 & 0 & 0 & 0 & \tilde{P}^{-1}(\theta_{k+1}) \\ 0 & I & 0 & 0 & 0 \\ M^T(\theta_k) & 0 & I & 0 & 0 \\ 0 & 0 & 0 & I & 0 \end{bmatrix}, \quad (3.46)$$

and on the right by its transpose, respectively, one gets:

$$\begin{bmatrix} -\tilde{Q}(\theta_{k+1}) & 0 & A(\theta_k) + B_f(\theta_k)M(\theta_k) & I \\ \star & -I & I & 0 \\ \star & \star & -\tilde{Q}^{-1}(\theta_k) & 0 \\ \star & \star & \star & -\sigma_a I \end{bmatrix} < 0. \quad (3.47)$$

Consider $x_{\Delta,k+1} = (A(\theta_k) + B_f(\theta_k)M(\theta_k))x_{\Delta,k} + w_k$ and use a Schur complement argument in (3.47), resulting in:

$$\begin{aligned} &\begin{bmatrix} -\tilde{P}(\theta_k) + I & 0 \\ \star & -\sigma_a I \end{bmatrix} + \begin{bmatrix} A(\theta_k) + B_f(\theta_k)M(\theta_k) & I \end{bmatrix}^T \\ &\quad \times \tilde{P}(\theta_{k+1}) \begin{bmatrix} A(\theta_k) + B_f(\theta_k)M(\theta_k) & I \end{bmatrix} < 0. \end{aligned} \quad (3.48)$$

Pre- and post-multiplying the inequality (3.48) by $\begin{bmatrix} x_{\Delta,k}^T & w_k^T \end{bmatrix}$ and its transpose, respectively, one obtains:

$$x_{\Delta,k+1}^T \tilde{P}(\theta_{k+1}) x_{\Delta,k+1} - x_{\Delta,k}^T \tilde{P}(\theta_k) x_{\Delta,k} \leq -x_{\Delta,k}^T x_{\Delta,k} + \sigma_a w_k^T w_k. \quad (3.49)$$

After this, using (3.40) and $w_k = B_{\Delta} u_{c,k} - L(\theta_k) C_f(\theta_k) e_k$ in (3.49), yields:

$$\tilde{V}(x_{\Delta,k+1}) - \tilde{V}(x_{\Delta,k}) \leq -\|x_{\Delta,k}\|^2 + \sigma_a \|B_{\Delta}\|^2 \|u_{c,k}\|^2 + \sigma_a c_1^2 c_2^2 \|e_k\|^2, \quad (3.50)$$

where $c_1 = \max_{1 \leq i \leq \bar{N}} \|L_i\|$ and $c_2 = \max_{1 \leq j \leq \bar{N}} \|C_{f_j}\|$.

Assuming the LMIs in (3.47) are feasible, then:

$$\begin{bmatrix} -I & I \\ \star & -\tilde{Q}(\theta_k)^{-1} \end{bmatrix} < 0 \quad \text{and} \quad \begin{bmatrix} -\tilde{Q}(\theta_{k+1}) & I \\ \star & -\sigma_a I \end{bmatrix} < 0. \quad (3.51)$$

Using a Schur complement argument, it follows that $\tilde{Q}(\theta_k)^{-1} = \tilde{P}(\theta_k) > I$ and $\tilde{Q}(\theta_{k+1})^{-1} = \tilde{P}(\theta_{k+1}) \leq \sigma_a I$, and consequently:

$$\|x_{\Delta,k}\|^2 \leq \tilde{V}(x_{\Delta,k}) \leq \sigma_a \|x_{\Delta,k}\|^2. \quad (3.52)$$

Then, by (3.50) and (3.52), the closed-loop system is input-to-state stable with respect to $u_{c,k}$ and e_k and following the similar steps as described in the proof of Theorem 3.1, it is possible to obtain the ISS gain with respect to $u_{c,k}$ and to e_k , as $\sigma_a \|B_{\Delta}\| \|u_c\|_{\infty}$ and $\sigma_a c_1 c_2 \|e\|_{\infty}$, respectively. This concludes the proof. \square

3.3.3 Combination of the virtual sensor with the virtual actuator

The interconnection between the virtual sensor and the virtual actuator is given by:

$$\begin{aligned} \begin{bmatrix} e_{k+1} \\ x_{\Delta,k+1} \end{bmatrix} &= \begin{bmatrix} A(\theta_k) + L(\theta_k) C_f(\theta_k) & 0 \\ -L(\theta_k) C_f(\theta_k) & A(\theta_k) + B_f(\theta_k) M(\theta_k) \end{bmatrix} \begin{bmatrix} e_k \\ x_{\Delta,k} \end{bmatrix} \\ &+ \begin{bmatrix} 0 \\ B_{\Delta} \end{bmatrix} u_{c,k} + \begin{bmatrix} -B_d \\ 0 \end{bmatrix} d_k, \end{aligned} \quad (3.53)$$

and according to [21], the following lemma can be stated.

Lemma 3.1 [21] *If the virtual sensor gains of the error system (3.12) and the virtual actuator gains of the difference state system (3.15) are designed by the conditions of Theorems 3.1 and 3.2, then the interconnection given in (3.53) is also input-to-state stable. Further, the ISS gain with respect to d_k is $c_3\sqrt{\mu\sigma_d c_5}\|d\|_\infty$ and with respect to $u_{c,k}$ is $c_4\sqrt{\sigma_a c_5}\|u_c\|_\infty$, with:*

$$\begin{aligned} c_1 &= \max_{1 \leq i \leq N} \|L_i\|, \quad c_2 = \max_{1 \leq j \leq N} \|C_{f_j}\|, \quad c_3 = \|B_d\|, \quad c_4 = \|B_\Delta\|, \\ \mu &= \sigma_a c_1^2 c_2^2 + 1, \quad c_5 = \max(\mu\sigma_d, \sigma_a). \end{aligned} \quad (3.54)$$

Proof. Following the same procedure of [21, Appendix A.3], consider:

$$\bar{V}(e_k, x_{\Delta,k}) = \mu V(e_k) + \tilde{V}(x_{\Delta,k}) \quad (3.55)$$

an ISS Lyapunov candidate function with $\mu > 0$ for the interconnection, $V(e_k)$ given by (3.18) and $\tilde{V}(x_{\Delta,k})$ by (3.40). Moreover,

$$\bar{V}(e_{k+1}, x_{\Delta,k+1}) - \bar{V}(e_k, x_{\Delta,k}) = \mu V(e_{k+1}) - \mu V(e_k) + \tilde{V}(x_{\Delta,k+1}) - \tilde{V}(x_{\Delta,k}). \quad (3.56)$$

From (3.29), (3.50) and with $v_k = -B_d d_k$, (3.56) can be written as:

$$\begin{aligned} \bar{V}(e_{k+1}, x_{\Delta,k+1}) - \bar{V}(e_k, x_{\Delta,k}) &\leq (\sigma_a c_1^2 c_2^2 - \mu) \|e_k\|^2 + \mu\sigma_d \|B_d\|^2 \|d_k\|^2 \\ &\quad - \|x_{\Delta,k}\|^2 + \sigma_a \|B_\Delta\|^2 \|u_{c,k}\|^2. \end{aligned} \quad (3.57)$$

Choosing $\mu = \sigma_a c_1^2 c_2^2 + 1$ and defining $c_3 = \|B_d\|$ and $c_4 = \|B_\Delta\|$, results in:

$$\begin{aligned} \bar{V}(e_{k+1}, x_{\Delta,k+1}) - \bar{V}(e_k, x_{\Delta,k}) &\leq -\|e_k\|^2 - \|x_{\Delta,k}\|^2 + \mu\sigma_d c_3^2 \|d_k\|^2 + \sigma_a c_4^2 \|u_{c,k}\|^2 \\ &\leq -\left\| \begin{bmatrix} e_k^T & x_{\Delta,k}^T \end{bmatrix} \right\|^2 + \mu\sigma_d c_3^2 \|d_k\|^2 + \sigma_a c_4^2 \|u_{c,k}\|^2. \end{aligned} \quad (3.58)$$

Thus, the interconnection (3.53) is input-to-state stable with respect to d_k and $u_{c,k}$. From (3.31) and (3.52), it can be written that:

$$\mu \|e_k\|^2 + \|x_{\Delta,k}\|^2 \leq \bar{V}(e_k, x_{\Delta,k}) \leq \mu\sigma_d \|e_k\|^2 + \sigma_a \|x_{\Delta,k}\|^2. \quad (3.59)$$

Defining $c_5 = \max(\mu\sigma_d, \sigma_a)$ and $e_r = \begin{bmatrix} e_k^T & x_{\Delta,k}^T \end{bmatrix}$ and replacing in (3.59), gives:

$$\|e_r\|^2 \leq \bar{V}(e_{r,k}) \leq c_5 \|e_{r,k}\|^2, \quad (3.60)$$

with $\mu \geq 1$. Performing a procedure similar to that presented in the proof of Theorem 3.1, the ISS gain of the interconnection (3.53) with respect to d_k and $u_{c,k}$ is given by $c_3\sqrt{\mu\sigma_d c_5}\|d\|_\infty$ and $c_4\sqrt{\sigma_a c_5}\|u_c\|_\infty$, respectively. \square

Notice that based on [21], the following theorem can also be presented.

Theorem 3.3 [21] *Consider the faulty LPV system (3.6) and assume that the nominal closed-loop system is composed of the nominal system (3.1) and the designed nominal controller characterized in Remark 2.1. If there exist virtual sensor gains as in (3.17) and virtual actuator gains as in (3.39) such that (3.16) and (3.38) are satisfied, then the reconfigured closed-loop system is input-to-output stable with respect to the input (r_k, d_k) and the output $(e_k, x_{\Delta,k})$.*

Proof. It follows similar steps as the one in [21, Appendix A.4], replacing B_f by $B_f(\theta_k)$, C_f by $C_f(\theta_k)$, B by $B(\theta_k)$ and C by $C(\theta_k)$.

Consider the fact that the IOS of the closed-loop system is equivalent to the IOS of the interconnection of the nominal system (3.1) with the nominal controller characterized in Remark 2.1 and the dynamics of the estimation error (3.12) with the dynamics of the difference state (3.15), as shown in Figure 6. Then, the reconfigured closed-loop system consists of the faulty system (3.6), the virtual sensor (3.10), the virtual actuator (3.13) and the nominal controller. With $x_{\Delta,k} = \tilde{x}_k - \hat{x}_{f,k}$ and $e_k = \hat{x}_{f,k} - x_{f,k}$, the following equations are obtained:

$$\Sigma_{\bar{P}} = \begin{cases} \tilde{x}_{k+1} = A(\theta_k)\tilde{x}_k + B(\theta_k)u_{c,k} \\ y_{c,k} = C(\theta_k)\tilde{x} \end{cases} \quad (3.61a)$$

$$\Sigma_C = \begin{cases} x_{c,k+1} = f_c(x_{c,k}, y_{c,k}, r_k) \\ u_{c,k} = h_c(x_{c,k}, y_{c,k}, r_k) \end{cases} \quad (3.61b)$$

$$e_{k+1} = (A(\theta_k) + L(\theta_k)C_f(\theta_k))e_k - B_d d_k \quad (3.61c)$$

$$x_{\Delta,k+1} = (A(\theta_k) + B_f(\theta_k)M(\theta_k))x_{\Delta,k} + L(\theta_k)C_f(\theta_k)e_k + B_\Delta u_{c,k}, \quad (3.61d)$$

where $\Sigma_{\bar{P}}$ in (3.61a) can be seen as the dynamics of the nominal system (3.1) and Σ_C is an arbitrary controller.

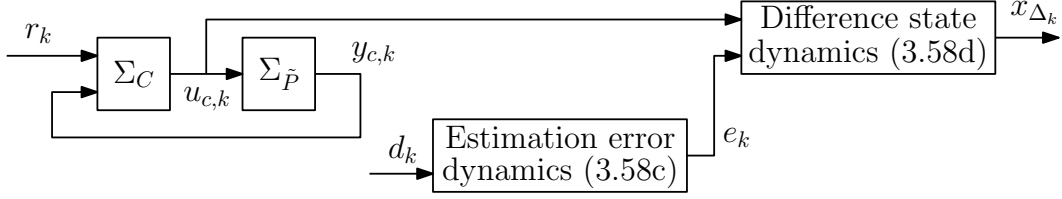


Figure 6: Closed-loop system as an interconnection of the nominal system (3.1) with the nominal controller (Remark 2.1) and the dynamics of the estimation error (3.61c) with the dynamics of the difference state (3.61d). Adapted from [21].

The system (3.61) can be considered as a cascade system, as depicted in the Figure 6. According to Remark 2.1, the closed-loop system composed of the nominal controller Σ_C and the system (3.61a) is also input-to-output stable with respect to the input (r_k, d_k) and with the output $(u_{c,k}, x_k)$. Moreover, from theorems 3.1 and 3.2, (3.61c) and (3.61d) are input-to-state stable with respect to d_k and $(u_{c,k}, e_k)$. From Lemma 3.1, the interconnection of (3.61c) with (3.61d) is input-to-state stable with respect to $(u_{c,k}, d_k)$, and, consequently, it is input-to-output stable with respect to the output $(e_k, x_{\Delta,k})$. Thus, according to [21, Theorem 2, Appendix A.4], it can be concluded that the connection (3.61) is input-to-output stable with respect to the input (r_k, d_k) and the output $(e_k, x_{\Delta,k})$. This concludes the proof. \square

Considering theorems 3.1 and 3.2 proposed in this chapter, notice that the fundamental difference with respect to [21, Theorem 3] and [21, Theorem 4] is that the input and output matrices of the faulty LPV model described in (3.16) and (3.38) are parameter-dependent. Thus, the main advantage and novelty of the proposed virtual sensor and actuator designs becomes evident. It should also be noticed that the reconfiguration block presented in [21] only allows its use for LPV systems with constant input and output matrices (B_f and C_f), therefore only matrix A may depend on the system time-varying parameters, which constraints its applicability as it is discussed in the experimental section in the sequel. Theorems 3.1 and 3.2, on the other hand, allow to deal with parameter-dependent matrices B_f and C_f , enabling the use of virtual sensors and actuators for a larger class of nonlinear systems that can be described by LPV models.

Another important issue is that in [21], the sensor and actuator faults are not considered as time-varying parameters, therefore, the design of the virtual sensor and actuator must be performed for each type and magnitude of fault that

occurs, individually. Then, for each new fault in the system, a new project must be carried out, updating the values of gains of the virtual sensor and the virtual actuator. That is, the conditions in [21, Theorem 3] and [21, Theorem 4] must be solved in real-time so that it can be used for each different fault that occurs. However, depending on the control system and the software used, this is often not possible. Moreover, the feasibility of the conditions is not ensured for a set of faults. On the other hand, using theorems 3.1 and 3.2, it is only necessary to define the maximum and minimum values of the faults that may occur in the sensors and actuators of the system and calculate the gains of the reconfiguration block only once, before executing the control algorithm in real-time. Thus, with only one reconfiguration block design, the system becomes robust to different types of faults that may occur, not depending on solving LMIs in real-time.

The previous comparisons can also be seen through the flowcharts in Figure 7, in which the approach proposed in this chapter and the one proposed in [21] are compared. It is important to note that in the left flowchart, the approach proposed in this work, the gains of the virtual sensor and the virtual actuator are calculated, respectively, by theorems 3.1 and 3.2, before the execution of the control algorithm. On the other hand, in the flowchart on the right, the gains are calculated by [21, Theorem 3] and [21, Theorem 4], for each new fault in the sensor and/or actuator. In addition, before executing the control algorithm, as there is still no fault detection, the reconfiguration block consists only of a virtual sensor, designed for the nominal system, i.e., with $C_f = C$.

3.4 EXPERIMENTAL RESULTS

The set-up of a nonlinear coupled tank system, as presented in Section 2.6, is used to illustrate the effectiveness of the new methodology proposed. Thus, a discrete-time model of (2.13) is obtained using Euler's method [115]. Thus:

$$\begin{cases} h_{k+1} &= \begin{bmatrix} 1 - \alpha_{1,k}\alpha_{3,k} & \alpha_{1,k}\alpha_{3,k} \\ \frac{\alpha_{1,k}}{S_2} & 1 - \frac{\alpha_{1,k} + \alpha_{2,k}}{S_2} \end{bmatrix} h_k + \begin{bmatrix} T_s K_{b_1} \alpha_{3,k} & T_s K_{b_2} \alpha_{3,k} \\ 0 & 0 \end{bmatrix} \tilde{u}_k \\ y_k &= \begin{bmatrix} 1 & 0 \\ 0 & 1 \end{bmatrix} h_k, \end{cases} \quad (3.62)$$

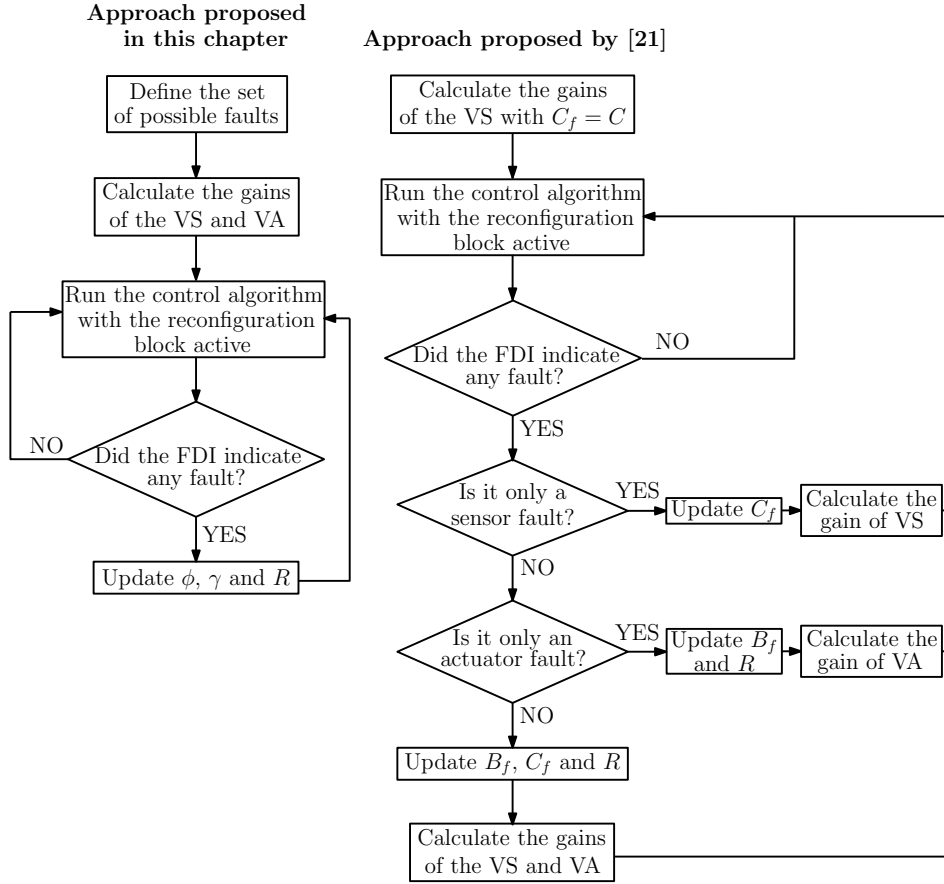


Figure 7: Comparative flowcharts of the methodology proposed in this chapter and the one proposed in [21]. In the left flowchart, the gains of the reconfiguration block are calculated by theorems 3.1 and 3.2 proposed in this chapter. In the right flowchart, the gains of the virtual sensor are calculated by [21, Theorem 3] and the gains of the virtual actuator by [21, Theorem 4].

where $\alpha_{1,k} = T_s/R_{12}(h_{1,k}, h_{2,k})$, $\alpha_{2,k} = T_s q_o(h_{2,k})/h_{2,k}$ and $\alpha_{3,k} = 1/S_1(h_{1,k})$ are the time-varying parameters grouped in the vector $\alpha_k = [\alpha_{1,k} \ \alpha_{2,k} \ \alpha_{3,k}]^T$, with $R_{12}(h_1(t), h_2(t)) = (0.412(h_1 - h_2) + 11.488) \times 10^{-3}$ and $q_o(h_2(t)) = 12.741h_2(t) + 817.674 \text{ cm}^3/\text{s}$. From (2.13), $q_{i_1}(u_1(t)) = K_{b_1}u_1 + 354.781 \text{ cm}^3/\text{s}$, $q_{i_2}(u_2(t)) = K_{b_2}u_2 + 220.085 \text{ cm}^3/\text{s}$, $K_{b_1} = 16.998$ and $K_{b_2} = 13.201$ are the pump static gains and $\tilde{u}_k = [\tilde{u}_{1,k} \ \tilde{u}_{2,k}]^T$, with $\tilde{u}_{1,k} = u_{1,k} + 354.781/K_{b_1}$ and $\tilde{u}_{2,k} = u_{2,k} + 220.085/K_{b_2}$. The sampling time $T_s = 2$ seconds is chosen so that the fastest time constant of the system stays between 7 and 8 samples [114]. For more details, return to Section 2.6.

Considering the range for $20 \text{ cm} \leq h_1 \leq 74 \text{ cm}$ and $12 \text{ cm} \leq h_2 \leq 50 \text{ cm}$, and also combining the maximum and minimum values of α_1 , α_2 , and α_3 , an LPV

model as described in (3.1) with $N = 8$ vertices is used to describe the nonlinear system (3.62), with the following matrices:

$$\begin{aligned}
A_1 &= \begin{bmatrix} 0.4809 & 0.5191 \\ 0.0358 & 0.9106 \end{bmatrix}; A_2 = \begin{bmatrix} 0.9567 & 0.0433 \\ 0.0358 & 0.9106 \end{bmatrix}; A_3 = \begin{bmatrix} 0.4809 & 0.5191 \\ 0.0358 & 0.9449 \end{bmatrix}; \\
A_4 &= \begin{bmatrix} 0.9567 & 0.0433 \\ 0.0358 & 0.9449 \end{bmatrix}; A_5 = \begin{bmatrix} 0.7008 & 0.2992 \\ 0.0206 & 0.9258 \end{bmatrix}; A_6 = \begin{bmatrix} 0.9751 & 0.0249 \\ 0.0206 & 0.9258 \end{bmatrix}; \\
A_7 &= \begin{bmatrix} 0.7008 & 0.2992 \\ 0.0206 & 0.9601 \end{bmatrix}; A_8 = \begin{bmatrix} 0.9751 & 0.0249 \\ 0.0206 & 0.9601 \end{bmatrix}; \quad C = \begin{bmatrix} 1 & 0 \\ 0 & 1 \end{bmatrix}; \\
B_1 = B_3 = B_5 = B_7 &= \begin{bmatrix} 0.1632 & 0.1267 \\ 0 & 0 \end{bmatrix}; \\
B_2 = B_4 = B_6 = B_8 &= \begin{bmatrix} 0.0136 & 0.0106 \\ 0 & 0 \end{bmatrix}.
\end{aligned} \tag{3.63}$$

3.4.1 Controller Design

The nominal gain-scheduled controller is designed according to the procedure presented in Section 2.6.1, where A_i and B_i are given in (3.63) and with $\tilde{N} = N$ in (2.15). The obtained gains are presented in Section A.1.

3.4.2 Design of Reconfiguration Blocks

To design the reconfiguration blocks, fault scenarios are considered for the two sensors and the two actuators of the process. Thus, the virtual sensor is designed for $\underline{\gamma}_{1,k} \leq \gamma_{1,k} \leq \bar{\gamma}_{1,k}$ and $\underline{\gamma}_{2,k} \leq \gamma_{2,k} \leq \bar{\gamma}_{2,k}$, with $\underline{\gamma}_{1,k} = 0$, $\bar{\gamma}_{1,k} = 1$, $\underline{\gamma}_{2,k} = 0.04$ and $\bar{\gamma}_{2,k} = 1$, and the virtual actuator for $\underline{\phi}_{1,k} \leq \phi_{1,k} \leq \bar{\phi}_{1,k}$ and $\underline{\phi}_{2,k} \leq \phi_{2,k} \leq \bar{\phi}_{2,k}$, with $\underline{\phi}_{1,k} = 0.5$, $\bar{\phi}_{1,k} = 1$, $\underline{\phi}_{2,k} = 0$ and $\bar{\phi}_{2,k} = 1$, that is, time-varying faults are allowed in the ranges given. Therefore, the faulty system has seven time-varying parameters, grouped in $\theta = [\alpha_1 \ \alpha_2 \ \alpha_3 \ \gamma_1 \ \gamma_2 \ \phi_1 \ \phi_2]^T$, each of them

with a maximum and a minimum value, resulting in an LPV system with $\bar{N} = 128$ vertices, given by the following matrices:

$$\left. \begin{array}{l} A_{\{q_1\}} = A_1; A_{\{q_2\}} = A_2 \\ A_{\{q_3\}} = A_3; A_{\{q_4\}} = A_4 \\ A_{\{q_5\}} = A_5; A_{\{q_6\}} = A_6 \\ A_{\{q_7\}} = A_7; A_{\{q_8\}} = A_8 \end{array} \right\} \begin{array}{l} \forall q_1 = 1, \dots, 16; q_2 = 17, \dots, 32; \\ q_3 = 33, \dots, 48; q_4 = 49, \dots, 64; \\ q_5 = 65, \dots, 80; q_6 = 81, \dots, 96; \\ q_7 = 97, \dots, 112; q_8 = 113, \dots, 128. \end{array} \quad (3.64)$$

$$\left. \begin{array}{l} B_{f_{\{r_1+16 \times l_1\}}} = B_1 \text{diag}\{\bar{\phi}_{1,k}, \bar{\phi}_{2,k}\} \\ B_{f_{\{r_2+16 \times l_1\}}} = B_1 \text{diag}\{\bar{\phi}_{1,k}, \underline{\phi}_{2,k}\} \\ B_{f_{\{r_3+16 \times l_1\}}} = B_1 \text{diag}\{\underline{\phi}_{1,k}, \bar{\phi}_{2,k}\} \\ B_{f_{\{r_4+16 \times l_1\}}} = B_1 \text{diag}\{\underline{\phi}_{1,k}, \underline{\phi}_{2,k}\} \\ B_{f_{\{r_1+16 \times l_2\}}} = B_2 \text{diag}\{\bar{\phi}_{1,k}, \bar{\phi}_{2,k}\} \\ B_{f_{\{r_2+16 \times l_2\}}} = B_2 \text{diag}\{\bar{\phi}_{1,k}, \underline{\phi}_{2,k}\} \\ B_{f_{\{r_3+16 \times l_2\}}} = B_2 \text{diag}\{\underline{\phi}_{1,k}, \bar{\phi}_{2,k}\} \\ B_{f_{\{r_4+16 \times l_2\}}} = B_2 \text{diag}\{\underline{\phi}_{1,k}, \underline{\phi}_{2,k}\} \end{array} \right\} \begin{array}{l} \forall r_1 = 1, 5, 9, 13; \\ r_2 = 2, 6, 10, 14; \\ r_3 = 3, 7, 11, 15; \\ r_4 = 4, 8, 12, 16; \\ l_1 = 0, 2, 4, 6; \\ l_2 = 1, 3, 5, 7. \end{array} \quad (3.65)$$

$$\left. \begin{array}{l} C_{f_{\{s_1+16 \times l_3\}}} = \text{diag}\{\bar{\gamma}_{1,k}, \bar{\gamma}_{2,k}\} C \\ C_{f_{\{s_2+16 \times l_3\}}} = \text{diag}\{\bar{\gamma}_{1,k}, \underline{\gamma}_{2,k}\} C \\ C_{f_{\{s_3+16 \times l_3\}}} = \text{diag}\{\underline{\gamma}_{1,k}, \bar{\gamma}_{2,k}\} C \\ C_{f_{\{s_4+16 \times l_3\}}} = \text{diag}\{\underline{\gamma}_{1,k}, \underline{\gamma}_{2,k}\} C \end{array} \right\} \begin{array}{l} \forall s_1 = 1, \dots, 4; s_2 = 5, \dots, 8; \\ s_3 = 9, \dots, 12; s_4 = 13, \dots, 16; \\ l_3 = 0, \dots, 7. \end{array} \quad (3.66)$$

From that, the virtual sensor is designed by Theorem 3.1 with (3.64) and (3.66) and using the software MOSEK[®] [116], the gains L_i given in (3.17), for $i = 1, \dots, \bar{N}$, presented in Section A.2, are found with a minimum value of $\sigma_d = 991.16$. Similarly, the virtual actuator is designed by Theorem 3.2 with (3.64) and (3.65) and the gains M_i in (3.39), for $i = 1, \dots, \bar{N}$, are calculated for the minimum value of $\sigma_a = 500.8$ and shown in Section A.3. In addition, the matrix $R(\theta_k)$ in (3.13) is designed such that $\|B_\Delta u_{c,k}\|$ is the minimum possible and is calculated according to the type of actuator faults, during the execution

of the control algorithm. In the presence of a total fault in the second actuator, the static gain matrix $R(\theta_k)$ is computed as follows:

$$R(\theta_k) = -\frac{1}{\phi_{1,k}} \begin{bmatrix} 1 & \frac{K_{b2}}{K_{b1}} \\ 0 & 0 \end{bmatrix}, \quad (3.67)$$

otherwise:

$$R(\theta_k) = -\begin{bmatrix} \frac{1}{\phi_{1,k}} & 0 \\ 0 & \frac{1}{\phi_{2,k}} \end{bmatrix}. \quad (3.68)$$

Remark 3.1 *Using the gain matrix $R(\theta_k)$ given in (3.67) and (3.68) for each type of fault, it is possible to notice that in all actuator fault scenarios of the experiments performed, $B_f(\theta_k)R(\theta_k) = -B(\theta_k)$, that is, $B_\Delta(\theta_k) = 0$. Thus, the control signal $u_{c,k}$ generated by the nominal controller does not interfere with the dynamics of the difference state (3.15) and $w_k = -L(\theta_k)C_f(\theta_k)e_k$.*

Remark 3.2 *Notice that, as the polytope of the faulty system is elaborated, it is not possible to contemplate total faults in all sensors and actuators of the process. This is because one of the vertices of the input and output matrices would include the total loss of system actuation and measurement, and the LMI conditions of theorems 3.1 and 3.2 become infeasible.*

In the following, the experimental results for three different fault scenarios: sensor faults, actuator faults, and simultaneous sensor and actuator faults are presented. The main objective is to evaluate the performance of the closed-loop system after the faults happen. For this, the process time-responses are analyzed and compared for three different methodologies: the robust FTC strategy proposed in this chapter (called **RFTC**, lines in **red**), the approach proposed in [21] (called **FTC[21]**, lines in **blue**), and the system without any FTC strategy, only with the nominal controller (2.16) (called **WFTC**, lines in **green**). In the latter, when there are faults in the sensors and/or actuators, no changes are made to the closed-loop system, thus, stability and performance may not be guaranteed by the controller. Also, it is assumed that it is not possible to design the virtual sensor and actuator gains in real-time. However, as discussed in the previous section and in the flowchart depicted in Figure 7, in order to use the reconfiguration block FTC presented in [21], it is necessary that the LMI conditions in [21, Theorem 3] and [21, Theorem 4] run in real-time. As this is not possible in this

case, the gains are obtained considering a constant value of the input matrix and fixed faults of the sensors and actuators, since the methodology does not allow the matrices B_f and C_f to be dependent on time-varying parameters. For this case, the input matrix is given by:

$$B = \begin{bmatrix} 0.0571 & 0.0443 \\ 0 & 0 \end{bmatrix}, \quad (3.69)$$

and the sensor and actuator faults used in the design are $\gamma_1 = 1$, $\gamma_2 = 0.5$, $\phi_1 = 0.85$, $\phi_2 = 1$. Through [21, Theorem 3] and [21, Theorem 4], the resulting gains are L_i , for $i = 1, \dots, N$, with the minimum $\sigma_d = 1.0013$, and M_i , for $i = 1, \dots, N$, with the minimum $\sigma_a = 495.10$. For the sake of space and to keep objectivity, the values of the gains are omitted in this chapter.

Furthermore, performance indices are calculated so that the system performance can be quantitatively evaluated. In particular, IVU1 and IVU2 denote the IVU index with respect to the first and second actuator, respectively. The values of IAE, ISE, IVU1 and IVU2 for **RFTC**, **WFTC** and **FTC** [21] are obtained and depicted in graphs, normalized with respect to the last one. It is important to notice that the lower the index, the better the performance. That is, the more interior the graph, the better the system performance.

3.4.3 Sensor faults

Experimental tests are performed to evaluate the performance of the closed-loop system after the occurrence of sensor faults for **RFTC**, **FTC** [21] and **WFTC**. The first test considers a partial fault of 50% in the measurement of the second sensor, namely ($\gamma_1 = 1$, $\gamma_2 = 0.5$, fault f_1) for $t \geq 300s$, and also a total loss in the measurement of the first sensor, i.e. ($\gamma_1 = 0$, $\gamma_2 = 0.5$, fault f_2) after $t \geq 900s$, as depicted in Figure 8. Notice from Figure 8 that after the occurrence of the first fault, no significant change in the system response can be observed for any strategy. This is because the fault of the second sensor does not interfere with the reference tracking, which is performed only for level h_1 . Moreover, the virtual sensors of **RFTC** and **FTC** [21] are designed to cover this fault. However, after the second fault, using **WFTC**, the system exceeds the security limit value and activates the plant protection system, which immediately shuts down the pumps preventing the overflow of the tank $T3$. With **FTC** [21], level h_1 becomes highly oscillatory, since its virtual sensor proposal is not designed for this type of fault.

Finally, with **RFTC**, the fault barely modifies the controlled outputs and the system continues to track the reference normally. Therefore, the reconfiguration block proposed in this chapter can maintain the closed-loop system behavior close to the nominal one, even with different sensor faults and even with the total loss of sensor measurement by which the reference is tracked.

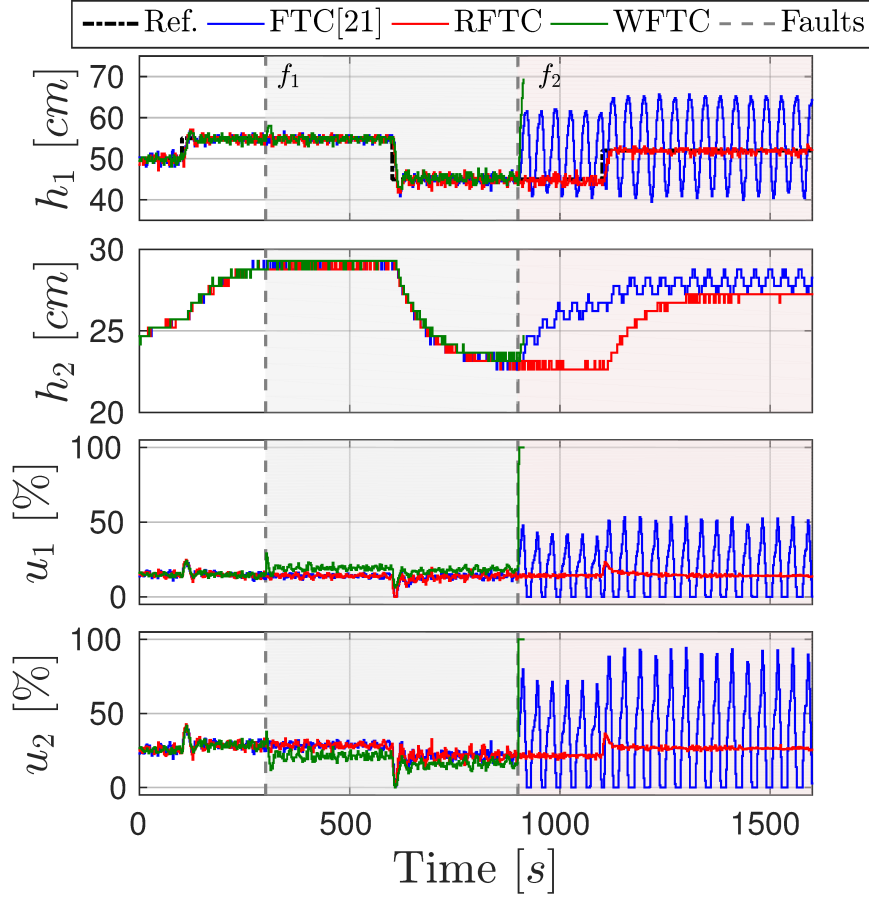


Figure 8: Experiments for sensor faults: Levels h_1 and h_2 (top) and control signals u_1 and u_2 (bottom).

Figure 9 presents the values of IAE, ISE, IVU1 and IVU2 for **RFTC**, **WFTC** and **FTC** [21]. In this case, it is evident that the performance of **RFTC** is significantly better than the others.

3.4.4 Actuator faults

The next experiments are performed to simulate actuator faults, as depicted in Figure 10, where a complete loss of the second actuator, namely ($\phi_1 = 1$, $\phi_2 = 0$, fault f_1), occurs from $t \geq 300s$ and also a partial fault of 15% in the

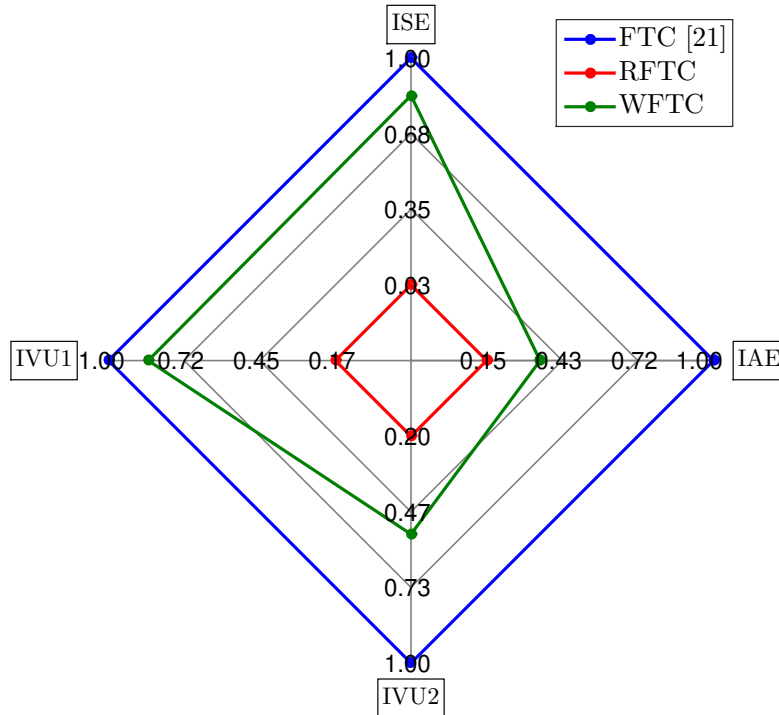


Figure 9: Performance indices for sensor faults normalized by the worst case (FTC [21]).

efficiency of the first pump, that is ($\phi_1 = 0.85$, $\phi_2 = 0$, fault f_2), occurs after $t \geq 900s$. As can be seen, after the first fault, the response of the system with the reconfiguration block FTC [21] becomes oscillatory and fails to track the reference, because its virtual actuator design does not address this type of fault and does not take into account an input matrix that is dependent on time-varying parameters. Moreover, from the graphs at the bottom of the Figure 10 it can be noticed that the control signal applied to pump 1 (u_1) varies aggressively between the maximum and minimum values, being saturated at many times and, even with total loss of the second actuator, a nonzero control signal continues to be applied to pump 2 (u_2). On the other hand, the system with WFTC can adjust the control signals to keep the system stable and tracking the reference, with a larger oscillation than RFTC around $t = 300s$, due to the integrator presence and process configuration. However, this is not appropriate as there is no guarantee of stability of the faulty system, and there is a continuity in the application of a control signal (often saturated) on pump 2. Finally, the system with RFTC remains stable and satisfactorily tracking the reference, even with a different loss of functionality of the actuators, as it has been designed to be robust to a set

of faults and not to compensate only one fault as the FTC [21]. Therefore, as expected, the reconfiguration block proposed in this chapter is more effective for reconfiguring a system subject to time-varying faults.

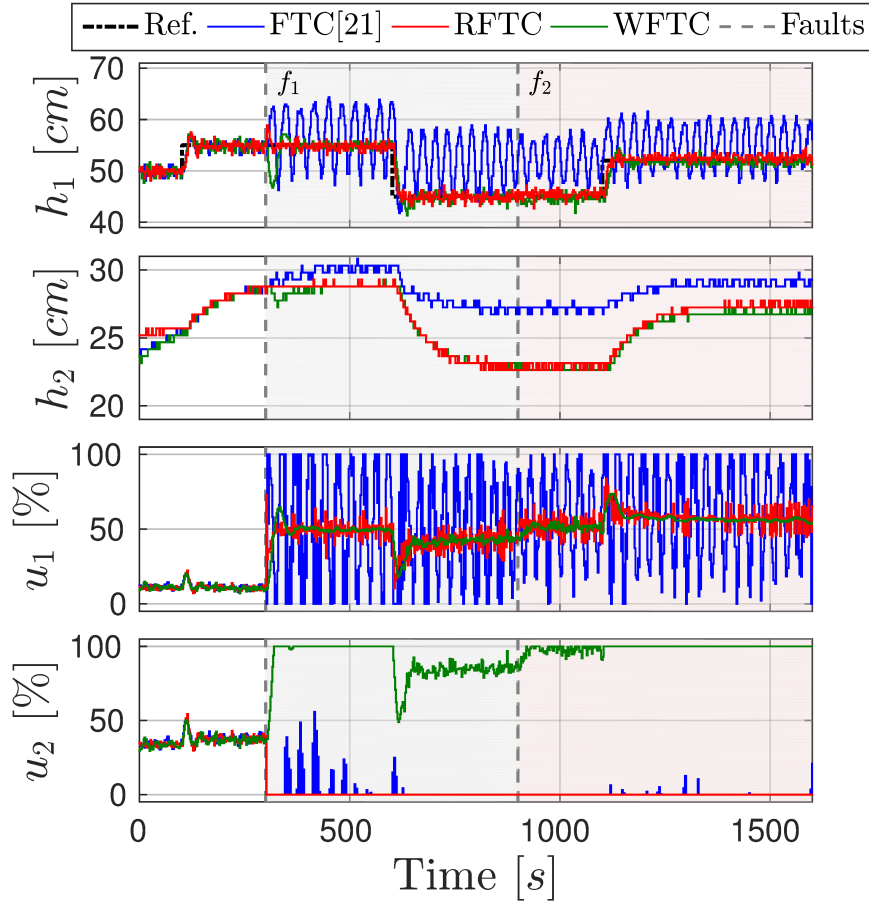


Figure 10: Experiments for actuator faults: Levels h_1 and h_2 (top) and control signals u_1 and u_2 (bottom).

Notice that the performance indices are shown in Figure 11, where a better performance of **RFTC** can be seen. The index IVU1 of **WFTC** is slightly lower than that of **RFTC**. However IVU2 is relatively higher, indicating that there is a greater control effort on the actuator that is not acting on the system.

3.4.5 Simultaneous sensor and actuator faults

Tests are also performed to evaluate the system responses for simultaneous actuators and sensor faults, as depicted in Figure 12. From $t \geq 300s$ there is a total loss of the second actuator, i.e. $(\gamma_1 = 1, \gamma_2 = 1, \phi_1 = 1, \phi_2 = 0, \text{ fault } f_1)$. From $t \geq 500s$ the second sensor has its measurement reduced by 50%, i.e.

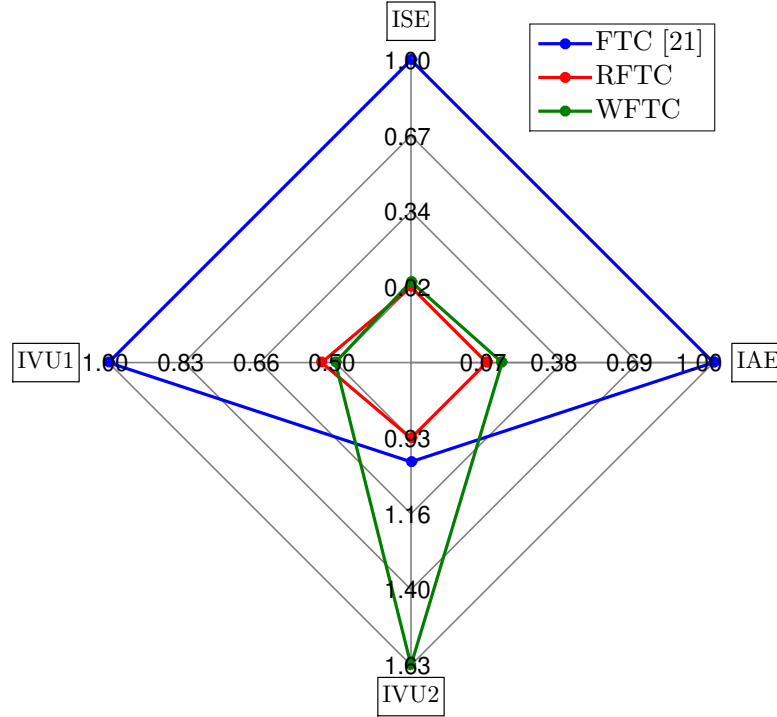


Figure 11: Performance indices for actuator faults normalized by the worst case (FTC [21]).

($\gamma_1 = 1, \gamma_2 = 0.5, \phi_1 = 1, \phi_2 = 0$, fault f_2). From $t \geq 900s$ the first actuator has 15% loss in efficiency, namely ($\gamma_1 = 1, \gamma_2 = 0.5, \phi_1 = 0.85, \phi_2 = 0$, fault f_3). Finally, from $t \geq 1200s$, there is also a complete loss of measurement provided by the first sensor, i.e. ($\gamma_1 = 0, \gamma_2 = 0.5, \phi_1 = 0.85, \phi_2 = 0$, fault f_4). In this case, FTC [21] is composed of a virtual sensor and a virtual actuator designed as presented in Section 3.4.2. However, similarly to the previous fault scenarios, that design does not allow the reconfiguration block to cover different faults. Thus, after the occurrence of the first fault, the variable h_1 becomes extremely oscillatory as well as the control signal, and reference tracking is no longer possible. Similar behavior also occurs to WFTC, where neither partial sensor faults nor actuator faults significantly affect the system time-responses. On the other hand, as seen before, when the first sensor fails completely, the nominal controller loses the measurement that provides information to track the reference, causing the control signal to saturate at the maximum and the level h_1 to increase to arm the security system. Finally, also as observed in other scenarios, as the RFTC design covers all faults that occur along the experiment, the system response is not significantly affected by the faults. In other words, the virtual sensor and

the actuator, as proposed in this chapter, are capable of keeping the closed-loop system stable and performing satisfactorily for the reference tracking case.

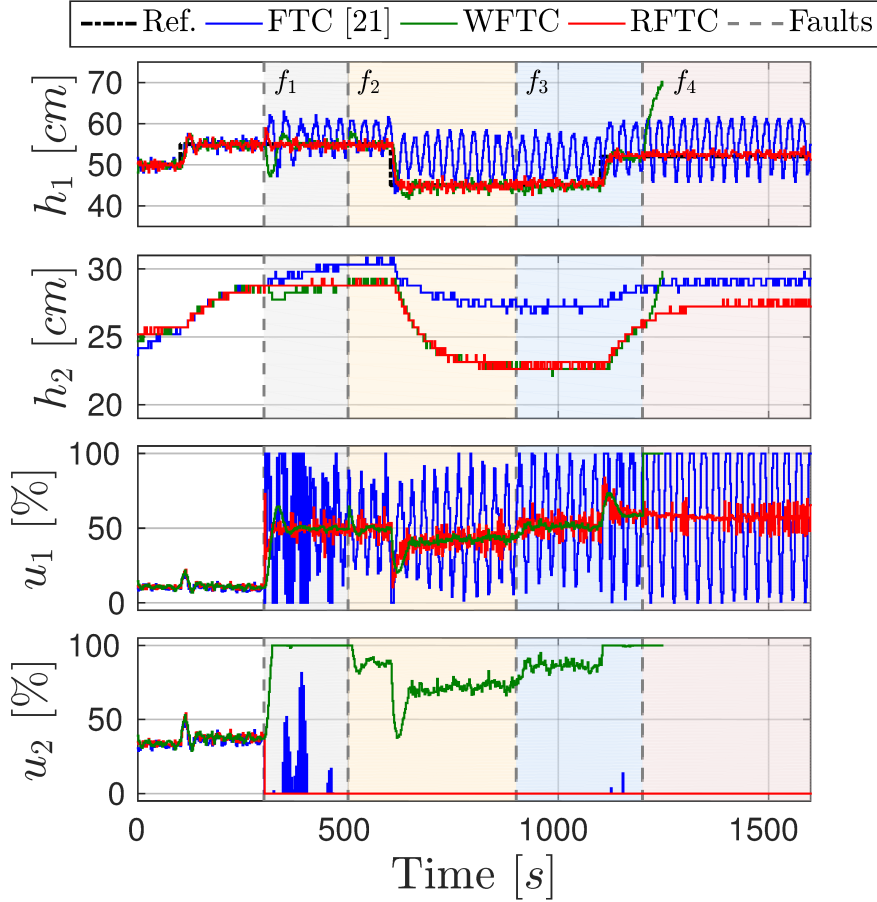


Figure 12: Experiments for sensor and actuator faults: Levels h_1 and h_2 (top) and control signals u_1 and u_2 (bottom).

Figure 13 shows the performance indices for simultaneous actuator and sensor faults. Again, it can be concluded that the proposed methodology provides better performance for the closed-loop system compared to the other approaches.

Remark 3.3 *Considering the various real-time experiments, it can be noticed that the reconfiguration block design proposed in this chapter is significantly more efficient and more general than that proposed by [21]. This can be concluded checking the graphs in Figures 9, 11 and 13, where in all cases, the performance obtained by FTC [21] is worse. Once more, this is due to the fact that the virtual sensor and the virtual actuator designs proposed in [21] are not robust to different types of faults that occur in the real-world experiments performed in the chapter, unlike RFTC. In addition, FTC [21] does not guarantee that the closed-loop system is stable or that it performs reasonably well. This is because*

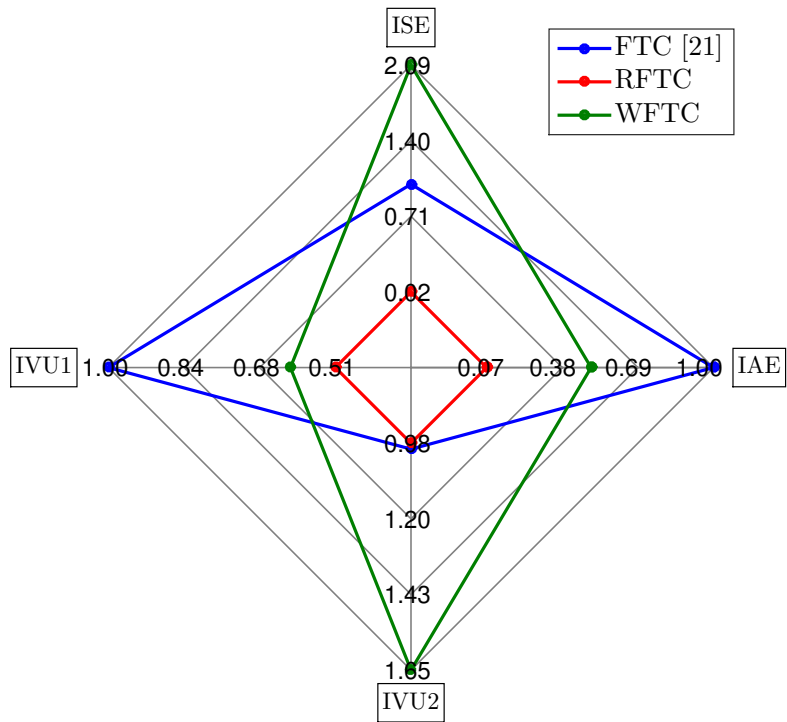


Figure 13: Performance indices for simultaneous actuator and sensor faults normalized by the worst case (FTC [21]).

the LPV model of the process has a parameter-dependent input matrix and its design is performed considering a constant input matrix.

FTC BASED ON UNKNOWN INPUT OBSERVER FOR
TAKAGI-SUGENO FUZZY SYSTEMS WITH UNMEASURED
PREMISE VARIABLES

This chapter proposes new sufficient conditions to guarantee the stability with H_∞ performance of the reconfiguration block based on Unknown Input Observer for TS fuzzy systems with unmeasured premise variables. In a single project, unlike [15, 20, 30], it is possible to ensure stability and the performance of the faulty system close to the nominal one, for different types and magnitudes of faults, which can be additive and/or multiplicative (partial and total) in both sensors and/or actuators. Moreover, the design of the reconfiguration block takes into account that the TS fuzzy model may be dependent on unmeasured premise variables, including those that become unmeasured due to sensor faults, in addition to being based on an UIO to deal with disturbances that may affect the system, a problem that is also not addressed in the current literature [15, 20, 30]. A case study is presented with computer simulations of the FTC strategy implemented in the control of the nonlinear coupled tanks system investigated in Section 2.6. At this time, the process is described by the TS fuzzy model.

4.1 FAULTY TAKAGI-SUGENO FUZZY SYSTEMS

Consider the discrete-time TS fuzzy system Σ_P , adapted from [32], given by:

$$\Sigma_P = \begin{cases} x_{k+1} &= \sum_{i=1}^{N_1} \sum_{j=1}^{N_2} \alpha_i(z_{\alpha,k}) \beta_j(z_{\beta,k}) (A_{ij}x_k + B_{ij}u_k + Dd_k) \\ &\triangleq A(\alpha_k, \beta_k)x_k + B(\alpha_k, \beta_k)u_{c,k} + Dd_k, \\ y_k &= Cx_k, \end{cases} \quad (4.1)$$

where $x_k \in \mathbb{R}^n$ represents the state vector, $u_k \in \mathbb{R}^m$ is the sequence of control inputs, $y_k \in \mathbb{R}^p$ is the output, and $d_k \in \mathbb{R}^d$ denotes an unknown disturbance sequence. Matrices $A(\alpha_k, \beta_k) \in \mathbb{R}^{n \times n}$, $B(\alpha_k, \beta_k) \in \mathbb{R}^{n \times m}$, $D \in \mathbb{R}^{n \times d}$, and $C \in \mathbb{R}^{p \times n}$ relate the dynamics and the output of the system. In addition $\alpha_i(z_{\alpha,k})$, $i = 1, \dots, N_1$, are the membership functions that depend only on the measured

premise variables and $\beta_j(z_{\beta,k})$, $j = 1, \dots, N_2$, are the membership functions that depend on at least one unmeasured premise variable.

The faulty model, denoted by Σ_{P_f} , is considered to be the same as the plant nominally represented by Σ_P in (4.1), but with the indications of sensor and actuator faults included in the multiplicative and additive forms in the dynamics and output equations:

$$\Sigma_{P_f} = \begin{cases} x_{f,k+1} &= \sum_{i=1}^{N_3} \sum_{j=1}^{N_4} \bar{\alpha}_i(\bar{z}_{\alpha,k}) \bar{\beta}_j(\bar{z}_{\beta,k}) (A_{ij} x_{f,k} + B_{ij} (\hat{\phi} u_{f,k} + f_{a,k}) + D d_k) \\ &\triangleq A(\bar{\alpha}_k, \bar{\beta}_k) x_{f,k} + B(\bar{\alpha}_k, \bar{\beta}_k) (\hat{\phi} u_{f,k} + f_{a,k}) + D d_k \\ y_{f,k} &= \hat{\gamma} C x_{f,k} + f_{s,k}, \end{cases} \quad (4.2)$$

where $f_{a,k} = [f_{a_{1,k}} \ \dots \ f_{a_{m,k}}]^T \in \mathbb{R}^m$ and $f_{s,k} = [f_{s_{1,k}} \ \dots \ f_{s_{p,k}}]^T \in \mathbb{R}^p$ represent the additive actuator and sensor fault vectors, respectively, $\hat{\phi} = \text{diag}\{\phi_{1,k}, \dots, \phi_{m,k}\}$ denotes the multiplicative actuator faults and $\hat{\gamma} = \text{diag}\{\gamma_{1,k}, \dots, \gamma_{p,k}\}$ the multiplicative sensor faults, with $\phi_{i,k}, \phi_{j,k} \in [0, 1]$, $\forall i, j$. It is important to note that, when certain premise variables depend on measurements provided by the system's sensors, in case of sensor faults, these measurements will obviously be corrupted and can be considered as unmeasured. Therefore, the membership functions $\bar{\beta}_j(\bar{z}_{\beta,k})$, $j = 1, \dots, N_4$, depend both on the unmeasured premise variables $z_{\beta,k}$ and on the premise variables that have their measurements affected by sensor faults, and the membership functions $\bar{\alpha}_i(\bar{z}_{\alpha,k})$, $i = 1, \dots, N_3$, depend only on the premise variables that remain measured after the occurrence of faults. In addition, if the measurements of the system's premise variables are not affected by sensor faults, $\bar{\alpha}_i(\bar{z}_{\alpha,k}) = \alpha_i(z_{\alpha,k})$, $i = 1, \dots, N_1$ with $N_1 = N_3$, and $\bar{\beta}_j(\bar{z}_{\beta,k}) = \beta_j(z_{\beta,k})$, $j = 1, \dots, N_2$ with $N_2 = N_4$.

Inspired by [117, 118], it is possible to describe the faulty system (4.2) as:

$$\Sigma_{P_f} = \begin{cases} x_{f,k+1} &= \sum_{i=1}^{N_3} \sum_{j=1}^{N_4} \bar{\alpha}_i(\bar{z}_{\alpha,k}) \bar{\beta}_j(\bar{z}_{\beta,k}) (A_{ij} x_{f,k} + B_{ij} (\hat{\phi} u_{f,k} + f_{a,k}) + D d_k \\ &\quad + B_{ij} u_{f,k} - B_{ij} u_{f,k}) \\ &\triangleq A(\bar{\alpha}_k, \bar{\beta}_k) x_{f,k} + B(\bar{\alpha}_k, \bar{\beta}_k) (u_{f,k} + \bar{f}_{a,k}) + D d_k, \\ y_{f,k} &= \hat{\gamma} C x_{f,k} + f_{s,k} + C x_{f,k} - C x_{f,k} = C x_{f,k} + F \bar{f}_{s,k}, \end{cases} \quad (4.3)$$

where $\bar{f}_{a,k} = (\hat{\phi} - I) u_{f,k} + f_{a,k}$, $\bar{f}_{s,k} = (\hat{\gamma} - I) C x_{f,k} + f_{s,k}$ and $F = I \in \mathbb{R}^{p \times p}$ is the sensor fault matrix. That is, the fault vectors $\bar{f}_{a,k}$ and $\bar{f}_{s,k}$ are seen by

the system in an additive way, but in reality they can represent both additive and/or multiplicative actuator and sensor faults, respectively.

Assumption 4.1 [118] *The matrices C and D in (4.3) are such that:*

$$\text{rank}(CD) = \text{rank}(D). \quad (4.4)$$

4.2 PROBLEM FORMULATION

Similar to the one presented in Chapter 3, in order to maintain the performance of the existing closed-loop system, it is proposed a reconfiguration block composed of a virtual sensor and a virtual actuator capable of hiding the faults of the nominal controller. Furthermore, the approach makes it possible to deal with unmeasured premise variables (from the system or affected by sensor faults) and with unknown input disturbances that may affect the system's behavior. As the virtual sensor can be seen as an observer of the faulty system, the methodologies proposed in [32] and [37] are used as inspiration for the problem formulation.

4.2.1 Virtual Sensor

The virtual sensor based on Unknown Input Observer, adapted from [37], is described by the following equations:

$$\left\{ \begin{array}{l} \hat{x}_{f,k+1} = \sum_{i=1}^{N_3} \sum_{j=1}^{N_4} \bar{\alpha}_i(\bar{z}_{\alpha,k}) \bar{\beta}_j(\hat{z}_{\beta,k}) \left(TA_{ij} \hat{x}_{f,k} + TB_{ij} (u_{f,k} + \bar{f}_{a,k}) + L_{ij} (y_{f,k} - \hat{y}_{f,k}) \right) \\ \quad + Ny_{f,k+1} - NF\bar{f}_{s,k+1} \\ \triangleq TA(\bar{\alpha}_k, \hat{\beta}_k) \hat{x}_{f,k} + TB(\bar{\alpha}_k, \hat{\beta}_k) (u_{f,k} + \bar{f}_{a,k}) + L(\bar{\alpha}_k, \hat{\beta}_k) (y_{f,k} - \hat{y}_{f,k}) \\ \quad + NCx_{f,k+1}, \\ \hat{y}_{f,k} = C\hat{x}_{f,k} + F\bar{f}_{s,k}, \end{array} \right. \quad (4.5)$$

where $\hat{x}_{f,k} \in \mathbb{R}^n$ is the estimated state by the virtual sensor of the faulty system, $u_{f,k} \in \mathbb{R}^m$ is the control sequence input generated by the virtual actuator defined

later in the next section, $T \in \mathbb{R}^{n \times n}$, $N \in \mathbb{R}^{n \times p}$, and $L(\bar{\alpha}_k, \hat{\beta}_k) \in \mathbb{R}^{n \times p}$ are design matrices, the latter being the virtual sensor gain matrix given by:

$$\sum_{i=1}^{N_3} \sum_{j=1}^{N_4} \bar{\alpha}_i(\bar{z}_{\alpha,k}) \bar{\beta}_j(\hat{z}_{\beta,k}) L_{ij} \triangleq L(\bar{\alpha}_k, \hat{\beta}_k). \quad (4.6)$$

The matrices T and N should be chosen so that the following equations are satisfied:

$$\begin{aligned} T + NC &= I, \\ TD &= 0, \end{aligned} \quad (4.7)$$

where N can be calculated as:

$$N = D(CD)^\dagger, \quad (4.8)$$

with the existence of the pseudo-inverse assured by Assumption 4.1.

Note that the membership functions $\bar{\beta}_j(\hat{z}_{\beta,k})$, $j = 1, \dots, N_4$, are the same used to describe the system in (4.3), but depending on the estimates of the premise variables that are not measured and/or affected by sensor faults.

Remark 4.1 *Note that the virtual sensor state equation (4.5) can be implemented as:*

$$\begin{cases} \epsilon_{1,k+1} = \sum_{i=1}^{N_3} \sum_{j=1}^{N_4} \bar{\alpha}_i(\bar{z}_{\alpha,k}) \bar{\beta}_j(\hat{z}_{\beta,k}) (TA_{ij} \hat{x}_{f,k} + TB_{ij} (u_{f,k} + \bar{f}_{a,k}) + L_{ij} (y_{f,k} - \hat{y}_{f,k})) \\ \quad \triangleq TA(\bar{\alpha}_k, \hat{\beta}_k) \hat{x}_{f,k} + TB(\bar{\alpha}_k, \hat{\beta}_k) (u_{f,k} + \bar{f}_{a,k}) + L(\bar{\alpha}_k, \hat{\beta}_k) (y_{f,k} - \hat{y}_{f,k}), \\ \hat{x}_{f,k} = \epsilon_{1,k} + Ny_{f,k} - NF\bar{f}_{s,k}, \end{cases}$$

where $\epsilon_{1,k} \in \mathbb{R}^n$ can be seen as an auxiliary variable.

The estimation error calculated between the state of the faulty system $x_{f,k}$ and the state estimated by the virtual sensor $\hat{x}_{f,k}$ is defined by $e_k = x_{f,k} - \hat{x}_{f,k}$ and has dynamics:

$$\begin{aligned} e_{k+1} &= (T + NC)x_{f,k+1} - \hat{x}_{f,k+1} \\ &\triangleq T \left(A(\bar{\alpha}_k, \bar{\beta}_k)x_{f,k} - A(\bar{\alpha}_k, \hat{\beta}_k)\hat{x}_{f,k} \right) + T \left(B(\bar{\alpha}_k, \bar{\beta}_k) - B(\bar{\alpha}_k, \hat{\beta}_k) \right) (u_{f,k} + \bar{f}_{a,k}) \\ &\quad - L(\bar{\alpha}_k, \hat{\beta}_k)Ce_k. \end{aligned} \quad (4.9)$$

As can be seen, equation (4.9) contains terms referring to the difference between the system matrices with the actual and estimated premise variables, requiring an methodology that makes it possible to deal with these differences. As the virtual sensor can be interpreted as an observer for the faulty system, the development presented below to deal with the problem is based on the approach proposed in [32] for the design of observers for continuous-time systems with unmeasured premise variables.

Replacing $\hat{x}_{f,k} = x_{f,k} - e_k$ in (4.9), results in:

$$e_{k+1} \triangleq T \left(A(\bar{\alpha}_k, \bar{\beta}_k) - A(\bar{\alpha}_k, \hat{\beta}_k) \right) x_{f,k} + T \left(B(\bar{\alpha}_k, \bar{\beta}_k) - B(\bar{\alpha}_k, \hat{\beta}_k) \right) \bar{u}_k + A_\delta(\bar{\alpha}_k, \hat{\beta}_k) e_k, \quad (4.10)$$

where $A_\delta(\bar{\alpha}_k, \hat{\beta}_k) = TA(\bar{\alpha}_k, \hat{\beta}_k) - L(\bar{\alpha}_k, \hat{\beta}_k)C$ and $\bar{u}_k = u_{f,k} + \bar{f}_{a,k}$. The differences between the dynamics and input matrices can be written as:

$$J(\bar{\alpha}_k, \bar{\beta}_k) - J(\bar{\alpha}_k, \hat{\beta}_k) = \sum_{i=1}^{N_3} \sum_{j=1}^{N_4} \bar{\alpha}_i(\bar{z}_{\alpha,k}) (\bar{\beta}_j(\bar{z}_{\beta,k}) - \bar{\beta}_j(\hat{z}_{\beta,k})) J_{ij}, \quad (4.11)$$

where $J(\cdot)$ can represent matrices $A(\cdot)$ and $B(\cdot)$. The estimation error of the premise variables can be defined as $e_{z,k} = \bar{z}_{\beta,k} - \hat{z}_{\beta,k}$, with $e_{z,k} = He_k$, where matrix $H \in \mathbb{R}^{N_\beta \times n}$ transforms the estimation error of the states into the estimation error of the premise variables, with N_β being the number of unmeasured premise variables of the system. Applying Lemma 2.3, there is a $c \in]\bar{z}_{\beta,k}, \hat{z}_{\beta,k}[$ so that (4.11) can be calculated by:

$$J(\bar{\alpha}_k, \bar{\beta}_k) - J(\bar{\alpha}_k, \hat{\beta}_k) = \sum_{i=1}^{N_3} \sum_{j=1}^{N_4} \bar{\alpha}_i(\bar{z}_{\alpha,k}) \nabla \bar{\beta}_j(c) e_{z,k} J_{ij} \triangleq \sum_{j=1}^{N_4} \nabla \bar{\beta}_j(c) e_{z,k} J_j(\bar{\alpha}_k), \quad (4.12)$$

where $\nabla \bar{\beta}_j(c) = \frac{\partial \bar{\beta}_j(c)}{\partial \bar{z}_{\beta,k}}$, $j = 1, \dots, N_4$. As $\sum_{j=1}^{N_4} (\bar{\beta}_j(\bar{z}_{\beta,k}) - \bar{\beta}_j(\hat{z}_{\beta,k})) = 0$, the following slack matrices can be inserted:

$$\begin{aligned} & \left(\sum_{j=1}^{N_4} (\bar{\beta}_j(\bar{z}_{\beta,k}) - \bar{\beta}_j(\hat{z}_{\beta,k})) \right) \left(Y(\bar{\alpha}_k, \hat{\beta}_k) x_{f,k} + Z(\bar{\alpha}_k, \hat{\beta}_k) \bar{u}_k \right) \\ & = \left(\sum_{j=1}^{N_4} \nabla \bar{\beta}_j(c) e_{z,k} \right) \left(Y(\bar{\alpha}_k, \hat{\beta}_k) x_{f,k} + Z(\bar{\alpha}_k, \hat{\beta}_k) \bar{u}_k \right) = 0, \end{aligned} \quad (4.13)$$

with $Y(\bar{\alpha}_k, \hat{\beta}_k) \in \mathbb{R}^{n \times n}$ and $Z(\bar{\alpha}_k, \hat{\beta}_k) \in \mathbb{R}^{n \times m}$. Considering (4.12) and (4.13), the estimation error dynamics in (4.10) can be given by:

$$e_{k+1} \triangleq \sum_{j=1}^{N_4} \left(\bar{A}_j(\bar{\alpha}_k, \hat{\beta}_k) x_{f,k} + \bar{B}_j(\bar{\alpha}_k, \hat{\beta}_k) \bar{u}_k \right) \nabla \bar{\beta}_j(c) H e_k + A_\delta(\bar{\alpha}_k, \hat{\beta}_k) e_k, \quad (4.14)$$

where $\bar{A}_j(\bar{\alpha}_k, \hat{\beta}_k) = T A_j(\bar{\alpha}_k) + Y(\bar{\alpha}_k, \hat{\beta}_k)$ and $\bar{B}_j(\bar{\alpha}_k, \hat{\beta}_k) = T B_j(\bar{\alpha}_k) + Z(\bar{\alpha}_k, \hat{\beta}_k)$. In addition, it can be written that:

$$\sum_{j=1}^{N_4} \bar{A}_j(\bar{\alpha}_k, \hat{\beta}_k) x_{f,k} \nabla \bar{\beta}_j(c) = R_A(\bar{\alpha}_k, \hat{\beta}_k) \Delta_A, \quad (4.15)$$

and

$$\sum_{j=1}^{N_4} \bar{B}_j(\bar{\alpha}_k, \hat{\beta}_k) \bar{u}_k \nabla \bar{\beta}_j(c) = R_B(\bar{\alpha}_k, \hat{\beta}_k) \Delta_B, \quad (4.16)$$

with

$$\begin{aligned} R_A(\bar{\alpha}_k, \hat{\beta}_k) &= [\bar{A}_1(\bar{\alpha}_k, \hat{\beta}_k) \ \dots \ \bar{A}_{N_4}(\bar{\alpha}_k, \hat{\beta}_k)], \quad \Delta_A = (I \otimes x_{f,k}) \nabla \bar{\beta}(c), \\ R_B(\bar{\alpha}_k, \hat{\beta}_k) &= [\bar{B}_1(\bar{\alpha}_k, \hat{\beta}_k) \ \dots \ \bar{B}_{N_4}(\bar{\alpha}_k, \hat{\beta}_k)], \quad \Delta_B = (I \otimes \bar{u}_k) \nabla \bar{\beta}(c), \end{aligned} \quad (4.17)$$

where \otimes is the classical Kronecker product and

$$\nabla \bar{\beta}(c) = \begin{bmatrix} \nabla \bar{\beta}_1(c) \\ \vdots \\ \nabla \bar{\beta}_{N_4}(c) \end{bmatrix}. \quad (4.18)$$

Then, (4.14) is given by:

$$e_{k+1} \triangleq \left(A_\delta(\bar{\alpha}_k, \hat{\beta}_k) + \bar{R}(\bar{\alpha}_k, \hat{\beta}_k) \bar{\Delta} H \right) e_k, \quad (4.19)$$

where $\bar{R}(\bar{\alpha}_k, \hat{\beta}_k) = [R_A(\bar{\alpha}_k, \hat{\beta}_k) \ R_B(\bar{\alpha}_k, \hat{\beta}_k)]$ and $\bar{\Delta} = [\Delta_A^T \ \Delta_B^T]^T$.

The following assumption is considered throughout this chapter.

Assumption 4.2 *The following bounds are considered: $\|x_{f,k}\| \leq \kappa_{x_f}$, $\|\bar{u}_k\| \leq \kappa_{\bar{u}}$, and $\left\| \frac{\partial \bar{\beta}_j}{\partial \bar{z}_\beta} \right\| \leq \kappa_{\bar{\beta}_j}$, with $j = 1, \dots, N_4$. The functions $\bar{\beta}_j(\cdot)$ are precisely known and continuously differentiable with a known and calculable derivative¹.*

¹ For more details see [32].

Thus, using Lemma 2.1, it is possible to obtain:

$$\nabla \bar{\beta}^T(c) \nabla \bar{\beta}(c) = \sum_{j=1}^{N_4} \nabla \bar{\beta}_j^T(c) \nabla \bar{\beta}_j(c) \leq \sum_{j=1}^{N_4} \kappa_{\bar{\beta}_j}^2 I. \quad (4.20)$$

From Assumption 4.2,

$$\begin{aligned} \nabla \bar{\beta}^T(c) \left(I \otimes (x_{f,k}^T x_{f,k} + \bar{u}_k^T \bar{u}_k) \right) \nabla \bar{\beta}(c) &= (x_{f,k}^T x_{f,k} + \bar{u}_k^T \bar{u}_k) \nabla \bar{\beta}^T(c) \nabla \bar{\beta}(c) \\ &\leq (\kappa_{x_f}^2 + \kappa_{\bar{u}}^2) \nabla \bar{\beta}^T(c) \nabla \bar{\beta}(c) \leq \kappa^2 I, \end{aligned} \quad (4.21)$$

with

$$\kappa = \sqrt{(\kappa_{x_f}^2 + \kappa_{\bar{u}}^2) \sum_{j=1}^{N_4} \kappa_{\bar{\beta}_j}^2}. \quad (4.22)$$

In addition,

$$\begin{aligned} \nabla \bar{\beta}^T(c) \left((I \otimes x_{f,k}^T)(I \otimes x_{f,k}) + (I \otimes \bar{u}_k^T)(I \otimes \bar{u}_k) \right) \nabla \bar{\beta}(c) \\ = \Delta_A^T \Delta_A + \Delta_B^T \Delta_B = \bar{\Delta}^T \bar{\Delta} \leq \kappa^2 I. \end{aligned} \quad (4.23)$$

4.2.2 Virtual Actuator

The virtual actuator can be described by the following equations:

$$\left\{ \begin{array}{l} \tilde{x}_{k+1} \triangleq TA(\bar{\alpha}_k, \hat{\beta}_k) \tilde{x}_k + TB(\bar{\alpha}_k, \hat{\beta}_k) u_{c,k} + Ny_{f,k+1} - NF \bar{f}_{s,k+1} \\ \quad \triangleq TA(\bar{\alpha}_k, \hat{\beta}_k) \tilde{x}_k + TB(\bar{\alpha}_k, \hat{\beta}_k) u_{c,k} + NCx_{f,k+1}, \\ u_{f,k} \triangleq -M(\bar{\alpha}_k, \hat{\beta}_k) x_{\Delta,k} + s_k, \\ y_{c,k} \triangleq C \tilde{x}_k, \end{array} \right. \quad (4.24)$$

where $\tilde{x}_k \in \mathbb{R}^n$ is the reference state computed by the virtual actuator, $u_{c,k} \in \mathbb{R}^m$ is the control sequence generated by the nominal controller, $u_{f,k} \in \mathbb{R}^m$ is the alternative control signal generated by the virtual actuator and used as input to the faulty system and $y_{c,k} \in \mathbb{R}^p$ is the output that is now supplied to the nominal controller. In addition, $s_k \in \mathbb{R}^m$ is a design signal and $M(\bar{\alpha}_k, \hat{\beta}_k) \in \mathbb{R}^{m \times n}$ is the virtual actuator gain matrix defined as:

$$\sum_{i=1}^{N_3} \sum_{j=1}^{N_4} \bar{\alpha}_i(\bar{z}_{\alpha,k}) \bar{\beta}_j(\hat{z}_{\beta,k}) M_{ij} \triangleq M(\bar{\alpha}_k, \hat{\beta}_k). \quad (4.25)$$

The difference between the reference state \tilde{x}_k and the state estimated by the virtual sensor $\hat{x}_{f,k}$ is called as difference state $x_{\Delta,k}$, i.e. $x_{\Delta,k} = \tilde{x}_k - \hat{x}_{f,k}$. This state has the following dynamics:

$$x_{\Delta,k+1} \triangleq \left(TA(\bar{\alpha}_k, \hat{\beta}_k) + TB(\bar{\alpha}_k, \hat{\beta}_k)M(\bar{\alpha}_k, \hat{\beta}_k) \right) x_{\Delta,k} + w_k, \quad (4.26)$$

where $w_k = -L(\bar{\alpha}_k, \hat{\beta}_k)Ce_k + TB(\bar{\alpha}_k, \hat{\beta}_k)(u_{c,k} - \bar{f}_{a,k} - s_k)$ can be seen as a disturbance to the dynamics of $x_{\Delta,k}$. Therefore, the signal s_k can be designed so that the norm of the second term of w_k has the smallest possible value.

Remark 4.2 *As the virtual actuator (4.24) and the dynamics of the difference state (4.26) depend only on the measured premise variables and those estimated by the virtual sensor, it is not necessary to use the methodology proposed in [32] to deal with differences between actual and estimated premise variables.*

Remark 4.3 *If the nominal controller has as inputs the membership functions $\alpha_\ell(z_{\alpha,k})$ and $\beta_j(z_{\beta,k})$, $\ell = 1, \dots, N_1$, $j = 1, \dots, N_2$, with the proposed reconfiguration block, these inputs can become the membership functions $\bar{\alpha}_\ell(\bar{z}_{\alpha,k})$ and $\bar{\beta}_j(\hat{z}_{\beta,k})$, $\ell = 1, \dots, N_3$, $j = 1, \dots, N_4$, that can be reorganized as estimates of $\alpha_\ell(z_{\alpha,k})$ and $\beta_j(z_{\beta,k})$.*

Remark 4.4 *Note that the virtual actuator state equation (4.24) can be implemented as:*

$$\begin{cases} \epsilon_{2,k+1} & \triangleq TA(\bar{\alpha}_k, \hat{\beta}_k)\tilde{x}_k + TB(\bar{\alpha}_k, \hat{\beta}_k)u_{c,k}, \\ \tilde{x}_k & \triangleq \epsilon_{2,k} + Ny_{f,k} - NF\bar{f}_{s,k}, \end{cases} \quad (4.27)$$

where $\epsilon_{2,k} \in \mathbb{R}^n$ can be seen as an auxiliary variable.

From the development presented above, the following problem is formulated.

Problem 4.1 *Determine the gains $L(\bar{\alpha}_k, \hat{\beta}_k)$ and $M(\bar{\alpha}_k, \hat{\beta}_k)$ of the virtual sensor (4.5) and the virtual actuator (4.24), respectively, for the faulty TS fuzzy system (4.3) with unmeasured premise variables and with unknown input disturbances that stabilize the proposed reconfiguration block with guaranteed H_∞ performance.*

4.3 TAKAGI-SUGENO FUZZY VIRTUAL SENSOR AND ACTUATOR

In the following, it is presented the main contributions in this chapter, which is concerned to the design of a virtual sensor and a virtual actuator based on Unknown Input Observers for TS fuzzy systems with unmeasured premise variables.

4.3.1 Virtual Sensor

Theorem 4.1 Consider the faulty Takagi-Sugeno fuzzy system in (4.3). The virtual sensor (4.5) with gain $L(\bar{\alpha}_k, \hat{\beta}_k)$ asymptotically stabilizes the estimation error system (4.19) if there exist symmetric positive definite matrices $P_{ij} \in \mathbb{R}^{n \times n}$, matrices $G_{ij} \in \mathbb{R}^{n \times n}$, $U_{ij} \in \mathbb{R}^{n \times p}$, $\bar{Y}_{ij} \in \mathbb{R}^{n \times nN_4}$, $\bar{Z}_{ij} \in \mathbb{R}^{n \times mN_4}$, and scalar $\mu_{ij} > 0$, $i = 1, \dots, N_3$, $j = 1, \dots, N_4$, such that the following LMIs are feasible:

$$\begin{bmatrix} P_{rs} - G_{ij} - G_{ij}^T & * & * & * \\ A_{ij}^T T^T G_{ij}^T - C^T U_{ij}^T & -P_{ij} + \mu_{ij} \kappa^2 H^T H & * & * \\ \bar{A}_i^T T^T G_{ij}^T + \bar{Y}_{ij}^T & 0 & -\mu_{ij} I & * \\ \bar{B}_i^T T^T G_{ij}^T + \bar{Z}_{ij}^T & 0 & 0 & -\mu_{ij} I \end{bmatrix} < 0, \quad (4.28)$$

$$\begin{aligned} \bar{A}_i &= [A_{i1} \ \dots \ A_{iN_4}], \quad \bar{B}_i = [B_{i1} \ \dots \ B_{iN_4}], \\ \bar{Y}_{ij} &= [Y_{ij} \ \dots \ Y_{ij}], \quad \bar{Z}_{ij} = [Z_{ij} \ \dots \ Z_{ij}], \end{aligned}$$

$\forall i, r = 1, \dots, N_3$, $\forall j, s = 1, \dots, N_4$, with $\bar{Z}_{ij} \in \mathbb{R}^{n \times mN_4}$, $\bar{Y}_{ij} \in \mathbb{R}^{n \times nN_4}$, $\bar{Y}_{ij} = G_{ij}^{-1} \bar{Y}_{ij}$ and $\bar{Z}_{ij} = G_{ij}^{-1} \bar{Z}_{ij}$. Moreover, the Takagi-Sugeno fuzzy virtual sensor gain in (4.6) is given by:

$$L_{ij} = G_{ij}^{-1} U_{ij}. \quad (4.29)$$

Proof. Consider the Lyapunov candidate function:

$$V(e_k) = e_k^T P(\bar{\alpha}_k, \hat{\beta}_k) e_k, \quad (4.30)$$

with $P(\bar{\alpha}_k, \hat{\beta}_k) = \sum_{i=1}^{N_3} \sum_{j=1}^{N_4} \bar{\alpha}_i(\bar{z}_{\alpha,k}) \bar{\beta}_j(\hat{z}_{\beta,k}) P_{ij}$. If (4.28) is feasible, then we have ensured the regularity of G_{ij} , this last one thanks to the positivity of P_{rs} , with $P(\bar{\alpha}_{k+1}, \hat{\beta}_{k+1}) = \sum_{r=1}^{N_3} \sum_{s=1}^{N_4} \bar{\alpha}_r(\bar{z}_{\alpha,k+1}) \bar{\beta}_s(\hat{z}_{\beta,k+1}) P_{rs}$. Now, define $U_{ij} = G_{ij} L_{ij}$, $\bar{Y}_{ij} = G_{ij} \bar{Y}_{ij}$ and $\bar{Z}_{ij} = G_{ij} \bar{Z}_{ij}$, and use in (4.28) the fact that $G_{ij} P_{ij}^{-1} G_{ij}^T \geq G_{ij} + G_{ij}^T - P_{ij}$, in order to obtain:

$$\begin{bmatrix} -G_{ij} P_{rs}^{-1} G_{ij}^T & * & * & * \\ A_{ij}^T G_{ij}^T & -P_{ij} + \mu_{ij} \kappa^2 H^T H & * & * \\ \bar{A}_i^T G_{ij}^T & 0 & -\mu_{ij} I & * \\ \bar{B}_i^T G_{ij}^T & 0 & 0 & -\mu_{ij} I \end{bmatrix} < 0, \quad (4.31)$$

with $\bar{A}_{ij} = T\tilde{A}_i + \tilde{Y}_{ij}$, $\bar{B}_{ij} = T\tilde{B}_i + \tilde{Z}_{ij}$ and $A_{\delta_{ij}} = TA_{ij} - L_{ij}C$. The inequality (4.31) is pre- and post-multiplied by $\text{diag}\{G_{ij}^{-1}, I, I, I\}$ and its transpose, respectively, and the resulting inequality is multiplied by $\bar{\alpha}_i(\bar{z}_{\alpha,k})$ and $\bar{\beta}_j(\bar{z}_{\beta,k})$ and summing it up for all $i = 1, \dots, N_3$ and $j = 1, \dots, N_4$, results in:

$$\begin{bmatrix} -P_{rs}^{-1} & \star & \star & \star \\ A_{\delta}(\bar{\alpha}_k, \hat{\beta}_k)^T & -P(\bar{\alpha}_k, \hat{\beta}_k) + \mu(\bar{\alpha}_k, \hat{\beta}_k)\kappa^2 H^T H & \star & \star \\ R_A(\bar{\alpha}_k, \hat{\beta}_k)^T & 0 & -\mu(\bar{\alpha}_k, \hat{\beta}_k)I & \star \\ R_B(\bar{\alpha}_k, \hat{\beta}_k)^T & 0 & 0 & -\mu(\bar{\alpha}_k, \hat{\beta}_k)I \end{bmatrix} < 0, \quad (4.32)$$

with $R_A(\bar{\alpha}_k, \hat{\beta}_k)$ and $R_B(\bar{\alpha}_k, \hat{\beta}_k)$ given in (4.17).

Then, pre- and post-multiplying the inequality (4.32) by $\text{diag}\{P_{rs}, I, I, I\}$ and its transpose, respectively, and multiplying the resulting inequality by $\bar{\alpha}_r(\bar{z}_{\alpha,k+1})$ and $\bar{\beta}_s(\bar{z}_{\beta,k+1})$ and summing it up for all $r = 1, \dots, N_3$ and $s = 1, \dots, N_4$, yields:

$$\begin{bmatrix} -P(\bar{\alpha}_{k+1}, \hat{\beta}_{k+1}) & \star & \star \\ A_{\delta}(\bar{\alpha}_k, \hat{\beta}_k)^T P(\bar{\alpha}_{k+1}, \hat{\beta}_{k+1}) & -P(\bar{\alpha}_k, \hat{\beta}_k) + \mu(\bar{\alpha}_k, \hat{\beta}_k)\kappa^2 H^T H & \star \\ \bar{R}(\bar{\alpha}_k, \hat{\beta}_k)^T P(\bar{\alpha}_{k+1}, \hat{\beta}_{k+1}) & 0 & -\mu(\bar{\alpha}_k, \hat{\beta}_k)I \end{bmatrix} < 0, \quad (4.33)$$

with $\bar{R}(\bar{\alpha}_k, \hat{\beta}_k) = [R_A(\bar{\alpha}_k, \hat{\beta}_k) \ R_B(\bar{\alpha}_k, \hat{\beta}_k)]$. Applying the Schur complement to eliminate the last diagonal term of (4.33), one obtains:

$$\begin{bmatrix} -P(\bar{\alpha}_{k+1}, \hat{\beta}_{k+1}) + \Phi_1 & \star \\ A_{\delta}(\bar{\alpha}_k, \hat{\beta}_k)^T P(\bar{\alpha}_{k+1}, \hat{\beta}_{k+1}) & -P(\bar{\alpha}_k, \hat{\beta}_k) + \mu(\bar{\alpha}_k, \hat{\beta}_k)\kappa^2 H^T H \end{bmatrix} < 0, \quad (4.34)$$

with $\Phi_1 = \mu(\bar{\alpha}_k, \hat{\beta}_k)^{-1} P(\bar{\alpha}_{k+1}, \hat{\beta}_{k+1}) \bar{R}(\bar{\alpha}_k, \hat{\beta}_k) \bar{R}(\bar{\alpha}_k, \hat{\beta}_k)^T P(\bar{\alpha}_{k+1}, \hat{\beta}_{k+1})$. Using (4.23), inequality (4.34) can be given by:

$$\begin{bmatrix} -P(\bar{\alpha}_{k+1}, \hat{\beta}_{k+1}) & \star \\ A_{\delta}(\bar{\alpha}_k, \hat{\beta}_k)^T P(\bar{\alpha}_{k+1}, \hat{\beta}_{k+1}) & -P(\bar{\alpha}_k, \hat{\beta}_k) \end{bmatrix} + \mu(\bar{\alpha}_k, \hat{\beta}_k) \Phi_2^T \Phi_2 + \mu(\bar{\alpha}_k, \hat{\beta}_k)^{-1} \Phi_3^T \Phi_3 < 0, \quad (4.35)$$

with $\Phi_2 = [0 \ \bar{\Delta}H]$ and $\Phi_3 = [\bar{R}(\bar{\alpha}_k, \hat{\beta}_k)^T P(\bar{\alpha}_k, \hat{\beta}_k) \ 0]$. Thus, considering Lemma 2.2 and (4.35), it is possible to obtain:

$$\begin{bmatrix} -P(\bar{\alpha}_{k+1}, \hat{\beta}_{k+1}) & \star \\ (A_{\delta}(\bar{\alpha}_k, \hat{\beta}_k) + \bar{R}(\bar{\alpha}_k, \hat{\beta}_k) \bar{\Delta}H)^T P(\bar{\alpha}_{k+1}, \hat{\beta}_{k+1}) & -P(\bar{\alpha}_k, \hat{\beta}_k) \end{bmatrix} < 0. \quad (4.36)$$

Thereby, (4.36) is pre- and post-multiplied by $\text{diag} \{P(\bar{\alpha}_{k+1}, \hat{\beta}_{k+1})^{-1}, I\}$ and its transpose, respectively, Schur complement is applied to the first diagonal term, and the resulting inequality is multiplied on the left and right by e_k^T and e_k , respectively, yielding:

$$e_k^T \chi e_k < 0, \quad (4.37)$$

with:

$$\begin{aligned} \chi = & \left(A_\delta(\bar{\alpha}_k, \hat{\beta}_k) + \bar{R}(\bar{\alpha}_k, \hat{\beta}_k) \bar{\Delta} H \right)^T P(\bar{\alpha}_{k+1}, \hat{\beta}_{k+1}) \left(A_\delta(\bar{\alpha}_k, \hat{\beta}_k) + \bar{R}(\bar{\alpha}_k, \hat{\beta}_k) \bar{\Delta} H \right) \\ & - P(\bar{\alpha}_k, \hat{\beta}_k). \end{aligned} \quad (4.38)$$

Then, (4.37) can be described as:

$$e_{k+1}^T P(\bar{\alpha}_{k+1}, \hat{\beta}_{k+1}) e_{k+1} - e_k^T P(\bar{\alpha}_k, \hat{\beta}_k) e_k < 0, \quad (4.39)$$

and consequently,

$$V(e_{k+1}) - V(e_k) < 0. \quad (4.40)$$

Since $P(\bar{\alpha}_k, \hat{\beta}_k) > 0$,

$$0 < \lambda_{\min}(P(\bar{\alpha}_k, \hat{\beta}_k)) e_k^T e_k \leq V(e_k) \leq \lambda_{\max}(P(\bar{\alpha}_k, \hat{\beta}_k)) e_k^T e_k, \quad (4.41)$$

where $\lambda_{\min}(\cdot)$ and $\lambda_{\max}(\cdot)$ are the minimum and maximum eigenvalues of the argument, respectively. Therefore, since (4.37) implies that the difference (4.40) is upper bounded by a negative definite function, $V(e_k)$ is a Lyapunov function and the gain $L(\bar{\alpha}_k, \hat{\beta}_k)$ designed by Theorem 4.1 asymptotically stabilizes the estimation error system (4.19). This concludes the proof. \square

4.3.2 Virtual Actuator

Theorem 4.2 *Consider the faulty Takagi-Sugeno fuzzy system (4.3). The virtual actuator (4.24) with gain $M(\bar{\alpha}_k, \hat{\beta}_k)$ stabilizes the difference system (4.26) with a guaranteed H_∞ performance η_1 of $x_{\Delta,k}$ with respect to w_k if there exist symmetric positive definite matrices $\tilde{Q}_{ij} \in \mathbb{R}^{n \times n}$, matrices $\tilde{G}_{ij} \in \mathbb{R}^{n \times n}$, $X_{ij} \in \mathbb{R}^{m \times n}$,*

$Z_{ij} \in \mathbb{R}^{m \times m}$, $i = 1, \dots, N_3$, $j = 1, \dots, N_4$, and a scalar $\eta_1 > 0$, such that the following LMIs are feasible:

$$\begin{bmatrix} \tilde{Q}_{rs} - TB_{ij}X_{rs} - X_{rs}^T B_{ij}^T T^T & \star & \star & \star & \star \\ 0 & I & \star & \star & \star \\ \tilde{G}_{ij}^T A_{ij}^T T^T & \tilde{G}_{ij}^T & \tilde{G}_{ij} + \tilde{G}_{ij}^T - \tilde{Q}_{ij} & \star & \star \\ I & 0 & 0 & \bar{\eta}_1 I & \star \\ -X_{rs} + Z_{rs}^T B_{ij}^T T^T & 0 & -Y_{ij} & 0 & Z_{rs} + Z_{rs}^T \end{bmatrix} > 0, \quad (4.42)$$

$\forall i, r = 1, \dots, N_3$, $\forall j, s = 1, \dots, N_4$ and with $\eta_1 = \sqrt{\bar{\eta}_1}$. Moreover, the Takagi-Sugeno fuzzy virtual actuator gain in (4.25) is given by:

$$M_{ij} = Y_{ij} \tilde{G}_{ij}^{-1}. \quad (4.43)$$

Proof. Consider:

$$\tilde{V}(x_{\Delta,k}) = x_{\Delta,k}^T \tilde{P}(\bar{\alpha}_k, \hat{\beta}_k) x_{\Delta,k}, \quad (4.44)$$

as a Lyapunov candidate function for the difference state (4.26) with $\tilde{P}(\bar{\alpha}_k, \hat{\beta}_k) = \sum_{i=1}^{N_3} \sum_{j=1}^{N_4} \bar{\alpha}_i(\bar{z}_{\alpha,k}) \bar{\beta}_j(\hat{z}_{\beta,k}) \tilde{P}_{ij}$ with $\tilde{P}_{ij} = \tilde{Q}_{ij}^{-1}$. Furthermore, $\tilde{P}(\bar{\alpha}_{k+1}, \hat{\beta}_{k+1}) = \sum_{r=1}^{N_3} \sum_{s=1}^{N_4} \bar{\alpha}_r(\bar{z}_{\alpha,k+1}) \bar{\beta}_s(\hat{z}_{\beta,k+1}) \tilde{P}_{rs}$.

Notice that \tilde{Q}_{ij} , \tilde{G}_{ij} and Z_{ij} are nonsingular. Defining $Y_{ij} = M_{ij} \tilde{G}_{ij}$ in (4.42) and using the fact that $\tilde{G}_{ij} \tilde{Q}_{ij}^{-1} \tilde{G}_{ij}^T \geq \tilde{G}_{ij} + \tilde{G}_{ij}^T - \tilde{Q}_{ij}$, it is possible to obtain:

$$\begin{bmatrix} \tilde{Q}_{rs} - TB_{ij}X_{rs} - X_{rs}^T B_{ij}^T T^T & \star & \star & \star & \star \\ 0 & I & \star & \star & \star \\ \tilde{G}_{ij}^T A_{ij}^T T^T & \tilde{G}_{ij}^T & \tilde{G}_{ij}^T \tilde{Q}_{ij}^{-1} \tilde{G}_{ij} & \star & \star \\ I & 0 & 0 & \bar{\eta}_2 I & \star \\ -X_{rs} + Z_{rs}^T B_{ij}^T T^T & 0 & -M_{ij} \tilde{G}_{ij} & 0 & Z_{rs} + Z_{rs}^T \end{bmatrix} > 0. \quad (4.45)$$

The inequality (4.45) is pre- and post-multiplied by $\text{diag}\{I, I, \tilde{G}_{ij}^{-T}, I, I\}$ and its transpose, respectively, resulting in:

$$\begin{bmatrix} \tilde{Q}_{rs} - TB_{ij}X_{rs} - X_{rs}^T B_{ij}^T T^T & \star & \star & \star & \star \\ 0 & I & \star & \star & \star \\ A_{ij}^T T^T & I & \tilde{Q}_{ij}^{-1} & \star & \star \\ I & 0 & 0 & \bar{\eta}_1 I & \star \\ -X_{rs} + Z_{rs}^T B_{ij}^T T^T & 0 & -M_{ij} & 0 & Z_{rs} + Z_{rs}^T \end{bmatrix} > 0. \quad (4.46)$$

In inequality (4.46), define $\tilde{P}_{ij} = \tilde{Q}_{ij}^{-1}$, $W_{ij} = Z_{ij}^{-T}$ and $F_{ij} = \tilde{P}_{ij} X_{ij}^T W_{ij}$, and one gets:

$$\begin{bmatrix} \varphi_1 & \star & \star & \star & \star \\ 0 & I & \star & \star & \star \\ A_{ij}^T T^T & I & \tilde{P}_{ij} & \star & \star \\ I & 0 & 0 & \bar{\eta}_1 I & \star \\ -W_{rs}^{-T} F_{rs}^T \tilde{P}_{rs}^{-1} + W_{rs}^{-1} B_{ij}^T T^T & 0 & -M_{ij} & 0 & W_{rs}^{-T} + W_{rs}^{-1} \end{bmatrix} > 0, \quad (4.47)$$

with $\varphi_1 = \tilde{P}_{rs}^{-1} - TB_{ij}W_{rs}^{-T}F_{rs}^T\tilde{P}_{rs}^{-1} - \tilde{P}_{rs}^{-1}F_{rs}W_{rs}^{-1}B_{ij}^T T^T$. Then, (4.47) is multiplied on the left by:

$$E_1 = \begin{bmatrix} 0 & 0 & 0 & 0 & W_{rs} \\ 0 & I & 0 & 0 & 0 \\ 0 & 0 & I & 0 & 0 \\ 0 & 0 & 0 & I & 0 \\ \tilde{P}_{rs} & 0 & 0 & 0 & F_{rs} \end{bmatrix}, \quad (4.48)$$

and on the right by its transpose, respectively, yielding:

$$\begin{bmatrix} W_{rs} + W_{rs}^T & \star & \star & \star & \star \\ 0 & I & \star & \star & \star \\ -M_{ij}^T W_{rs}^T & I & \tilde{P}_{ij} & \star & \star \\ 0 & 0 & 0 & \bar{\eta}_1 I & \star \\ \tilde{P}_{rs} T B_{ij} + F_{rs} & 0 & \tilde{P}_{rs} T A_{ij} - F_{rs} M_{ij} & \tilde{P}_{rs} & \tilde{P}_{rs} \end{bmatrix} > 0. \quad (4.49)$$

Thereafter, multiply the inequality (4.49) by $\bar{\alpha}_i(\bar{z}_{\alpha,k})$, $\bar{\beta}_j(\hat{z}_{\beta,k})$, $\bar{\alpha}_r(\bar{z}_{\alpha,k+1})$ and $\bar{\beta}_s(\hat{z}_{\beta,k+1})$ and summing it up for all $i,r = 1, \dots, N_3$ and $j,s = 1, \dots, N_4$, results in:

$$\begin{bmatrix} \varphi_2 & \star & \star & \star & \star \\ 0 & I & \star & \star & \star \\ \varphi_3 & I & \tilde{P}(\bar{\alpha}_k, \hat{\beta}_k) & \star & \star \\ 0 & 0 & 0 & \bar{\eta}_1 I & \star \\ \varphi_4 & 0 & \varphi_5 & \tilde{P}(\bar{\alpha}_{k+1}, \hat{\beta}_{k+1}) & \tilde{P}(\bar{\alpha}_{k+1}, \hat{\beta}_{k+1}) \end{bmatrix} > 0. \quad (4.50)$$

$$\begin{aligned} \varphi_2 &= W(\bar{\alpha}_{k+1}, \hat{\beta}_{k+1}) + W(\bar{\alpha}_{k+1}, \hat{\beta}_{k+1})^T, \quad \varphi_3 = -M(\bar{\alpha}_k, \hat{\beta}_k)^T W(\bar{\alpha}_{k+1}, \hat{\beta}_{k+1})^T, \\ \varphi_4 &= \tilde{P}(\bar{\alpha}_{k+1}, \hat{\beta}_{k+1}) T B(\bar{\alpha}_k, \hat{\beta}_k) + F(\bar{\alpha}_{k+1}, \hat{\beta}_{k+1}), \\ \varphi_5 &= \tilde{P}(\bar{\alpha}_{k+1}, \hat{\beta}_{k+1}) T A(\bar{\alpha}_k, \hat{\beta}_k) - F(\bar{\alpha}_{k+1}, \hat{\beta}_{k+1}) M(\bar{\alpha}_k, \hat{\beta}_k). \end{aligned}$$

Then, pre- and post-multiplying (4.50) on the left by:

$$E_2 = \begin{bmatrix} 0 & 0 & 0 & 0 & \tilde{P}(\bar{\alpha}_{k+1}, \hat{\beta}_{k+1})^{-1} \\ 0 & I & 0 & 0 & 0 \\ M(\bar{\alpha}_k, \hat{\beta}_k)^T & 0 & I & 0 & 0 \\ 0 & 0 & 0 & I & 0 \end{bmatrix}, \quad (4.51)$$

and on the right by its transpose, respectively, one gets:

$$\begin{bmatrix} \tilde{Q}(\bar{\alpha}_{k+1}, \hat{\beta}_{k+1}) & \star & \star & \star \\ 0 & I & \star & \star \\ A_\zeta(\bar{\alpha}_k, \hat{\beta}_k)^T & I & \tilde{Q}(\bar{\alpha}_k, \hat{\beta}_k)^{-1} & \star \\ I & 0 & 0 & \bar{\eta}_1 I \end{bmatrix} < 0, \quad (4.52)$$

with $A_\zeta(\bar{\alpha}_k, \hat{\beta}_k) = T A(\bar{\alpha}_k, \hat{\beta}_k) + T B(\bar{\alpha}_k, \hat{\beta}_k) M(\bar{\alpha}_k, \hat{\beta}_k)$.

Replacing $\eta_1 = \sqrt{\bar{\eta}_1}$ in (4.52), and pre- and post-multiplying the resulting inequality by $\text{diag}\{\tilde{P}(\bar{\alpha}_{k+1}, \hat{\beta}_{k+1}), I, I, I\}$ and its transpose, respectively, yields:

$$\begin{bmatrix} \tilde{P}(\bar{\alpha}_{k+1}, \hat{\beta}_{k+1}) & \star & \star & \star \\ 0 & I & \star & \star \\ A_\zeta(\bar{\alpha}_k, \hat{\beta}_k)^T \tilde{P}(\bar{\alpha}_{k+1}, \hat{\beta}_{k+1}) & I & \tilde{P}(\bar{\alpha}_k, \hat{\beta}_k) & \star \\ \tilde{P}(\bar{\alpha}_{k+1}, \hat{\beta}_{k+1}) & 0 & 0 & \eta_1^2 I \end{bmatrix} > 0. \quad (4.53)$$

Consider $x_{\Delta,k+1} = A_\zeta(\bar{\alpha}_k, \hat{\beta}_k)x_{\Delta,k} + w_k$ and use a Schur complement argument in (4.53), resulting in:

$$\begin{bmatrix} \varphi_6 & \star \\ \tilde{P}(\bar{\alpha}_{k+1}, \hat{\beta}_{k+1})A_\zeta(\bar{\alpha}_k, \hat{\beta}_k) & \tilde{P}(\bar{\alpha}_{k+1}, \hat{\beta}_{k+1}) - \eta_1^2 I \end{bmatrix} < 0, \quad (4.54)$$

with $\varphi_6 = A_\zeta(\bar{\alpha}_k, \hat{\beta}_k)^T \tilde{P}(\bar{\alpha}_{k+1}, \hat{\beta}_{k+1}) A_\zeta(\bar{\alpha}_k, \hat{\beta}_k) - \tilde{P}(\bar{\alpha}_k, \hat{\beta}_k) + I$.

Pre- and post-multiplying the inequality (4.54) by $\begin{bmatrix} x_{\Delta,k}^T & w_k^T \end{bmatrix}$ and its transpose, respectively, one obtains:

$$x_{\Delta,k+1}^T \tilde{P}(\bar{\alpha}_{k+1}, \hat{\beta}_{k+1}) x_{\Delta,k+1} - x_{\Delta,k}^T \tilde{P}(\bar{\alpha}_k, \hat{\beta}_k) x_{\Delta,k} + x_{\Delta,k}^T x_{\Delta,k} - \eta_1^2 w_k^T w_k \leq 0. \quad (4.55)$$

After this, using (4.44) and $w_k = -L(\bar{\alpha}_k, \hat{\beta}_k)C e_k + TB(\bar{\alpha}_k, \hat{\beta}_k)(u_{c,k} - \bar{f}_{a,k} - s_k)$ in (4.55), yields:

$$\tilde{V}(x_{\Delta,k+1}) - \tilde{V}(x_{\Delta,k}) + \|x_{\Delta,k}\|^2 - \eta_1^2 \|w_k\|^2 \leq 0. \quad (4.56)$$

Then, based on the Bounded Real Lemma, and considering zero initial conditions, $\tilde{V}(x_{\Delta,k}) > 0$ is a Lyapunov function and the H_∞ criterion for the difference system (4.26) is given by:

$$\sup_{\|w_k\|_2 \neq 0} \frac{\|x_{\Delta,k}\|_2}{\|w_k\|_2} \leq \eta_1, \quad (4.57)$$

with $w_k \in \ell_2^n$ and $x_{\Delta,k} \in \ell_2^n$. This concludes the proof. \square

4.3.3 Combination of the virtual sensor with the virtual actuator

From equations (4.19) and (4.26), the interconnection system of the TS fuzzy virtual sensor with the virtual actuator is given by:

$$\begin{aligned} \begin{bmatrix} e_{k+1} \\ x_{\Delta,k+1} \end{bmatrix} &= \begin{bmatrix} A_\delta(\bar{\alpha}_k, \hat{\beta}_k) + \bar{R}(\bar{\alpha}_k, \hat{\beta}_k)\bar{\Delta}T & 0 \\ -L(\bar{\alpha}_k, \hat{\beta}_k)C & A_\zeta(\bar{\alpha}_k, \hat{\beta}_k) \end{bmatrix} \begin{bmatrix} e_k \\ x_{\Delta,k} \end{bmatrix} \\ &+ \begin{bmatrix} 0 \\ TB(\bar{\alpha}_k, \hat{\beta}_k) \end{bmatrix} (u_{c,k} - \bar{f}_{a,k} - s_k), \end{aligned} \quad (4.58)$$

with $A_\zeta(\bar{\alpha}_k, \hat{\beta}_k) = TA(\bar{\alpha}_k, \hat{\beta}_k) + TB(\bar{\alpha}_k, \hat{\beta}_k)M(\bar{\alpha}_k, \hat{\beta}_k)$. Thus, the stability with H_∞ performance of the system (4.58) can be verified through the following lemma.

Lemma 4.1 *If the virtual sensor gain $L(\bar{\alpha}_k, \hat{\beta}_k)$ of the error system (4.19) and the virtual actuator gain $M(\bar{\alpha}_k, \hat{\beta}_k)$ of the difference system (4.26) are designed by the conditions of theorems 4.1 and 4.2, then the interconnection given in (4.58) is also stable with guaranteed H_∞ performance η_2 computed by $\eta_2 = \eta_1 c_2$, with:*

$$c_2 = \max_{\substack{1 \leq i \leq N_3 \\ 1 \leq j \leq N_4}} \|TB_{ij}\|. \quad (4.59)$$

Proof. Consider:

$$\bar{V}(e_k, x_{\Delta, k}) = \xi V(e_k) + \tilde{V}(x_{\Delta, k}) \quad (4.60)$$

as a Lyapunov candidate function with $\xi > 0$ for the interconnection, $V(e_k)$ given by (4.30) and $\tilde{V}(x_{\Delta, k})$ by (4.44). Then,

$$\bar{V}(e_{k+1}, x_{\Delta, k+1}) - \bar{V}(e_k, x_{\Delta, k}) = \xi V(e_{k+1}) - \xi V(e_k) + \tilde{V}(x_{\Delta, k+1}) - \tilde{V}(x_{\Delta, k}). \quad (4.61)$$

Considering (4.37), (4.38) and (4.40), it follows that:

$$V(e_{k+1}) - V(e_k) = e_k^T \chi e_k \leq -\nu \|e_k\|^2 < 0, \quad (4.62)$$

where $-\nu = \lambda_{\max}(\chi)$ is negative definite and is the maximum eigenvalue of χ .

From (4.56) and (4.62), with $w_k = -L(\bar{\alpha}_k, \hat{\beta}_k)C e_k + TB(\bar{\alpha}_k, \hat{\beta}_k)\tilde{u}_k$ and $\tilde{u}_k = u_{c, k} - \bar{f}_{a, k} - s_k$, (4.61) can be described as:

$$\bar{V}(e_{k+1}, x_{\Delta, k+1}) - \bar{V}(e_k, x_{\Delta, k}) \leq -\xi \nu \|e_k\|^2 - \|x_{\Delta, k}\|^2 + \eta_1^2 c_1^2 \|e_k\|^2 + \eta_1^2 c_2^2 \|\tilde{u}_k\|^2, \quad (4.63)$$

with $c_1 = \max_{\substack{1 \leq i \leq N_3 \\ 1 \leq j \leq N_4}} \|L_{ij}C\|$ and c_2 given in (4.59), which yields:

$$\bar{V}(e_{k+1}, x_{\Delta, k+1}) - \bar{V}(e_k, x_{\Delta, k}) \leq (\eta_1^2 c_1^2 - \xi \nu) \|e_k\|^2 - \|x_{\Delta, k}\|^2 + \eta_1^2 c_2^2 \|\tilde{u}_k\|^2. \quad (4.64)$$

Defining $\xi = \frac{1 + \eta_1^2 c_1^2}{\nu}$, (4.64) results in:

$$\begin{aligned} \bar{V}(e_{k+1}, x_{\Delta, k+1}) - \bar{V}(e_k, x_{\Delta, k}) &\leq -\|e_k\|^2 - \|x_{\Delta, k}\|^2 + \eta_1^2 c_2^2 \|\tilde{u}_k\|^2 \\ &\leq -\left\| \begin{bmatrix} e_k^T & x_{\Delta, k}^T \end{bmatrix} \right\|^2 + \eta_2^2 \|\tilde{u}_k\|^2, \end{aligned} \quad (4.65)$$

with $\eta_2 = \eta_1 c_2$. Thus, the interconnection (4.58) is stable with guaranteed H_∞ performance η_2 for the virtual sensor gain $L(\bar{\alpha}_k, \hat{\beta}_k)$ and virtual actuator gain $M(\bar{\alpha}_k, \hat{\beta}_k)$ designed by the conditions of theorems 4.1 and 4.2, respectively. This concludes the proof. \square

Remark 4.5 *It is important to note that if it is possible to design the virtual actuator signal s_k so that $\eta_2^2 \|\tilde{u}_k\|^2$ is null, the interconnection will be asymptotically stable.*

Theorem 4.3 *Consider the faulty Takagi-Sugeno fuzzy model (4.3) and assume that the nominal closed-loop system is composed of the nominal system (4.1) and the designed nominal controller characterized in Remark 2.1. If there exist virtual sensor gains as in (4.29) and virtual actuator gains as in (4.43) such that the conditions (4.28) and (4.42) are satisfied, then the controller design is independent of the virtual sensor and actuator designs through theorems 4.1 and 4.2, respectively.*

Proof. Consider the Remark 4.3 and a generic nominal controller given by:

$$\Sigma_C = \begin{cases} x_{c, k+1} &= A_c(\bar{\alpha}_k, \hat{\beta}_k)x_{c, k} + B_c(\bar{\alpha}_k, \hat{\beta}_k)y_{c, k} + E_c(\bar{\alpha}_k, \hat{\beta}_k)r_k, \\ u_{c, k} &= C_c(\bar{\alpha}_k, \hat{\beta}_k)x_{c, k} + D_c(\bar{\alpha}_k, \hat{\beta}_k)y_{c, k} + F_c(\bar{\alpha}_k, \hat{\beta}_k)r_k, \end{cases} \quad (4.66)$$

where $x_{c, k}$ is the internal state of the controller, $y_{c, k}$ is given in (4.24) and $u_{c, k}$ is the control sequence computed by the controller. Matrices $A_c(\bar{\alpha}_k, \hat{\beta}_k)$, $B_c(\bar{\alpha}_k, \hat{\beta}_k)$, $E_c(\bar{\alpha}_k, \hat{\beta}_k)$, $C_c(\bar{\alpha}_k, \hat{\beta}_k)$, $D_c(\bar{\alpha}_k, \hat{\beta}_k)$ and $F_c(\bar{\alpha}_k, \hat{\beta}_k)$ have appropriate dimensions and are determined according to the design of the controller.

Then, the reconfigured closed-loop system consists of the faulty system (4.3), the virtual sensor (4.5), the virtual actuator (4.24) and the nominal controller (4.66). With $e_k = x_{f, k} - \hat{x}_{f, k}$ and $x_{\Delta, k} = \tilde{x}_k - \hat{x}_{f, k}$, its dynamics can be given by the estimation error dynamics (4.19), together with the dynamics of the difference state (4.26), the controller (4.66) and the virtual actuator (4.24). It is important

to notice that the nominal controller does not interact directly with the faulty system (4.3), but with the nominal system given by the virtual actuator equations (4.24). The faulty system state ($x_{f,k}$) is included in the estimation error dynamics (4.19), and consequently, in the difference state dynamics (4.26).

The first part of this proof consists in demonstrating that the dynamics of the reference state of the virtual actuator (4.24) can be seen as the dynamics of the nominal system (4.1).

Consider:

$$\tilde{x}_{k+1} = A(\bar{\alpha}_k, \hat{\beta}_k)\tilde{x}_k + B(\bar{\alpha}_k, \hat{\beta}_k)u_{c,k}, \quad (4.67)$$

which can be written as:

$$\begin{aligned} \tilde{x}_{k+1} &\triangleq (T + NC) \left[A(\bar{\alpha}_k, \hat{\beta}_k)\tilde{x}_k + B(\bar{\alpha}_k, \hat{\beta}_k)u_{c,k} \right] \\ &\triangleq TA(\bar{\alpha}_k, \hat{\beta}_k)\tilde{x}_k + TB(\bar{\alpha}_k, \hat{\beta}_k)u_{c,k} + NC \left(A(\bar{\alpha}_k, \hat{\beta}_k)\tilde{x}_k + B(\bar{\alpha}_k, \hat{\beta}_k)u_{c,k} \right) \\ &\triangleq TA(\bar{\alpha}_k, \hat{\beta}_k)\tilde{x}_k + TB(\bar{\alpha}_k, \hat{\beta}_k)u_{c,k} + NC\tilde{x}_{k+1}, \end{aligned} \quad (4.68)$$

with $(T + NC) = I$, as given in (4.7).

As the dynamics of the reference state \tilde{x}_k of the virtual actuator is presented in (4.24), it must be similar to the one given in (4.68). For this, it is necessary to verify that $NC\tilde{x}_{k+1} = NCx_{f,k+1}$, with:

$$NC\tilde{x}_{k+1} = NCT \left(A(\bar{\alpha}_k, \hat{\beta}_k)\tilde{x}_k + B(\bar{\alpha}_k, \hat{\beta}_k)u_{c,k} \right) + NCNCx_{f,k+1}. \quad (4.69)$$

Then, it is necessary that the following equations are proven:

$$\begin{aligned} NCT &= 0 \\ NCNC &= NC. \end{aligned} \quad (4.70)$$

Since N is calculated as shown in (4.8), it follows that:

$$\begin{aligned} NCNC &= D \left(D^T C^T C D \right)^{-1} D^T C^T C D \left(D^T C^T C D \right)^{-1} D^T C^T C \\ &= D \left(D^T C^T C D \right)^{-1} D^T C^T C = NC. \end{aligned} \quad (4.71)$$

From (4.71), it is possible to demonstrate that:

$$\begin{aligned} NC(T + NC) &= NC \\ NCT + NCNC &= NC \\ NCT &= 0. \end{aligned} \quad (4.72)$$

As the equations in (4.70) are satisfied, it can be ensured that $NC\tilde{x}_{k+1} = NCx_{f,k+1}$ and that the reference state dynamics in (4.24), (4.67) and (4.68) are equivalent. Furthermore, the dynamics of the virtual actuator that directly interacts with the designed controller can be written as (4.67).

The second part of the proof is to demonstrate that the controller design is independent of the reconfiguration block design, considering the Remark 4.3 and a generic controller given in (4.66). Writing a closed-loop system composed of (4.19), (4.26), (4.66) and (4.67), one obtains:

$$\begin{aligned} \begin{bmatrix} x_{\Delta,k+1} \\ e_{k+1} \\ \tilde{x}_{k+1} \\ x_{c,k+1} \end{bmatrix} &= \begin{bmatrix} A_{\zeta}(\bar{\alpha}_k, \hat{\beta}_k) & -L(\bar{\alpha}_k, \hat{\beta}_k)C & B_{\zeta_1}(\bar{\alpha}_k, \hat{\beta}_k) & B_{\zeta_2}(\bar{\alpha}_k, \hat{\beta}_k) \\ 0 & \bar{A}_{\delta}(\bar{\alpha}_k, \hat{\beta}_k) & 0 & 0 \\ 0 & 0 & A_{\sigma}(\bar{\alpha}_k, \hat{\beta}_k) & B_{\sigma}(\bar{\alpha}_k, \hat{\beta}_k) \\ 0 & 0 & B_c(\bar{\alpha}_k, \hat{\beta}_k)C & A_c(\bar{\alpha}_k, \hat{\beta}_k) \end{bmatrix} \begin{bmatrix} x_{\Delta,k} \\ e_k \\ \tilde{x}_k \\ x_{c,k} \end{bmatrix} \\ &+ \begin{bmatrix} -TB(\bar{\alpha}_k, \hat{\beta}_k) \\ 0 \\ 0 \\ 0 \end{bmatrix} (\bar{f}_{a,k} + s_k) + \begin{bmatrix} TB(\bar{\alpha}_k, \hat{\beta}_k)F_c(\bar{\alpha}_k, \hat{\beta}_k) \\ 0 \\ B(\bar{\alpha}_k, \hat{\beta}_k)F_c(\bar{\alpha}_k, \hat{\beta}_k) \\ E_c(\bar{\alpha}_k, \hat{\beta}_k) \end{bmatrix} r_k, \end{aligned} \quad (4.73)$$

with:

$$\begin{aligned} A_{\zeta}(\bar{\alpha}_k, \hat{\beta}_k) &= TA(\bar{\alpha}_k, \hat{\beta}_k) + TB(\bar{\alpha}_k, \hat{\beta}_k)M(\bar{\alpha}_k, \hat{\beta}_k), \\ B_{\zeta_1}(\bar{\alpha}_k, \hat{\beta}_k) &= TB(\bar{\alpha}_k, \hat{\beta}_k)D_c(\bar{\alpha}_k, \hat{\beta}_k)C, \\ B_{\zeta_2}(\bar{\alpha}_k, \hat{\beta}_k) &= TB(\bar{\alpha}_k, \hat{\beta}_k)C_c(\bar{\alpha}_k, \hat{\beta}_k), \\ \bar{A}_{\delta}(\bar{\alpha}_k, \hat{\beta}_k) &= A_{\delta}(\bar{\alpha}_k, \hat{\beta}_k) + \bar{R}(\bar{\alpha}_k, \hat{\beta}_k)\bar{\Delta}H, \\ A_{\sigma}(\bar{\alpha}_k, \hat{\beta}_k) &= A(\bar{\alpha}_k, \hat{\beta}_k) + B(\bar{\alpha}_k, \hat{\beta}_k)D_c(\bar{\alpha}_k, \hat{\beta}_k)C, \\ B_{\sigma}(\bar{\alpha}_k, \hat{\beta}_k) &= B(\bar{\alpha}_k, \hat{\beta}_k)C_c(\bar{\alpha}_k, \hat{\beta}_k). \end{aligned}$$

The dynamics matrix consists of two blocks, an upper one composed by the dynamics of the difference state and the estimation error and one at the bottom

composed by the dynamics of the nominal system and the controller. As can be seen, the block at the bottom is not affected by the dynamics of the upper block. Therefore, the design of the reconfiguration block can be carried out independently of the nominal system and the controller. On the other hand, the design of the controller is also carried out independently of the virtual sensor and the virtual actuator and should take into account only the dynamics of the nominal system. This concludes the proof. \square

From the problem formulation and theorems 4.1 and 4.2, it is possible to notice the main differences compared to the approach proposed in Chapter 3. One of them is that sensor and actuator faults are described in an additive way, while in the LPV methodology, they are described as multiplicative. This implies that the proposed TS fuzzy methodology makes it possible to contemplate a greater variety of faults, both multiplicative and additive, including total faults in both sensors and actuators, in addition to describing the system in a simpler way. This is because the description of faults does not affect the input and output matrices of the system, unlike the strategy presented in the previous chapter. That is, the LMI conditions of theorems 4.1 and 4.2 depend only on the nominal matrices of the system (B and C), while the conditions of theorems 3.1 and 3.2 depend on the faulty system matrices (B_f and C_f) and, consequently, on the indications of sensor and actuator faults which are described as time-varying parameters of the system. Therefore, it is evident that the same nonlinear system with faults, described by the LPV model in (3.6) and by the TS fuzzy model in (4.3) will have a lower number of vertices/rules if modeled as TS fuzzy with additive faults (4.3), as shown in the following example.

Example 4.1. A nonlinear system with two sensors and two actuators described as LPV (3.1) with $N = 8$ vertices, when subject to faults, includes them as time-varying parameters in its model (3.6), increasing the number of vertices to $\bar{N} = 128$, as shown in equation (3.5). On the other hand, the same system described as TS fuzzy (with 8 rules), when subject to faults, continues with the same number of rules, but with the premise variables rearranged into vectors $\bar{z}_{\alpha,k}$ and $\bar{z}_{\beta,k}$.

Another difference is that the LPV approach proposed in Chapter 3 considers that time-varying parameters are measured independently of the occurrence of faults (Assumption 3.1), unlike the methodology proposed in this chapter, which

is capable of dealing with unmeasured premise variables, even those that become unmeasured due to the occurrence of sensor faults. Depending on the real-world application, the requirement to measure the premise variables may be a problem, since the measurement of these variables (or time-varying parameters) generally depends on the reading of the signals provided by sensors. If the sensors are affected by faults, the measurements used to have the premise variables (or time-varying parameters) can be compromised as well as the computation of the gains and states of the reconfiguration block and the controller (when applicable). Thus, the performance of the system as a whole can deteriorate and stability is no longer guaranteed. With the use of the proposed methodology, however, it becomes possible to implement a reconfiguration block capable of maintaining the stability and performance of the faulty system, even those that have premise variables affected by faults.

Finally, another significant contribution to the methodology presented in the previous chapter is the way the disturbance is handled in the reconfiguration block design. In this chapter, a strategy based on unknown input observer is proposed, which allows the estimation error of the virtual sensor to be independent of the disturbance. On the other hand, the design in the LPV context is only able to guarantee system stability with respect to the disturbance with an ISS gain. So, depending on the controller design, using the TS fuzzy approach, it is possible for the system output to continue tracking the reference with a performance close to that of the nominal system, while with the LPV strategy, a tracking error may arise during the disturbed period. Notice that the estimation error also affects the performance of the virtual actuator and, consequently, of the reconfiguration block as a whole.

It is important to emphasize that the approaches of [20, 30] propose FTC strategies for TS fuzzy systems with only actuator faults, the first one only contemplates multiplicative faults in a single actuator and the last one covers multiplicative and additive faults, but with different virtual actuator designs that depend on the type of the fault. The methodology in [15], on the other hand, is proposed for TS fuzzy continuous-time systems and allows the occurrence of sensor and actuator faults, as long as they are multiplicative and a reconfiguration block design must be carried out for each new fault that occurs. Then, the contribution of the proposed approach is evident, since it includes additive and multiplicative faults of sensors and actuators, which can be total in both sensors and/or actuators, and only one reconfiguration block design for different types and magnitudes of faults is needed. In [29] a virtual sensor based on unknown

input observer is proposed for LPV systems with additive and multiplicative faults, but which only contemplates sensor faults and considers that time-varying parameters are given. Regarding the use of reconfiguration blocks based on unknown input observer for TS fuzzy systems with unmeasured premise variables or in the LPV context with unmeasured time-varying parameters and subject to sensor and actuator faults (additive and multiplicative), similar methodologies are not found in the current literature.

Algorithm 1 presents to the reader a guide with the steps implementing the proposed technique when applied to a faulty system. Such algorithm is used in the next section to implement the proposed approach to control a nonlinear coupled tank system under both sensor and actuators faults, with unmeasured premise variables and disturbance.

Algorithm 1 Simplified algorithm for implementing the proposed approach.

- 1: Determine the unmeasured premise variables (that can be affected by total losses the sensors).
 - 2: Rearrange the premise variable vectors, separating those that are measured from those that are unmeasured ($\bar{z}_{\alpha,k}$ and $\bar{z}_{\beta,k}$).
 - 3: Determine the value of κ and of the matrix H .
 - 4: Determine the matrices N and T .
 - 5: Determine the matrices A_{ij} , B_{ij} , \tilde{A}_i , \tilde{B}_i , for $i = 1, \dots, N_3$ and $j = 1, \dots, N_4$.
 - 6: Calculate the gains of the virtual sensor and the virtual actuator using theorems 4.1 and 4.2.
 - 7: Design the signal s_k according to the possible actuator faults and such that $\|TB(\bar{\alpha}_k, \hat{\beta}_k)(u_{c,k} - \bar{f}_{a,k} - s_k)\|_2$ is the minimum possible.
 - 8: Run the control algorithm with the reconfiguration block active for the nominal conditions ($\phi_{i,k} = 1$ and $\gamma_{j,k} = 1$, for $i = 1, \dots, m$ and $j = 1, \dots, p$).
 - 9: **if** the FDI module indicates a fault **then**
 - 10: Update $\phi_{i,k}$, $\gamma_{j,k}$, for $i = 1, \dots, m$ and $j = 1, \dots, p$, and s_k .
 - 11: **else**
 - 12: Run the control algorithm with the reconfiguration block active for the nominal conditions.
 - 13: **end if**
-

4.4 CASE STUDY - COUPLED TANKS SYSTEM

In order to evaluate the methodology proposed in this chapter, computer simulations are carried out using the nonlinear model that represents the coupled tank system presented in Section 2.6. From the equations describing the system's behavior given in (2.13), a translation is done in the dynamics equations so that the desired equilibrium point becomes the state space's origin. Thus, the following

discrete-time TS fuzzy model, with an added disturbance, is obtained by using Euler method [115]:

$$\left\{ \begin{array}{l} \delta h_{k+1} = \begin{bmatrix} 1 + z_{1,k} z_{2,k} (-1 + r_{12} q_{io}) & z_{1,k} z_{2,k} (1 - r_{12} q_{io}) \\ (1 - r_{12} q_{oo}) \frac{z_{2,k}}{S_2} & 1 + \frac{z_{2,k} (-1 + r_{12} q_{oo}) - g T_s}{S_2} \end{bmatrix} \delta h_k \\ + \begin{bmatrix} T_s K_{b_1} z_{1,k} & T_s K_{b_2} z_{1,k} \\ 0 & 0 \end{bmatrix} \delta u_k + \begin{bmatrix} 0 \\ 1 \end{bmatrix} d_k, \\ \delta y_k = \begin{bmatrix} 1 & 0 \\ 0 & 1 \end{bmatrix} \delta h_k, \end{array} \right. \quad (4.74)$$

where $\delta h_k = [\delta h_{1,k} \quad \delta h_{2,k}]^T = [h_{1,k} - h_{1o} \quad h_{2,k} - h_{2o}]^T$, with $h_{1o} = 0.5798$ m and $h_{2o} = 0.3112$ m being the state equilibrium values, $\delta u_k = [\delta u_{1,k} \quad \delta u_{2,k}]^T = [u_{1,k} - u_{1o} \quad u_{2,k} - u_{2o}]^T$, with $u_{1o} = 0.2330$ and $u_{2o} = 0.2330$ being the input equilibrium values, $K_{b_1} = 15.5980 \times 10^{-4}$ and $K_{b_2} = 12.2010 \times 10^{-4}$ the static gains of the pumps, $q_{io} = q_{i1o} + q_{i2o}$, with $q_{i1o} = K_{b_1} u_{1o} + 270.3400 \times 10^{-6}$ m³/s and $q_{i2o} = K_{b_2} u_{2o} + 272.5260 \times 10^{-6}$ m³/s the equilibrium values of the input flows, $g = 12.9410 \times 10^{-4}$ and $q_{oo} = g h_{2o} + 787.5860 \times 10^{-6}$ m³/s being the equilibrium value of the output flow. In addition, $z_{1,k} = 1/S_1(h_{1,k})$ and $z_{2,k} = T_s/R_{12}(h_{1,k}, h_{2,k})$ are the measured premise variables grouped in the vector $z_{\alpha,k} = [z_{1,k} \quad z_{2,k}]^T$, with $R_{12}(h_{1,k}, h_{2,k}) = r_{12}(h_{1,k} - h_{2,k}) + 114.8800$ and $r_{12} = 412$. Once again, the sampling time $T_s = 2$ seconds is chosen so that the fastest time constant of the system stays between 7 and 8 samples [114]. For more details, see Section 2.6.

Considering that $0.48 \leq h_{1,k} \leq 0.68$ m and $0.165 \leq h_{1,k} - h_{2,k} \leq 0.5$ m, the minimum and maximum values of the premises variables are obtained, and given by:

$$\begin{aligned} a_1 &= \max_{h_{1,k}} z_{1,k} = 48.1534; & a_2 &= \min_{h_{1,k}} z_{1,k} = 6.4234; \\ b_1 &= \max_{h_{1,k}, h_{2,k}} z_{2,k} = 109.3733 \times 10^{-4}; & b_2 &= \min_{h_{1,k}, h_{2,k}} z_{2,k} = 62.3286 \times 10^{-4}. \end{aligned} \quad (4.75)$$

Using the sector nonlinearity approach, the premise variables can be written as $z_{1,k} = \sum_{i=1}^2 \psi_{1_i}(z_{1,k}) a_i$ and $z_{2,k} = \sum_{j=1}^2 \psi_{2_j}(z_{2,k}) b_j$, with:

$$\begin{aligned} \psi_{1_1}(z_{1,k}) &= \frac{z_{1,k} - a_2}{a_1 - a_2}, & \psi_{1_2}(z_{1,k}) &= \frac{a_1 - z_{1,k}}{a_1 - a_2}, \\ \psi_{2_1}(z_{2,k}) &= \frac{z_{2,k} - b_2}{b_1 - b_2}, & \psi_{2_2}(z_{2,k}) &= \frac{b_1 - z_{2,k}}{b_1 - b_2}, \end{aligned} \quad (4.76)$$

and the membership functions $\alpha_\ell(z_{\alpha,k})$ given in (4.1) are computed as:

$$\alpha_\ell(z_{\alpha,k}) = \psi_{1_i}(z_{1,k}) \psi_{2_j}(z_{2,k}), \quad (4.77)$$

where $\ell = 2(i-1) + j$, for $\ell = 1, \dots, 4$ and $i, j = 1, 2$.

Thus, combining the maximum and minimum values given in (4.75), a TS fuzzy model as presented in (4.1), with $N_1 = 4$ and $N_2 = 0$ rules, is used to describe the nonlinear system (4.74), with the following matrices:

$$\begin{aligned} A_1 &= \begin{bmatrix} 0.7317 & 0.2683 \\ 0.0185 & 0.9730 \end{bmatrix}; & A_2 &= \begin{bmatrix} 0.8471 & 0.1529 \\ 0.0105 & 0.9809 \end{bmatrix}; & C &= \begin{bmatrix} 1 & 0 \\ 0 & 1 \end{bmatrix}; \\ A_3 &= \begin{bmatrix} 0.9642 & 0.0358 \\ 0.0185 & 0.9730 \end{bmatrix}; & A_4 &= \begin{bmatrix} 0.9796 & 0.0204 \\ 0.0105 & 0.9809 \end{bmatrix}; & D &= \begin{bmatrix} 0 \\ 1 \end{bmatrix}; \\ B_1 = B_2 &= \begin{bmatrix} 0.1502 & 0.1175 \\ 0 & 0 \end{bmatrix}; & B_3 = B_4 &= \begin{bmatrix} 0.0200 & 0.0157 \\ 0 & 0 \end{bmatrix}. \end{aligned} \quad (4.78)$$

4.4.1 Controller Design

The nominal TS fuzzy controller is designed according to the methodology presented in Section 2.6.1, where A_i and B_i are given in (4.78) and with $\tilde{N} = N_1$ in (2.15). The obtained gains are presented in Section B.1.

4.4.2 Reconfiguration Block Design

As sensor and actuator faults are modeled as faults added to the system dynamics and output equations, the structure of the input and output matrices are not modified as in the methodology proposed in Chapter 3. Therefore, the virtual sensor and the virtual actuator are designed using the same matrices as the nom-

inal system (4.1), with some adjustments related to the dependence of premise variables that become unmeasured due to faults.

According to the description of the faulty system, total faults in both sensors are considered in the proposed approach. Then, it is pertinent to assume that the measurements from the two level sensors that provide the values of $h_{1,k}$ and $h_{2,k}$ may be corrupted. Consequently, as the premise variables $z_{1,k}$ and $z_{2,k}$ depend on these measurements, their values can be affected by sensor faults and are considered unmeasured (step 1 of Algorithm 1). Thus, the faulty system becomes dependent only on unmeasured premise variables, organized in the vector $\bar{z}_{\beta,k} = [\bar{z}_{\beta_{1,k}} \quad \bar{z}_{\beta_{2,k}}]^T$, as defined in (4.3), and with a change of variables, $\bar{z}_{\beta_{1,k}} = h_{1,k}$ and $\bar{z}_{\beta_{2,k}} = h_{1,k} - h_{2,k}$ (step 2 of Algorithm 1). From this, it follows that:

$$z_{1,k} = \frac{1}{S_1(\bar{z}_{\beta_{1,k}})}, \quad z_{2,k} = \frac{T_s}{r_{12}\bar{z}_{\beta_{2,k}} + 114.88}, \quad (4.79)$$

with $S_1(\bar{z}_{\beta_{1,k}})$ given in (2.14), and the membership functions ψ_{1_i} and ψ_{2_j} , $i, j = 1, 2$, concerned with the unmeasured premise variables in (4.76), can be rewritten as:

$$\begin{aligned} \psi_{1_1}(\bar{z}_{\beta_{1,k}}) &= \frac{1}{\frac{S_1(\bar{z}_{\beta_{1,k}})}{a_1} - a_2}, & \psi_{2_1}(\bar{z}_{\beta_{2,k}}) &= \frac{\frac{T_s}{r_{12}\bar{z}_{\beta_{2,k}} + 114.88} - b_2}{b_1 - b_2}, \\ \psi_{1_2}(\bar{z}_{\beta_{1,k}}) &= \frac{a_1 - \frac{1}{S_1(\bar{z}_{\beta_{1,k}})}}{a_1 - a_2}, & \psi_{2_2}(\bar{z}_{\beta_{2,k}}) &= \frac{b_1 - \frac{T_s}{r_{12}\bar{z}_{\beta_{2,k}} + 114.88}}{b_1 - b_2}. \end{aligned} \quad (4.80)$$

The membership functions of the faulty model (4.3) are given by:

$$\bar{\beta}_\ell(\bar{z}_{\beta,k}) = \psi_{1_i}(\bar{z}_{\beta_{1,k}})\psi_{2_j}(\bar{z}_{\beta_{2,k}}), \quad (4.81)$$

where $\ell = 2(i-1) + j$, for $\ell = 1, \dots, N_4$ and $i, j = 1, 2$, with $N_4 = 4$ and ψ_{1_i} and ψ_{2_j} given in (4.80).

According to step 3 of Algorithm 1, in order to use the conditions of Theorem 4.1 to determine the virtual sensor gains, it is necessary to define the value of κ and of the matrix H so that $e_{z,k} = He_k$. Considering Assumption 4.2, for this case study, the levels of tanks $T3$ and $T4$ can vary up to 0.2 m and 0.14 m around the equilibrium point, respectively, and the control signal $\bar{u}_k = u_{f,k} + \bar{f}_{a,k}$ can vary up to 0.23 around the operation point, leading to $\kappa_{x_f} = 0.2202$, $\kappa_{\bar{u}} = 0.3253$,

$\kappa_{\beta_1} = 2.2709$, $\kappa_{\beta_2} = 2.2709$, $\kappa_{\beta_3} = 3.1590$ and $\kappa_{\beta_4} = 3.1229$, resulting in $\kappa = 2.1532$. The matrix H is given by:

$$H = \begin{bmatrix} 1 & 0 \\ 1 & -1 \end{bmatrix}, \quad (4.82)$$

since $h_{1,k}$ and $h_{2,k}$ are not measured.

Following step 4 of Algorithm 1, matrix N is designed according to equation (4.8) and then matrix T is calculated using the first equation of (4.7), obtaining:

$$N = \begin{bmatrix} 0 & 0 \\ 0 & 1 \end{bmatrix}, \quad T = \begin{bmatrix} 1 & 0 \\ 0 & 0 \end{bmatrix}. \quad (4.83)$$

Thus, applying steps 5 and 6 of Algorithm 1, the virtual sensor can be designed according to the information presented above and, using Theorem 4.1 and the solver MOSEK[®] [116], the gains L_j , for $j = 1, \dots, N_4$, given in (4.29) are calculated and presented in Section B.2. Also using the solver MOSEK[®] [116], the virtual actuator is designed using Theorem 4.2 and the gains M_j , for $j = 1, \dots, N_4$, in (4.43) are calculated for the minimum guaranteed H_∞ performance $\eta_1 = 2.5140$ and shown in Section B.3. Moreover, following step 7 of Algorithm 1, the signal s_k in (4.24) is designed such that $\|TB(\bar{\alpha}_k, \hat{\beta}_k)(u_{c,k} - \bar{f}_{a,k} - s_k)\|_2$ is the minimum possible and is calculated according to the type of actuator faults, during the execution of the control algorithm. For cases of multiplicative partial faults and/or additive faults in one or both actuators, s_k is given by:

$$s_k = \begin{bmatrix} \frac{1}{\phi_{1,k}} & 0 \\ 0 & \frac{1}{\phi_{2,k}} \end{bmatrix} (u_{c,k} - \bar{f}_{a,k}). \quad (4.84)$$

On the other hand, when there is a total fault in one of the actuators, the equivalent control signal must be routed to the remaining actuator. For total fault of the first pump, one gets:

$$s_k = \frac{1}{\phi_{2,k}} \begin{bmatrix} 0 & 0 \\ \frac{K_{b1}}{K_{b2}} & 1 \end{bmatrix} (u_{c,k} - \bar{f}_{a,k}), \quad (4.85)$$

and for total fault of the second pump:

$$s_k = \frac{1}{\phi_{1,k}} \begin{bmatrix} 1 & \frac{K_{b2}}{K_{b1}} \\ 0 & 0 \end{bmatrix} (u_{c,k} - \bar{f}_{a,k}). \quad (4.86)$$

Note that to implement the reconfiguration block, the control signals applied to the system must take into account the equilibrium input values compensated according to the faults.

Remark 4.6 Using the signal s_k given in (4.84), (4.85) and (4.86) for each type of fault, it is possible to observe that in all cases $TB(\bar{\alpha}_k, \hat{\beta}_k)(u_{c,k} - \bar{f}_{a,k} - s_k) = 0$. Thus, the disturbance w_k in (4.26) is given by $w_k = -L(\bar{\alpha}_k, \hat{\beta}_k)Ce_k$, not depending on nominal control signal $u_{c,k}$ nor actuator fault $\bar{f}_{a,k}$.

From this, the computer simulations are performed for different scenarios of sensor faults, actuator faults, simultaneous sensor and actuator faults and disturbance. In order to verify the performance of the system, its time-responses are analyzed for the methodology proposed in this chapter, applying steps 8-13 of Algorithm 1, (called **UIO_{FTC}**, lines in red) and with faults; for the system with nominal controller, without any FTC strategy and without faults (called **WFTC_N**, lines in blue); and for the system with the nominal controller, without any FTC strategy and with faults (called **WFTC**, lines in green). Notice that, as the nominal controller is designed for the nominal system (4.1), stability and performance of the closed-loop system with **WFTC** are not guaranteed in the presence of faults. In addition, as sensor faults affect the measurement of the premise variables, the computation of the controller gain, in the case of the **WFTC** simulations, is also affected.

Computer simulations are also performed to compare performance with the approach proposed in Chapter 3 (called **RFTC**, lines in magenta), considering that the system parameters are calculated from the measurements of the level sensors and, therefore, can be affected by sensor faults. The reconfiguration block composed of a virtual sensor and a virtual actuator is designed for the system described in (4.74) with matrices (4.78), subject to sensor and actuator faults for $\underline{\gamma}_{1,k} \leq \gamma_{1,k} \leq \bar{\gamma}_{1,k}$, $\underline{\gamma}_{2,k} \leq \gamma_{2,k} \leq \bar{\gamma}_{2,k}$, $\underline{\phi}_{1,k} \leq \phi_{1,k} \leq \bar{\phi}_{1,k}$ and $\underline{\phi}_{2,k} \leq \phi_{2,k} \leq \bar{\phi}_{2,k}$, with $\underline{\gamma}_{1,k} = 0$, $\bar{\gamma}_{1,k} = 1$, $\underline{\gamma}_{2,k} = 0.1$, $\bar{\gamma}_{2,k} = 1$, $\underline{\phi}_{1,k} = 0.5$, $\bar{\phi}_{1,k} = 1$, $\underline{\phi}_{2,k} = 0$ and $\bar{\phi}_{2,k} = 1$. Therefore, only faults in these ranges are guaranteed by the design. Also note that additive faults are not covered, as well as total faults

in both sensors and actuators. The resulting faulty system (3.6) has six time-varying parameters, resulting in an LPV system with $\bar{N} = 64$ vertices, with appropriately calculated matrices $B_f(\theta_k)$ and $C_f(\theta_k)$, similar to that shown in (3.65) and (3.66), respectively. Matrix $R(\theta_k)$ is given in (3.67) for total fault of the first pump, in (3.68) for partial faults and for total fault of the second pump is given by:

$$R(\theta_k) = -\frac{1}{\phi_{2,k}} \begin{bmatrix} 0 & 0 \\ \frac{K_{b1}}{K_{b2}} & 1 \end{bmatrix}. \quad (4.87)$$

From that, the virtual sensor is designed by Theorem 3.1 and using the software MOSEK[®] [116], the gains L_i given in (3.17), for $i = 1, \dots, \bar{N}$, are found with a minimum value of $\sigma_d = 1075.79$. Similarly, the virtual actuator is designed by Theorem 3.2 and the gains M_i in (3.39), for $i = 1, \dots, \bar{N}$, are calculated for the minimum value of $\sigma_a = 1464.31$. For the sake of space and to keep objectivity, the values of the gains are omitted in this chapter.

Similar to the previous chapter, the performance of the system is evaluated quantitatively by means of the performance indices IAE, ISE, IVU1 and IVU2, which are depicted in graphs. Note that the lower the index, the better the performance. Then, the more interior the graph, the better the system performance.

4.4.3 Sensor Faults

To evaluate the performance of the closed-loop system subject to sensor faults, computer simulations are performed considering piecewise constant faults f_i , with $i = 1, \dots, 5$. The first fault occurs for $t \geq 500$ s, when there is a partial fault of 20% in the second sensor, i.e. ($\gamma_{1,k} = 1$, $\gamma_{2,k} = 0.8$, $f_{s_{1,k}} = 0$, $f_{s_{2,k}} = 0$, fault f_1), and the second after $t \geq 1000$ s, when there is a partial fault of 50% in first sensor and the second sensor fails completely, namely ($\gamma_{1,k} = 0.5$, $\gamma_{2,k} = 0$, $f_{s_{1,k}} = 0$, $f_{s_{2,k}} = 0$, fault f_2), as depicted in figures 14 and 15. For $t \geq 2000$ s, the first sensor fails completely and a partial fault of 50% occurs in the second sensor, i.e. ($\gamma_{1,k} = 0$, $\gamma_{2,k} = 0.5$, $f_{s_{1,k}} = 0$, $f_{s_{2,k}} = 0$, fault f_3), for $t \geq 3000$ s, the first sensor recovers 50% of its efficiency, namely ($\gamma_{1,k} = 0.5$, $\gamma_{2,k} = 0.5$, $f_{s_{1,k}} = 0$, $f_{s_{2,k}} = 0$, fault f_4), and for $t \geq 4000$ s, additive faults with values of -0.1 m and 0.05 m occur in the first and second sensor, respectively, i.e. ($\gamma_{1,k} = 0.5$, $\gamma_{2,k} = 0.5$, $f_{s_{1,k}} = -0.1$, $f_{s_{2,k}} = 0.05$, fault f_5). In addition, for $5000 \leq t < 6000$, a disturbance d_k is inserted in tank $T4$, equivalent to applying a control signal to the second pump with an amplitude of 0.1 .

The instants of faults f_i , $i = 1, \dots, 5$, are shown in figures 14 and 15 by dashed gray lines, while their durations are represented by the colored backgrounds. These faults can be summarized as:

$$\begin{cases} f_1 : \gamma_{1,k} = 1, & \gamma_{2,k} = 0.8, & f_{s_{1,k}} = 0, & f_{s_{2,k}} = 0, & 500 \leq t < 1000s, \\ f_2 : \gamma_{1,k} = 0.5, & \gamma_{2,k} = 0, & f_{s_{1,k}} = 0, & f_{s_{2,k}} = 0, & 1000 \leq t < 2000s, \\ f_3 : \gamma_{1,k} = 0, & \gamma_{2,k} = 0.5, & f_{s_{1,k}} = 0, & f_{s_{2,k}} = 0, & 2000 \leq t < 3000s, \\ f_4 : \gamma_{1,k} = 0.5, & \gamma_{2,k} = 0.5, & f_{s_{1,k}} = 0, & f_{s_{2,k}} = 0, & 3000 \leq t < 4000s, \\ f_5 : \gamma_{1,k} = 0.5, & \gamma_{2,k} = 0.5, & f_{s_{1,k}} = -0.1, & f_{s_{2,k}} = 0.05, & t \geq 4000s. \end{cases} \quad (4.88)$$

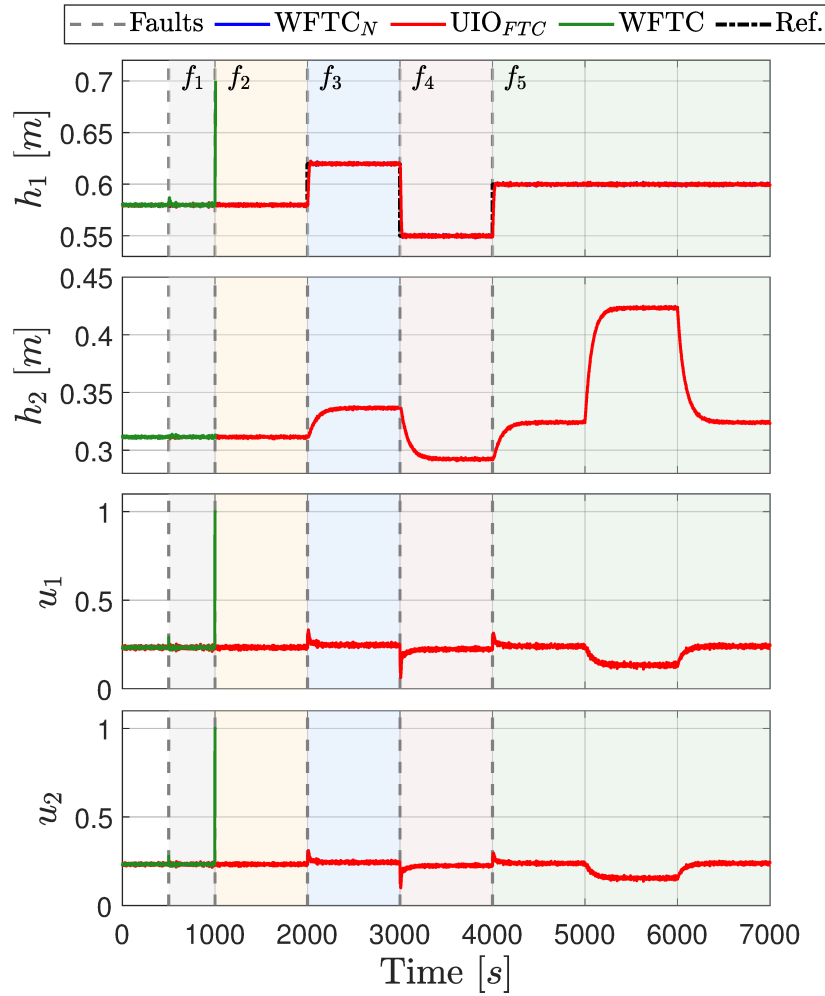


Figure 14: Simulations for sensor faults and disturbance for $WFTC_N$, $WFTC$, and UIO_{FTC} : Levels h_1 and h_2 (top) and control signals u_1 and u_2 (bottom).

From Figure 14 it is possible to notice that with the occurrence of fault f_2 , the system with **WFTC** has an increase in the control signal and in the level h_1 , so that it exceeds 0.7 m and activates the process security system, turning it off (the simulation is stopped) and preventing the tank $T3$ from overflowing. This is because the controller is not designed to compensate fault occurrences and when the measurement of the levels are incorrect, the system exceeds the maximum allowed safety limit. On the other hand, with the use of the **UIO_{FTC}** strategy, the faults hardly affect the control signal and the real output of the system. Thus, their time-responses are similar to those obtained with the implementation of **WFTC_N**, when no faults and no FTC strategy are considered. Furthermore, the disturbance does not affect the reference tracking, due to the use of the unknown input observer-based approach. From Figure 15, in which the methodologies **RFTC** and **UIO_{FTC}** are compared, it is possible to observe that after the occurrence of the fault f_3 , the system using the **RFTC** strategy exceeds the maximum level value allowed in the tank $T3$, activating the security system and disabling the operation of the process. Although the fault f_3 is considered in the design of the virtual sensor, it affects the measurements of the system time-varying parameters, resulting in an inadequate computation of gains and states of the virtual sensor, virtual actuator and controller, and causing the system to exceed the maximum security limit. Therefore, the reconfiguration block **UIO_{FTC}** proposed in this chapter is able to keep the system response close to the nominal one and with reference tracking, even in the presence of different sensor faults (multiplicative and additive), with unmeasured premise variables and disturbance.

The performance indices of the system are normalized with respect to the **WFTC** and presented in Figure 16, in which it can be noticed that the system performance with **UIO_{FTC}** is close to that of the nominal system with **WFTC_N**, being, in general, significantly better than the system with **WFTC**. Regarding the error, the methodology **UIO_{FTC}** presents better performance than the **RFTC**, but the latter has slightly better values of IVU1 and IVU2, since the simulation was interrupted at the beginning, not showing, for example, the control signal variations caused by changes in the reference value.

An important detail is that, as the sensor faults affect the measurement of all the premise variables, the gain calculated by the implemented controller becomes inadequate since it depends on its value. However, with the use of the proposed virtual sensor, the estimates of these premise variables are provided to the controller, allowing an adequate computation of its gain.

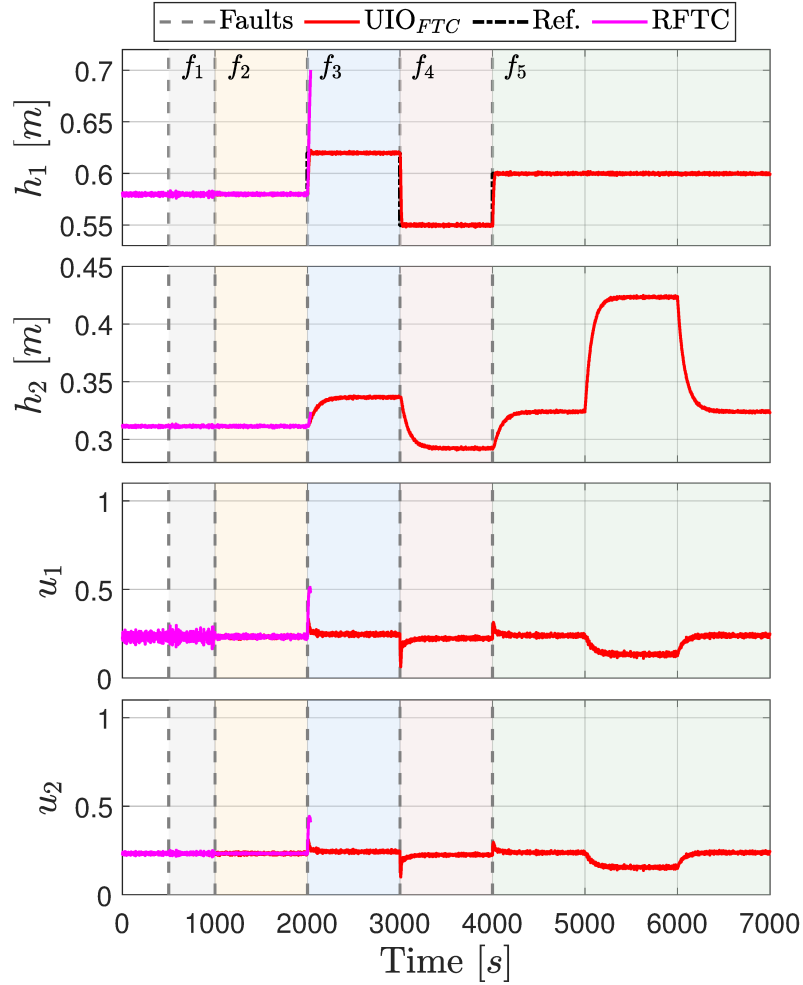


Figure 15: Simulations for sensor faults and disturbance for UIO_{FTC} and $RFTC$: Levels h_1 and h_2 (top) and control signals u_1 and u_2 (bottom).

Figure 17 presents the simulation graphs for the system with UIO_{FTC} to visualize the states of the reconfiguration block ($\hat{x}_{f,k}$ and \tilde{x}_k) compared to the system state ($x_{f,k}$) and also the nominal control signal ($u_{c,k}$) compared to the reconfigured control signal ($u_{f,k}$) applied to the process actuators. As can be seen, the virtual sensor and virtual actuator states resemble the system state, even in the presence of different sensor faults, allowing sensor faults to be hidden from the nominal controller. Similarly, as in this case there are no actuator faults, $u_{f,k}$ is practically identical to the control signal $u_{c,k}$ generated by the nominal controller.

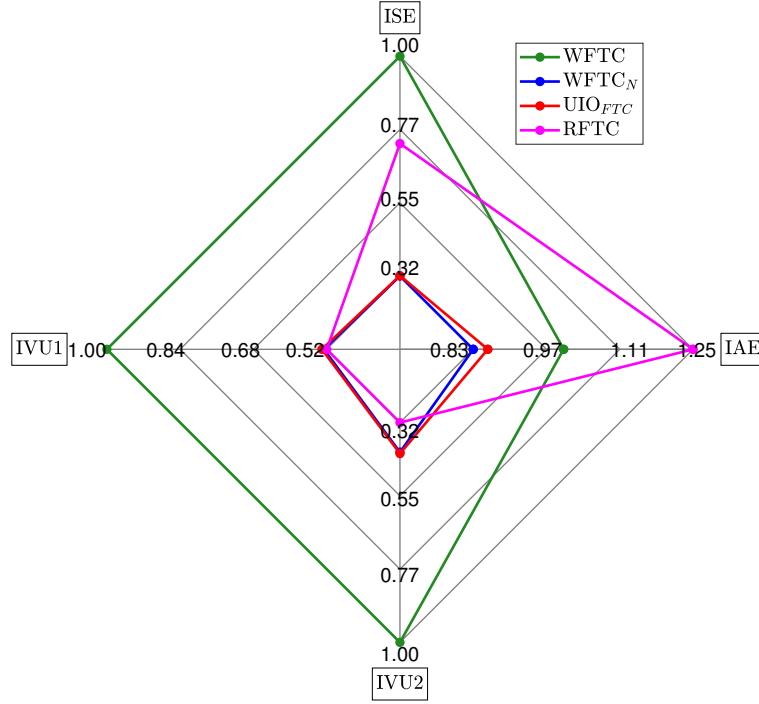


Figure 16: Performance indices for sensor faults and disturbance normalized with respect to **WFTC**.

4.4.4 Actuator Faults

Simulations are also performed to verify the performance of the system subject to piecewise constant actuator faults f_i , $i = 1, \dots, 5$, as depicted in figures 18 and 19. The first fault occurs for $t \geq 500$ s, when there is a partial fault of 20% in the first actuator and of 10% in the second actuator, namely $(\phi_{1,k} = 0.8, \phi_{2,k} = 0.9, f_{a_{1,k}} = 0, f_{a_{2,k}} = 0, \text{fault } f_1)$, and the second for $t \geq 1500$ s, with a total loss of the first actuator, i.e. $(\phi_{1,k} = 0, \phi_{2,k} = 0.9, f_{a_{1,k}} = 0, f_{a_{2,k}} = 0, \text{fault } f_2)$. For $t \geq 2500$ s, there is a recovery of 90% of the efficiency of the first pump and a total loss of the second pump, namely $(\phi_{1,k} = 0.9, \phi_{2,k} = 0, f_{a_{1,k}} = 0, f_{a_{2,k}} = 0, \text{fault } f_3)$, for $t \geq 3500$ s, the second actuator fully recovers, i.e. $(\phi_{1,k} = 0.9, \phi_{2,k} = 1, f_{a_{1,k}} = 0, f_{a_{2,k}} = 0, \text{fault } f_4)$, and for $t \geq 4500$ s, additive faults occur with values of 0.05 and 0.08 in the first and second pump, respectively, namely $(\phi_{1,k} = 0.9, \phi_{2,k} = 1, f_{a_{1,k}} = 0.05, f_{a_{2,k}} = 0.08, \text{fault } f_5)$. A disturbance d_k with the same amplitude and duration as the one in the previous section is also inserted.

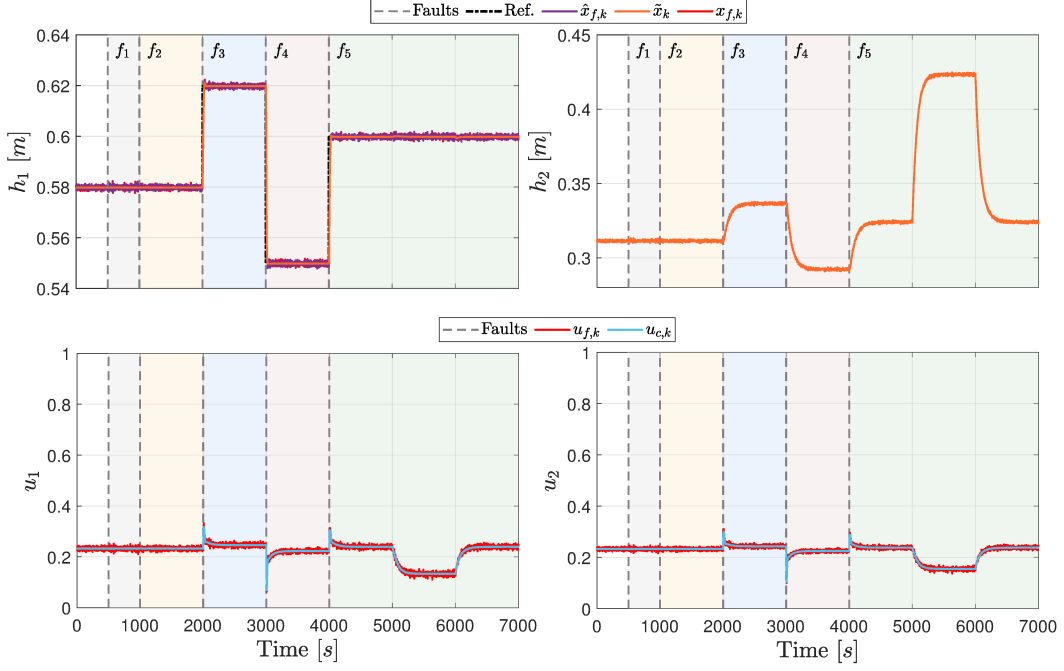


Figure 17: Simulation for sensor faults and disturbance for **UIO_{FTC}**: System ($x_{f,k}$) and reconfiguration block states ($\hat{x}_{f,k}$ and \tilde{x}_k) (top), nominal ($u_{c,k}$) and reconfigured control signals ($u_{f,k}$) (bottom).

Once again, the faults f_i , $i = 1, \dots, 5$, occur, respectively, at the time instants represented in figures 18 and 19 by the dashed lines, while their durations are represented by the colored backgrounds. These faults can be summarized as:

$$\left\{ \begin{array}{llll} f_1 : \phi_{1,k} = 0.8, & \phi_{2,k} = 0.9, & f_{a_{1,k}} = 0, & f_{a_{2,k}} = 0, & 500 \leq t < 1500s, \\ f_2 : \phi_{1,k} = 0, & \phi_{2,k} = 0.9, & f_{a_{1,k}} = 0, & f_{a_{2,k}} = 0, & 1500 \leq t < 2500s, \\ f_3 : \phi_{1,k} = 0.9, & \phi_{2,k} = 0, & f_{a_{1,k}} = 0, & f_{a_{2,k}} = 0, & 2500 \leq t < 3500s, \\ f_4 : \phi_{1,k} = 0.9, & \phi_{2,k} = 1, & f_{a_{1,k}} = 0, & f_{a_{2,k}} = 0, & 3500 \leq t < 4500s, \\ f_5 : \phi_{1,k} = 0.9, & \phi_{2,k} = 1, & f_{a_{1,k}} = 0.05, & f_{a_{2,k}} = 0.08, & t \geq 4500s. \end{array} \right. \quad (4.89)$$

As can be noticed in Figure 18, the system with **WFTC** is able to continue tracking the reference even in the presence of different actuator faults. However, this is not guaranteed, since the controller is designed for the nominal system. In addition, whenever a fault occurs, the system is disturbed and variations in the system output are noticed. These variations can be of great amplitude, such as the one that appears close to the occurrence of the fault f_2 . Another observation is that there is the application of control signals in the pumps, even when they are in total fault. On the other hand, using **UIO_{FTC}** methodology,

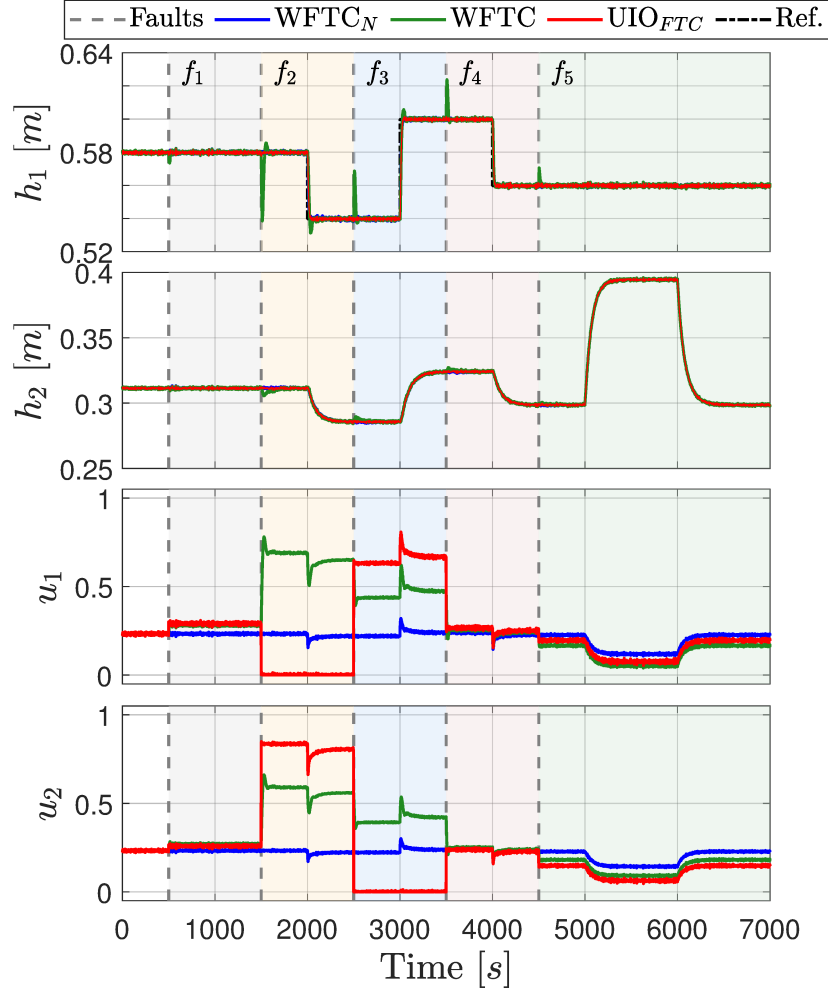


Figure 18: Simulations for actuator faults and disturbance for $WFTC_N$, $WFTC$, and UIO_{FTC} : Levels h_1 and h_2 (top) and control signals u_1 and u_2 (bottom).

the reconfiguration block is able to maintain the performance of the system close to the nominal $WFTC_N$, via adjustments made to its control signal to compensate the faults and the disturbance. Note that, after the total loss of the actuators in f_2 and f_3 , the control signal for the pump with total fault becomes practically null and the remaining actuator becomes responsible for the actuation of the whole system. The system with $RFTC$, on the other hand, has a behavior similar to the UIO_{FTC} up to the time of fault f_5 , as can be seen in Figure 19. After that, it no longer follows the reference, due to additive faults that are not included in its design and the system stability is just guaranteed with respect to the disturbance with an ISS gain. It is worth noting that, although the total fault of the first actuator is compensated by the reconfiguration block (thanks to the use of the matrix $R(\theta_k)$ in (4.87)), there is no guarantee of stability by the

design, in which only the total fault of the second actuator is ensured. Thus, the approach proposed in this chapter prove to be adequate and efficient even with the presence of different types of faults, including total faults on both actuators, and disturbance.

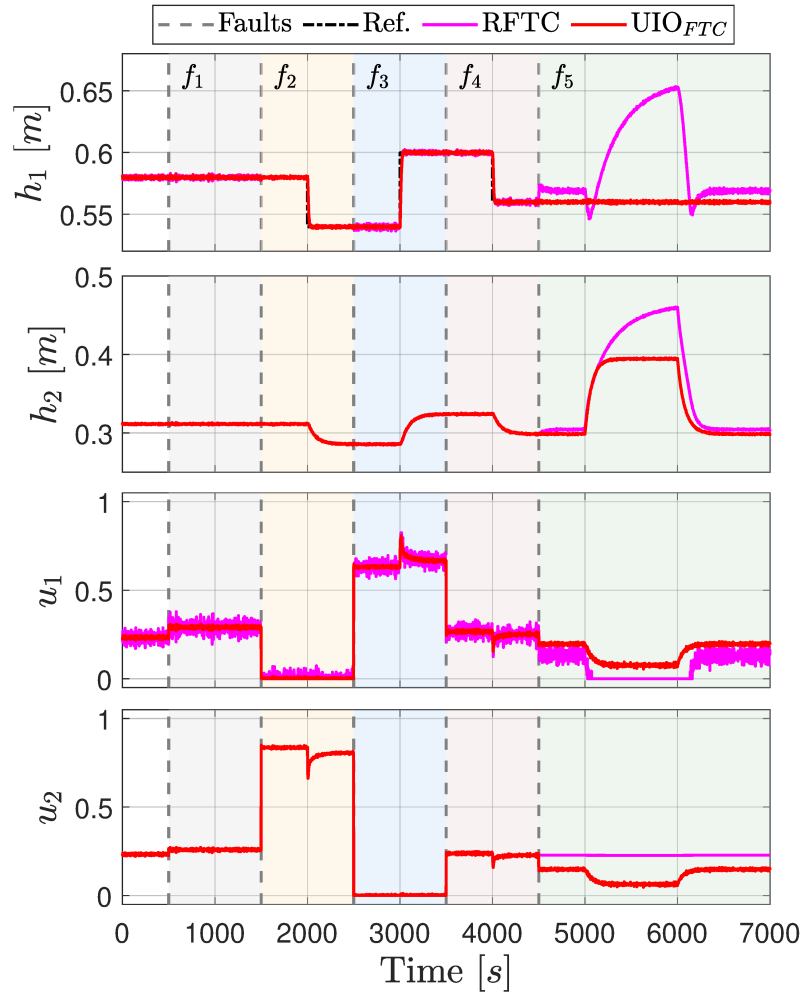


Figure 19: Simulations for actuator faults and disturbance for UIO_{FTC} and $RFTC$: Levels h_1 and h_2 (top) and control signals u_1 and u_2 (bottom).

Figure 20 illustrates the performance indices for the system with the simulated methodologies, normalized in relation to the $WFTC$, being evident that the $RFTC$ approach presents the worst performance in this scenario. Regarding the error, the system with UIO_{FTC} has similar indices to the nominal system $WFTC_N$ and has higher values of IVU_1 and IVU_2 , due to the adjustments made to the control signal to compensate the actuator faults. The system with $WFTC$, on the other hand, has an IAE about 30% higher and ISE 43% higher than the

system with UIO_{FTC} , with lower values of IVU1 and IVU2. However, there is the application of control signal in actuators that are in total fault.

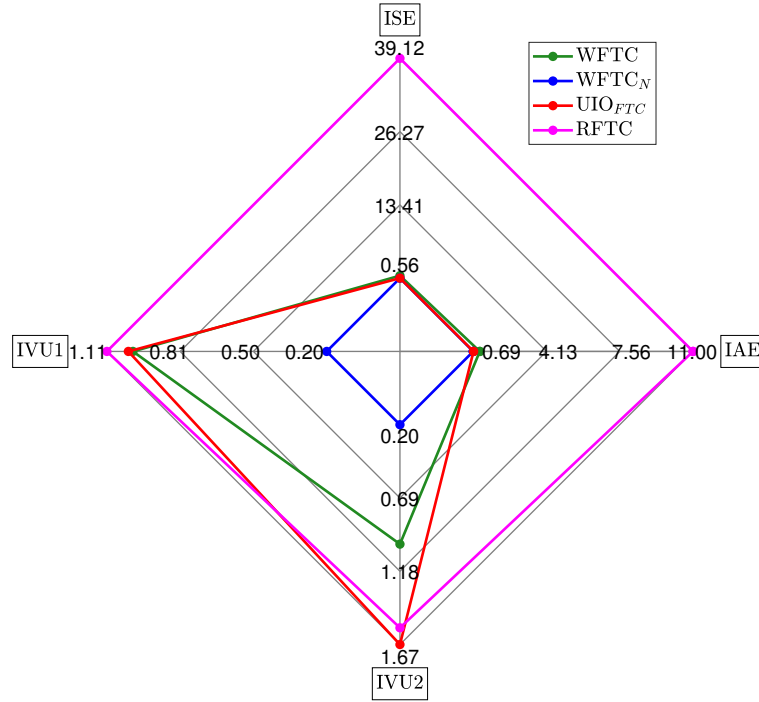


Figure 20: Performance indices for actuator faults and disturbance normalized with respect to $WFTC$.

From Figure 21, it is possible to verify that the states of the reconfiguration block ($\hat{x}_{f,k}$ and \tilde{x}_k) are similar to the system state ($x_{f,k}$) regardless of faults. On the other hand, the reconfigured control signal ($u_{f,k}$) differs significantly from the control signal ($u_{c,k}$) generated by the nominal controller. This is because the virtual actuator modifies the nominal control signal so that actuator faults are compensated and do not interfere with the system behavior. Note also that when there are no faults, the control signals $u_{f,k}$ and $u_{c,k}$ are similar.

4.4.5 Simultaneous Sensor and Actuator Faults

In these computer simulations are considered simultaneous sensor and actuator faults and disturbance, as depicted in figures 22 and 23. From $t \geq 500$ s, the second sensor has its measurement reduced by 20%, and the first and second actuators have 20% and 10% loss in their efficiencies, respectively, namely ($\gamma_{1,k} = 1$, $\gamma_{2,k} = 0.8$, $f_{s1,k} = 0$, $f_{s2,k} = 0$, $\phi_{1,k} = 0.8$, $\phi_{2,k} = 0.9$, $f_{a1,k} = 0$, $f_{a2,k} = 0$,

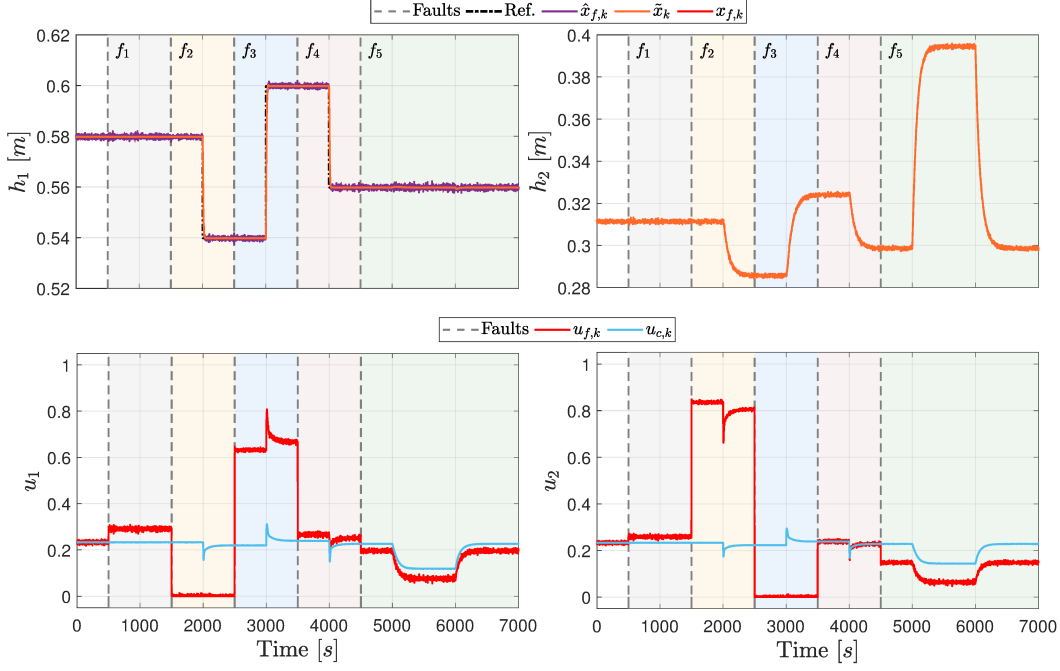


Figure 21: Simulation for actuator faults and disturbance for UIO_{FTC} : System $(x_{f,k})$ and reconfiguration block states $(\hat{x}_{f,k}$ and \tilde{x}_k) (top), nominal $(u_{c,k})$ and reconfigured control signals $(u_{f,k})$ (bottom).

fault f_1), and from $t \geq 1500$ s there is a partial fault of 50% in the first sensor, and total faults in the second sensor and the first actuator, i.e. $(\gamma_{1,k} = 0.5, \gamma_{2,k} = 0, f_{s_{1,k}} = 0, f_{s_{2,k}} = 0, \phi_{1,k} = 0, \phi_{2,k} = 0.9, f_{a_{1,k}} = 0, f_{a_{2,k}} = 0, \text{fault } f_2)$. For $t \geq 2500$ s, the second sensor recovers 50% of its efficiency and the first pump recovers 90%, and the first sensor and second pump fail completely, namely $(\gamma_{1,k} = 0, \gamma_{2,k} = 0.5, f_{s_{1,k}} = 0, f_{s_{2,k}} = 0, \phi_{1,k} = 0.9, \phi_{2,k} = 0, f_{a_{1,k}} = 0, f_{a_{2,k}} = 0, \text{fault } f_3)$. From $t \geq 3500$ s, the first sensor recovers 50% of its efficiency, while the second actuator fully recovers, i.e. $(\gamma_{1,k} = 0.5, \gamma_{2,k} = 0.5, f_{s_{1,k}} = 0, f_{s_{2,k}} = 0, \phi_{1,k} = 0.9, \phi_{2,k} = 1, f_{a_{1,k}} = 0, f_{a_{2,k}} = 0, \text{fault } f_4)$. Finally, for $t \geq 4500$ s, additive faults occur in sensors and actuators, with values of -0.1 m, 0.05 m, 0.05 and 0.08 , respectively, namely $(\gamma_{1,k} = 0.5, \gamma_{2,k} = 0.5, f_{s_{1,k}} = -0.1, f_{s_{2,k}} = 0.05, \phi_{1,k} = 0.9, \phi_{2,k} = 1, f_{a_{1,k}} = 0.05, f_{a_{2,k}} = 0.08, \text{fault } f_5)$. Moreover, a disturbance d_k with the same amplitude and duration as the one in the previous sections is inserted in tank T_4 .

Following similar steps as in the other graphs, the fault instants f_i , $i = 1, \dots, 5$, are indicated by the dashed gray lines and the colored backgrounds illustrate their duration intervals. These faults can be summarized as:

$$\left\{ \begin{array}{ll} f_1 : \gamma_{1,k} = 1, & \gamma_{2,k} = 0.8, \quad f_{s_{1,k}} = 0, \quad f_{s_{2,k}} = 0, \\ & \phi_{1,k} = 0.8, \quad \phi_{2,k} = 0.9, \quad f_{a_{1,k}} = 0, \quad f_{a_{2,k}} = 0, & 500 \leq t < 1500s, \\ f_2 : \gamma_{1,k} = 0.5, & \gamma_{2,k} = 0, \quad f_{s_{1,k}} = 0, \quad f_{s_{2,k}} = 0, \\ & \phi_{1,k} = 0, \quad \phi_{2,k} = 0.9, \quad f_{a_{1,k}} = 0, \quad f_{a_{2,k}} = 0, & 1500 \leq t < 2500s, \\ f_3 : \gamma_{1,k} = 0, & \gamma_{2,k} = 0.5, \quad f_{s_{1,k}} = 0, \quad f_{s_{2,k}} = 0, \\ & \phi_{1,k} = 0.9, \quad \phi_{2,k} = 0, \quad f_{a_{1,k}} = 0, \quad f_{a_{2,k}} = 0, & 2500 \leq t < 3500s, \\ f_4 : \gamma_{1,k} = 0.5, & \gamma_{2,k} = 0.5, \quad f_{s_{1,k}} = 0, \quad f_{s_{2,k}} = 0, \\ & \phi_{1,k} = 0.9, \quad \phi_{2,k} = 1, \quad f_{a_{1,k}} = 0, \quad f_{a_{2,k}} = 0, & 3500 \leq t < 4500s, \\ f_5 : \gamma_{1,k} = 0.5, & \gamma_{2,k} = 0.5, \quad f_{s_{1,k}} = -0.1, \quad f_{s_{2,k}} = 0.05, \\ & \phi_{1,k} = 0.9, \quad \phi_{2,k} = 1, \quad f_{a_{1,k}} = 0.05, \quad f_{a_{2,k}} = 0.08, & t \geq 4500s. \end{array} \right. \quad (4.90)$$

Through Figure 22, notice that the output corresponding to the tank $T3$ level of the system with **WFTC** exceeds the maximum safety limit of 0.7 m right after the fault f_2 , causing the simulation to be interrupted. As seen previously, this is due to the fact that sensor faults have occurred and the controller loses the correct measurement information to continue tracking the reference. The system with **UIO_{FTC}**, on the other hand, maintains the output at the desired level, and close to the nominal **WFTC_N**, regardless of the occurrence of different sensor and actuator faults and disturbance. Furthermore, it can be seen that the inserted disturbance is compensated by the system, so that it continues the reference tracking without offset errors. From Figure 23, it is possible to notice that the performance of the system with **RFTC** is affected by the faults that occur and after the reference change during fault f_3 , the output of tank $T3$ reaches the maximum allowed value and the simulation is interrupted. This is due to the occurrence of faults that are not covered in the reconfiguration block design and the inadequate supply of the time-varying parameters that become unmeasured due to sensor faults. Thus, it is important to note that the reconfiguration block **UIO_{FTC}** proposed in this chapter is capable of ensure stability and performance, even when there are different simultaneous sensor and actuator faults, including total loss in measurement and actuation. In addition, the loss of both sensors also causes all premise variables to be unmeasured. However, with the proposed

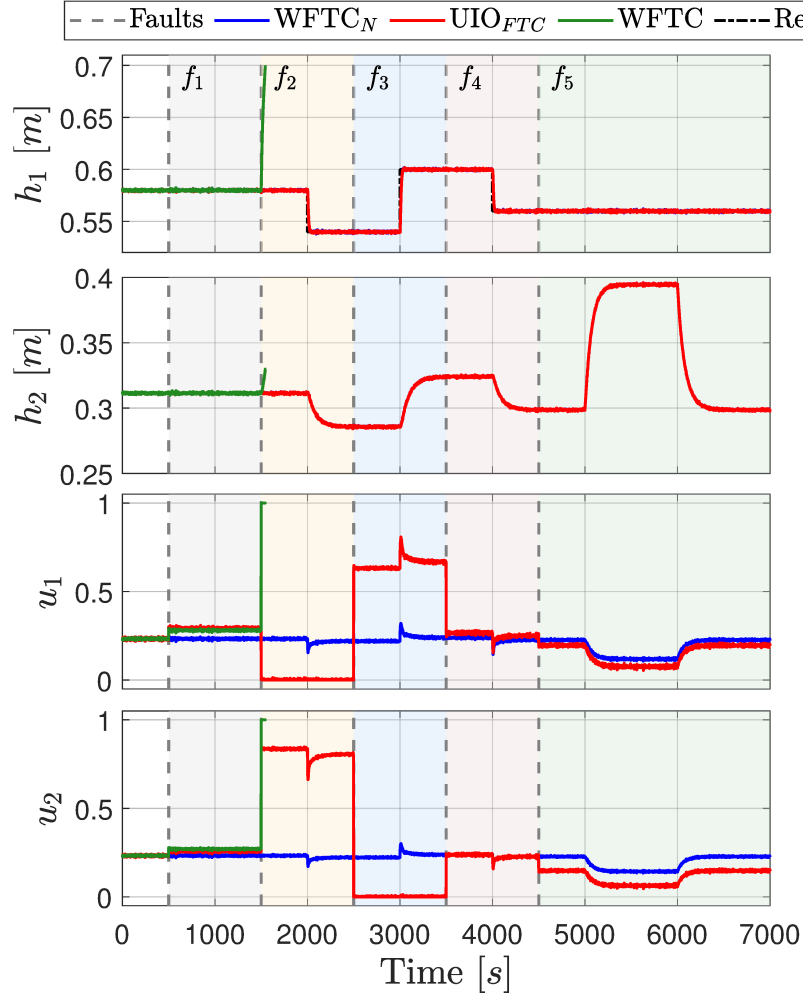


Figure 22: Simulations for simultaneous sensor and actuator faults and disturbance for WFTC_N , WFTC , and UIO_{FTC} : Levels h_1 and h_2 (top) and control signals u_1 and u_2 (bottom).

virtual sensor and virtual actuator, its estimates are used to calculate the gains of the controller and the reconfiguration block itself.

The performance indices of the system are normalized with respect to WFTC and are presented in Figure 24. Regarding the error, the system with UIO_{FTC} presents indices close to the nominal system WFTC_N , while it has higher values of IVU1 and IVU2, due to the compensation of the control signal because of actuator faults. Overall, the system with RFTC shows worse performance, followed by the system with WFTC .

It is also possible to analyze the behavior of the reconfiguration block through Figure 25. As shown for the other fault scenarios, the virtual sensor and virtual actuator states ($\hat{x}_{f,k}$ and \tilde{x}_k) are similar to the system state ($x_{f,k}$), even when

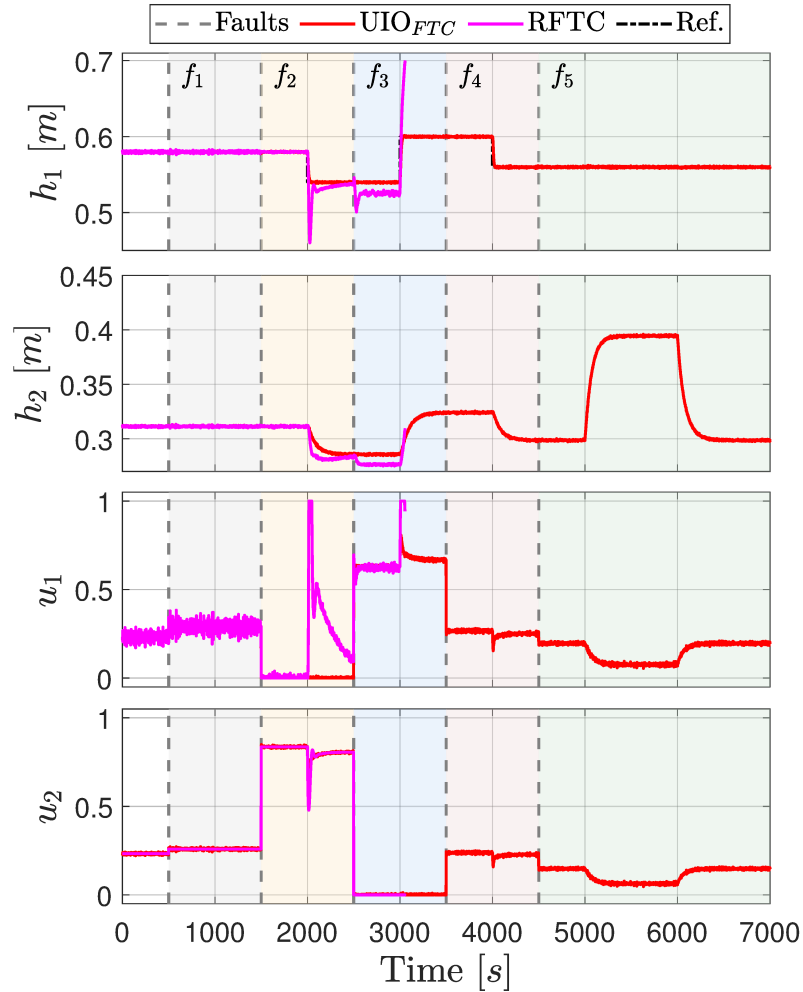


Figure 23: Simulations for simultaneous sensor and actuator faults and disturbance for **UIO_{FTC}** and **RFTC**: Levels h_1 and h_2 (top) and control signals u_1 and u_2 (bottom).

different sensor and actuator faults occur. Thus, sensor faults are hidden from the controller, as the output provided to it depends on the state of the virtual actuator and not on the faulty output. On the other hand, the control signal generated by the virtual actuator ($u_{f,k}$) modifies the control signal of the nominal controller ($u_{c,k}$), in order to compensate the actuator faults that occur during the simulated period.

4.4.6 Piecewise Constant Disturbance

Finally, simulations are performed to analyze the performance of the system when it is subject to disturbances. For this, it is considered a piecewise constant

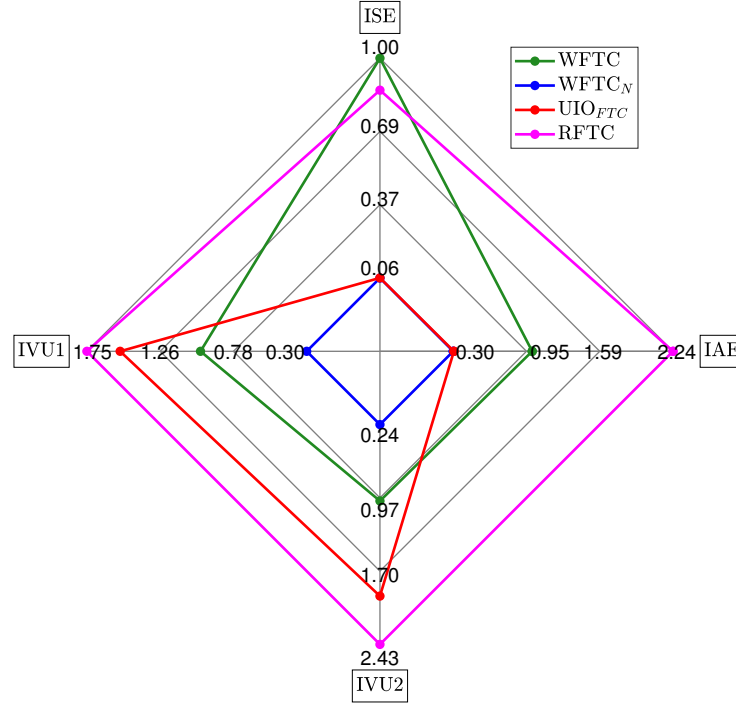


Figure 24: Performance indices for simultaneous sensor and actuator faults and disturbance normalized with respect to **WFTC**.

disturbance that occurs in the range $1000 \leq t \leq 3000$ s, as depicted in Figure 26. The disturbance d_k is inserted in the tank $T4$, equivalent to applying a control signal to second pump with an amplitude of 0.1. For a better analysis of the system performance in the presence of disturbance, it is considered that it operates without sensor and actuator faults, namely ($\gamma_{1,k} = 1$, $\gamma_{2,k} = 1$, $f_{s_{1,k}} = 0$, $f_{s_{2,k}} = 0$, $\phi_{1,k} = 1$, $\phi_{2,k} = 1$, $f_{a_{1,k}} = 0$, $f_{a_{2,k}} = 0$), and therefore, simulations are performed only for the system with **UIO_{FTC}**, **RFTC** and **WFTC_N** are analyzed. As can be seen, the system with **UIO_{FTC}** has practically the same performance as the nominal system with **WFTC_N**, even during the disturbance period, rejecting it completely. This is due to the action of the reconfiguration block based on unknown input observer that estimates the system states independent of the input d_k . On the other hand, the **RFTC** approach is not able to reject the disturbance, presenting an error of approximately four centimeters during the evaluated period. This is because the reconfiguration block design is performed only to guarantee the system stability with respect to the disturbance with an ISS gain. That is, even for the system subject to disturbance, but without faults, there is a better performance of the **UIO_{FTC}** approach proposed in this chapter in relation to the **RFTC** proposed in Chapter 3.

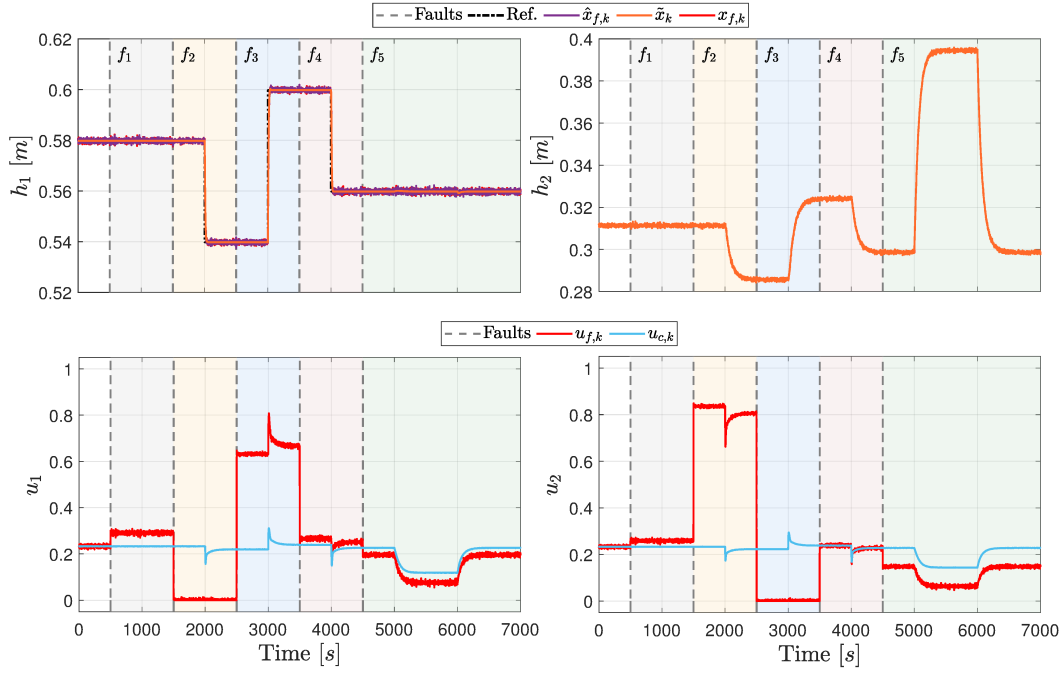


Figure 25: Simulation for simultaneous sensor and actuator faults and disturbance for UIO_{FTC} : System ($x_{f,k}$) and reconfiguration block states ($\hat{x}_{f,k}$ and \tilde{x}_k) (top), nominal ($u_{c,k}$) and reconfigured control signals ($u_{f,k}$) (bottom).

Figure 27 presents the performance indices for the evaluated methodologies and which are normalized in relation to the RFTC . It can be observed that the system with UIO_{FTC} has a performance similar to the nominal system WFTC_N , since all calculated indices have very close values. Furthermore, they presented lower values than the system with RFTC in all indices, except for IVU_2 . However, it is possible to note that this is because the latter does not make any adjustments to the control signal of the second pump to deal with the disturbance, unlike the UIO_{FTC} and WFTC_N .

Remark 4.7 *After analyzing the system performance through different computer simulations, it is possible to notice that the TS fuzzy reconfiguration block proposed in this chapter is able to guarantee the stability of the closed-loop system with a certain performance even when it is subject to different sensor and actuator faults, being they multiplicative and/or additive, including total losses in both sensors and actuators. From the proposed methodology, it is also possible to deal with systems that have unmeasured premise variables, even when they become unmeasured due to sensor faults. Furthermore, through an approach based on unknown input observer, it is obtained a reconfiguration block design with the dynamics of the estimation error and state difference independent of the distur-*

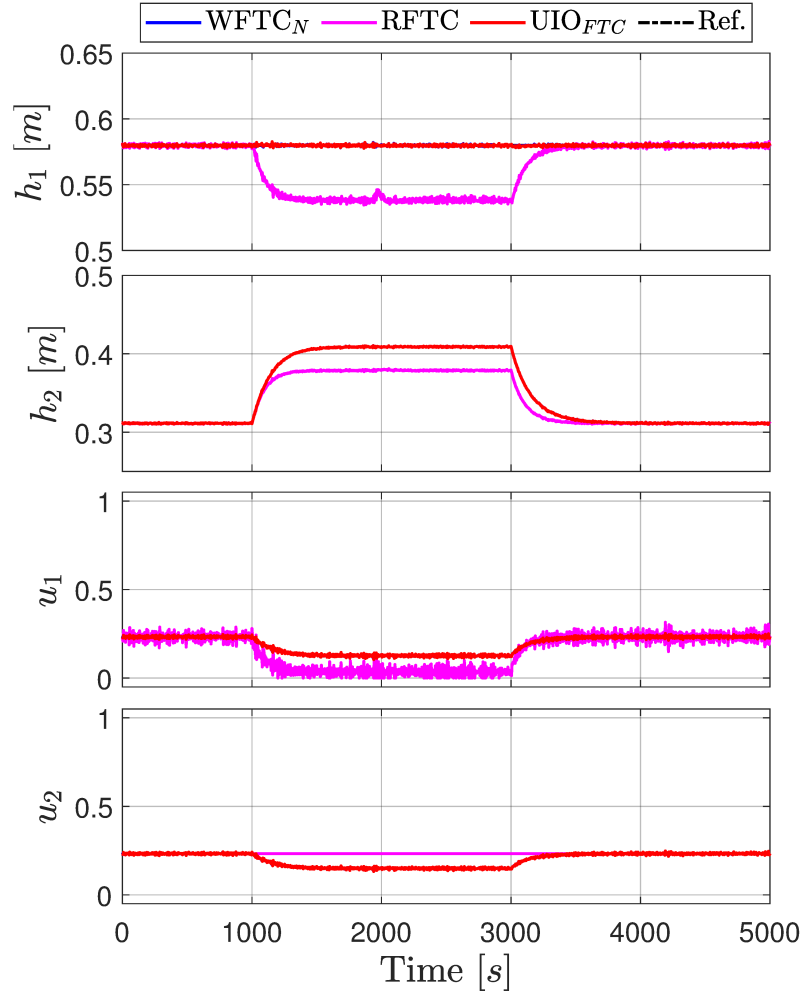


Figure 26: Simulations for disturbance for $WFTC_N$, UIO_{FTC} , and $RFTC$: Levels h_1 and h_2 (top) and control signals u_1 and u_2 (bottom).

bance, keeping the reference tracking with performance close to the nominal one. It is important to emphasize that no work in the literature addresses the design of a reconfiguration block based on UIO for TS fuzzy systems subject to sensor and actuator faults with unmeasured premise variables. It is also noted that the proposed methodology is capable of dealing with additive faults and has virtual sensor and virtual actuator design conditions independent of the faulty model, unlike the LPV approach presented in Chapter 3. Consequently, the proposed strategy leads to a lower number of rules used to describe the problem.

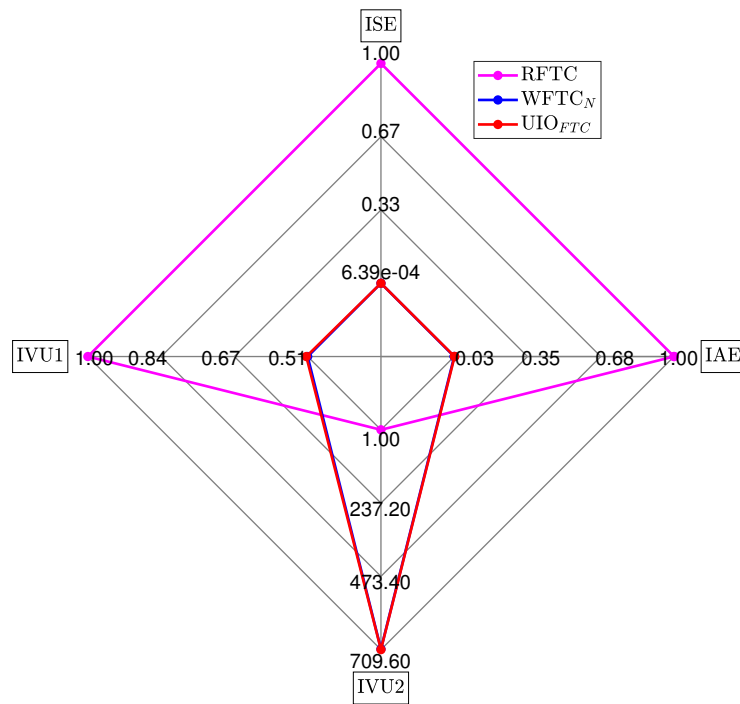


Figure 27: Performance indices for disturbance normalized with respect to RFTC.

Part III

FINAL DISCUSSIONS AND APPENDICES

CONCLUSIONS

This Thesis aims to develop new FTC strategies based on the fault hiding methodology for nonlinear systems. For this, reconfiguration blocks composed of virtual sensors and actuators are proposed, capable of ensuring the stability and performance of systems described by discrete-time TS fuzzy and LPV models, even in the presence of sensor and actuator faults. As discussed along this Thesis, different methodologies for the design of LPV and TS fuzzy reconfiguration blocks have been proposed in the literature, but they usually need to use different reconfiguration block designs for each type of fault. In order to overcome such limitations, this Thesis has presented new robust LPV and TS fuzzy reconfiguration blocks, capable of dealing with different types and magnitudes of sensor and actuator faults.

The methodology proposed in Chapter 3 provides improved fault hiding approach for nonlinear systems described by LPV models with input and output matrices dependent on time-varying parameters. This approach produces an LPV reconfiguration block that is robust to different fault scenarios and magnitudes by enabling to design a single reconfiguration block for a set of faults. Therefore, a single virtual sensor and virtual actuator design can be used throughout the execution of the control algorithm, being able to cover various types and magnitudes of faults that may occur. These faults can be of sensor and/or actuator, partial of different magnitudes and/or total faults. The effectiveness of the proposed methodology for the LPV case has been verified via experiments in a real-world nonlinear level-control process and it has been compared with other approaches found in the literature by means of performance indices. The experimental evaluation indicates that the proposed approach is able to mitigate the fault effects in different scenarios by means of the robust LPV virtual sensor and actuator. Furthermore, the IAE, IVU and ISE indices indicated that the performance of the reconfiguration blocks obtained by means of the proposed conditions outperform the literature results.

The FTC approach presented in Chapter 4 proposes a TS fuzzy reconfiguration block based on unknown input observer for systems with sensor and actuator faults and with unmeasured premise variables, even when these become unmea-

sured due to sensor faults. By describing the faults as additives, it is possible to design a virtual sensor and actuator with a smaller number of rules, since the input and output matrices of the faulty model do not depend on the indications of sensor and actuator faults. Thus, a single reconfiguration block design is carried out, which includes additive and multiplicative faults of different magnitudes, the latter being partial and/or total in both sensors and/or actuators. Furthermore, unlike other approaches in the literature, the system may have unmeasured premise variables and disturbances, and even so, the proposed FTC strategy continues to guarantee stability and performance similar to the nominal system. The efficiency for the TS fuzzy case has been assessed using computer simulations of the coupled tanks nonlinear system subject to different fault scenarios and disturbance. Through the analysis of graphs and performance indices, the time-responses of the system with the proposed reconfiguration block have been compared with those obtained by the closed-loop system without any FTC strategy implemented and with the system with the methodology proposed in Chapter 3. Thus, it has been possible to verify that, in all cases, only the reconfiguration block based on UIO of the Chapter 4 is able to ensure the stability and performance of the faulty system.

Therefore, the main results presented throughout this Thesis can be summarized as follows.

1. Novel sufficient LMI conditions for the design of virtual sensors and actuators for nonlinear systems described by LPV models with parameter-dependent input and output matrices. The reconfiguration block designed has the ISS guaranteed and ensures the IOS of the closed-loop system.
2. Novel sufficient LMI conditions for the design of virtual sensors and actuators based on UIO for nonlinear systems represented by TS fuzzy models with unmeasured premise variables and subject to disturbances. The reconfiguration block obtained is stable with guaranteed H_∞ performance and the performance of the faulty system is similar to the nominal one.
3. Inclusion of sensor and actuator faults in a polytopic representation of the faulty LPV model.
4. Novel robust LPV and TS fuzzy reconfiguration blocks composed of a virtual sensor and a virtual actuator. From its use, the closed-loop system has guaranteed stability for a set of faults. Thus, partial faults of different magnitudes are addressed, as well as total losses of sensors and actuators.

For the fuzzy TS case, additive faults of different magnitudes are also contemplated.

5. Evaluation and validation of the efficiency of the proposed LPV approach for real-time experiments in MIMO nonlinear level-control system in comparison with other methodologies. From the results obtained, a better performance is verified in different fault scenarios of the proposed reconfiguration block.
6. Verification and analysis of the performance obtained by the proposed TS fuzzy reconfiguration block, in comparison with the performance of the system without any FTC strategy implemented and with the proposed LPV methodology, through computer simulations and for a faulty system with unmeasured premise variables and subject to disturbances. Through the analysis of the obtained results, a better performance with the proposed FTC TS fuzzy strategy is observed.

As a possibility of continuing the work and future contributions, a limitation of the reconfiguration blocks as proposed in this work (Chapters 3 and 4) and in the literature [15, 20, 21, 23, 30] can be highlighted. This limitation is the explicit dependence on an FDI module to provide information about the faults, as seen in Assumption 2.1. The dynamics of the virtual sensor and actuator are directly related to this fault information, through fault indications expressed by time-varying parameters and by additive terms of faults. However, the fault estimation made by the FDI module may not indicate an event of fault or even to indicate a false alarm. Thus, the stability and performance of the closed-loop system can be deteriorated and a possible future direction is to investigate methodologies that guarantee stability and performance even in the presence of errors in the fault detection and isolation module. In the literature, different approaches are proposed, through the description of the uncertainties of fault estimation as disturbances [20], or with the use of an adaptive fault estimator together with a virtual sensor [29]. Both methodologies address the isolated case of a virtual actuator [20] or a virtual sensor [29]. Therefore, a future contribution would be the proposal of designing a robust reconfiguration block to different types of sensor and actuator faults with possibly errors in the FDI system and with unmeasured premise variables.

In addition, it is intended to implement the reconfiguration block proposed in Chapter 4, as well as the future methodologies to be developed, in the test

bed of coupled tanks, analyzing its performance in different fault scenarios, as presented in Section 4.4, in comparison to other strategies.

The results presented in Chapter 3 are based on the content of the following article published in the ISA Transactions and part of the results presented in Chapter 4 has been submitted in the Information Sciences.

- M. M. Quadros, I. V. Bessa, V. J. S. Leite, and R. M. Palhares. “Fault Tolerant Control for Linear Parameter Varying Systems: An Improved Robust Virtual Actuator and Sensor Approach”. In: *ISA Transactions* (2020). <https://doi.org/10.1016/j.isatra.2020.05.010>
- M. M. Quadros, V. J. S. Leite, and R. M. Palhares. “Robust Fault Hiding Approach for T–S Fuzzy Systems with Unmeasured Premise Variables”. *Submitted*.



CONTROLLER AND RECONFIGURATION BLOCK GAINS COMPUTED IN CHAPTER 3

A.1 CONTROLLER GAINS

$$\begin{aligned} K_1 &= \begin{bmatrix} -2.4034 & -2.0259 & 0.3192; & -1.8664 & -1.5732 & 0.2479 \end{bmatrix}; \\ K_2 &= \begin{bmatrix} -7.8176 & -1.3646 & 0.6772; & -6.0709 & -1.0597 & 0.5259 \end{bmatrix}; \\ K_3 &= \begin{bmatrix} -2.4280 & -2.0191 & 0.3189; & -1.8855 & -1.5680 & 0.2476 \end{bmatrix}; \\ K_4 &= \begin{bmatrix} -7.8202 & -1.4164 & 0.6781; & -6.0729 & -1.0999 & 0.5266 \end{bmatrix}; \\ K_5 &= \begin{bmatrix} -3.0544 & -1.2427 & 0.3020; & -2.3719 & -0.9650 & 0.2345 \end{bmatrix}; \\ K_6 &= \begin{bmatrix} -7.9322 & -1.2667 & 0.6781; & -6.1599 & -0.9837 & 0.5266 \end{bmatrix}; \\ K_7 &= \begin{bmatrix} -3.0590 & -1.2603 & 0.3010; & -2.3755 & -0.9787 & 0.2338 \end{bmatrix}; \\ K_8 &= \begin{bmatrix} -7.9324 & -1.3247 & 0.6789; & -6.1600 & -1.0287 & 0.5272 \end{bmatrix}. \end{aligned} \tag{A.1}$$

A.2 VIRTUAL SENSOR GAINS

$$\begin{aligned} L_{1,2,3,4} &= \begin{bmatrix} -0.3191 & -1.0587 \\ -0.0266 & -1.2246 \end{bmatrix}; & L_{5,6,7,8} &= \begin{bmatrix} -0.3313 & -3.0296 \\ -0.0413 & -3.2741 \end{bmatrix}; \\ L_{9,10,11,12} &= \begin{bmatrix} -0.2895 & -1.2636 \\ -0.0229 & -1.2404 \end{bmatrix}; & L_{13,14,15,16} &= \begin{bmatrix} -0.3266 & -3.7168 \\ -0.0335 & -3.3358 \end{bmatrix}; \\ L_{17,18,19,20} &= \begin{bmatrix} -0.5840 & -0.8513 \\ -0.0245 & -1.2266 \end{bmatrix}; & L_{21,22,23,24} &= \begin{bmatrix} -0.6018 & -2.6222 \\ -0.0413 & -3.2700 \end{bmatrix}; \\ L_{25,26,27,28} &= \begin{bmatrix} -0.4709 & -1.2924 \\ -0.0195 & -1.2425 \end{bmatrix}; & L_{29,30,31,32} &= \begin{bmatrix} -0.4489 & -3.9588 \\ -0.0306 & -3.3428 \end{bmatrix}; \end{aligned}$$

$$\begin{aligned}
L_{33,34,35,36} &= \begin{bmatrix} -0.3191 & -1.0587 \\ -0.0267 & -1.2697 \end{bmatrix}; & L_{37,38,39,40} &= \begin{bmatrix} -0.3193 & -3.0856 \\ -0.0417 & -3.3891 \end{bmatrix}; \\
L_{41,42,43,44} &= \begin{bmatrix} -0.2895 & -1.2636 \\ -0.0230 & -1.2855 \end{bmatrix}; & L_{45,46,47,48} &= \begin{bmatrix} -0.3243 & -3.7020 \\ -0.0349 & -3.4408 \end{bmatrix}; \\
L_{49,50,51,52} &= \begin{bmatrix} -0.5840 & -0.8513 \\ -0.0246 & -1.2717 \end{bmatrix}; & L_{53,54,55,56} &= \begin{bmatrix} -0.5853 & -2.7282 \\ -0.0429 & -3.3807 \end{bmatrix}; \\
L_{57,58,59,60} &= \begin{bmatrix} -0.4709 & -1.2925 \\ -0.0195 & -1.2876 \end{bmatrix}; & L_{61,62,63,64} &= \begin{bmatrix} -0.4206 & -3.8292 \\ -0.0228 & -3.5039 \end{bmatrix}; \\
L_{65,66,67,68} &= \begin{bmatrix} -0.4486 & -0.9561 \\ -0.0160 & -1.2333 \end{bmatrix}; & L_{69,70,71,72} &= \begin{bmatrix} -0.4643 & -2.8285 \\ -0.0326 & -3.2834 \end{bmatrix}; \\
L_{73,74,75,76} &= \begin{bmatrix} -0.3979 & -1.2551 \\ -0.0131 & -1.2424 \end{bmatrix}; & L_{77,78,79,80} &= \begin{bmatrix} -0.4403 & -3.8650 \\ -0.0244 & -3.3284 \end{bmatrix}; \\
L_{81,82,83,84} &= \begin{bmatrix} -0.5902 & -0.8474 \\ -0.0152 & -1.2341 \end{bmatrix}; & L_{85,86,87,88} &= \begin{bmatrix} -0.6109 & -2.6083 \\ -0.0334 & -3.2774 \end{bmatrix}; \\
L_{89,90,91,92} &= \begin{bmatrix} -0.4523 & -1.2383 \\ -0.0094 & -1.2431 \end{bmatrix}; & L_{93,94,95,96} &= \begin{bmatrix} -0.4521 & -3.8174 \\ -0.0088 & -3.3852 \end{bmatrix}; \\
L_{97,98,99,100} &= \begin{bmatrix} -0.4486 & -0.9561 \\ -0.0161 & -1.2784 \end{bmatrix}; & L_{101,102,103,104} &= \begin{bmatrix} -0.4483 & -2.9215 \\ -0.0345 & -3.3911 \end{bmatrix}; \\
L_{105,106,107,108} &= \begin{bmatrix} -0.3979 & -1.2552 \\ -0.0131 & -1.2875 \end{bmatrix}; & L_{109,110,111,112} &= \begin{bmatrix} -0.4380 & -3.9001 \\ -0.0265 & -3.4366 \end{bmatrix}; \\
L_{113,114,115,116} &= \begin{bmatrix} -0.5901 & -0.8474 \\ -0.0152 & -1.2792 \end{bmatrix}; & L_{117,118,119,120} &= \begin{bmatrix} -0.5947 & -2.7351 \\ -0.0366 & -3.3792 \end{bmatrix}; \\
L_{121,122,123,124} &= \begin{bmatrix} -0.4414 & -1.2213 \\ -0.0013 & -1.2879 \end{bmatrix}; & L_{125,126,217,128} &= \begin{bmatrix} -0.4575 & -3.8377 \\ -0.0163 & -3.4656 \end{bmatrix}.
\end{aligned}$$

(A.2)

A.3 VIRTUAL ACTUATOR GAINS

$$\begin{aligned}
M_{1,5,9,13} &= \begin{bmatrix} -3.1631 & -6.3457 \\ -1.1029 & -1.0082 \end{bmatrix}; & M_{2,6,10,14} &= \begin{bmatrix} -3.8300 & -6.9745 \\ -0.1185 & -0.1661 \end{bmatrix}; \\
M_{3,7,11,15} &= \begin{bmatrix} -3.4090 & -8.5158 \\ -1.9079 & -2.8006 \end{bmatrix}; & M_{4,8,12,16} &= \begin{bmatrix} -4.5262 & -10.2217 \\ -0.3651 & -0.5845 \end{bmatrix}; \\
M_{17,21,25,29} &= \begin{bmatrix} -13.3957 & -10.6644 \\ -3.0753 & -1.6469 \end{bmatrix}; & M_{18,22,26,30} &= \begin{bmatrix} -14.2618 & -11.1269 \\ -2.3644 & -1.2764 \end{bmatrix}; \\
M_{19,23,27,31} &= \begin{bmatrix} -15.3126 & -12.1013 \\ -3.6672 & -2.0190 \end{bmatrix}; & M_{20,24,28,32} &= \begin{bmatrix} -16.5737 & -12.8469 \\ -2.7795 & -1.5034 \end{bmatrix}; \\
M_{33,37,41,45} &= \begin{bmatrix} -3.1627 & -6.4470 \\ -1.1018 & -0.9659 \end{bmatrix}; & M_{34,38,42,46} &= \begin{bmatrix} -3.8291 & -7.0416 \\ -0.1179 & -0.1499 \end{bmatrix}; \\
M_{35,39,43,47} &= \begin{bmatrix} -3.4140 & -8.7009 \\ -1.9030 & -2.7373 \end{bmatrix}; & M_{36,40,44,48} &= \begin{bmatrix} -4.5300 & -10.3642 \\ -0.3597 & -0.5357 \end{bmatrix}; \\
M_{49,53,57,61} &= \begin{bmatrix} -13.4187 & -11.0317 \\ -3.0691 & -1.6651 \end{bmatrix}; & M_{50,54,58,62} &= \begin{bmatrix} -14.2876 & -11.5067 \\ -2.3565 & -1.2842 \end{bmatrix}; \\
M_{51,55,59,63} &= \begin{bmatrix} -15.4441 & -12.6391 \\ -3.6053 & -1.9876 \end{bmatrix}; & M_{52,56,60,64} &= \begin{bmatrix} -16.9943 & -13.5131 \\ -2.5008 & -1.3258 \end{bmatrix}; \\
M_{65,69,73,77} &= \begin{bmatrix} -4.4998 & -5.0346 \\ -1.5966 & -0.5153 \end{bmatrix}; & M_{66,70,74,78} &= \begin{bmatrix} -5.4678 & -5.3739 \\ -0.1611 & -0.1039 \end{bmatrix}; \\
M_{67,71,75,79} &= \begin{bmatrix} -4.7944 & -7.1867 \\ -2.7370 & -1.9933 \end{bmatrix}; & M_{68,72,76,80} &= \begin{bmatrix} -6.4097 & -8.4080 \\ -0.5112 & -0.4219 \end{bmatrix}; \\
M_{81,85,89,93} &= \begin{bmatrix} -13.4932 & -10.5310 \\ -3.1087 & -1.6232 \end{bmatrix}; & M_{82,86,90,94} &= \begin{bmatrix} -14.3696 & -10.9744 \\ -2.3893 & -1.2611 \end{bmatrix}; \\
M_{83,87,91,95} &= \begin{bmatrix} -15.4176 & -11.8800 \\ -3.7121 & -2.0034 \end{bmatrix}; & M_{84,88,92,96} &= \begin{bmatrix} -16.6925 & -12.5607 \\ -2.8235 & -1.5212 \end{bmatrix};
\end{aligned}$$

$$\begin{aligned}
M_{97,101,105,109} &= \begin{bmatrix} -4.5408 & -5.0584 \\ -1.5348 & -0.4489 \end{bmatrix}; & M_{98,102,106,110} &= \begin{bmatrix} -5.5263 & -5.3654 \\ -0.0184 & -0.0040 \end{bmatrix}; \\
M_{99,103,107,111} &= \begin{bmatrix} -4.8110 & -7.3219 \\ -2.6962 & -1.8506 \end{bmatrix}; & M_{100,104,108,112} &= \begin{bmatrix} -6.3388 & -8.4226 \\ -0.2744 & -0.2186 \end{bmatrix}; \\
M_{113,117,121,125} &= \begin{bmatrix} -13.6041 & -10.6640 \\ -3.0891 & -1.5653 \end{bmatrix}; & M_{114,118,122,126} &= \begin{bmatrix} -14.4879 & -11.1098 \\ -2.3633 & -1.2008 \end{bmatrix}; \\
M_{115,119,123,127} &= \begin{bmatrix} -15.6925 & -12.1643 \\ -3.6284 & -1.9281 \end{bmatrix}; & M_{116,120,124,128} &= \begin{bmatrix} -17.0792 & -12.8991 \\ -2.6345 & -1.4089 \end{bmatrix}.
\end{aligned}$$

(A.3)

B

CONTROLLER AND RECONFIGURATION BLOCK GAINS COMPUTED IN CHAPTER 4

B.1 CONTROLLER GAINS

$$\begin{aligned} K_1 &= \begin{bmatrix} -2.9282 & -1.0485 & 0.3142; & -2.2905 & -0.8201 & 0.2458 \end{bmatrix}; \\ K_2 &= \begin{bmatrix} -3.2069 & -0.6802 & 0.3053; & -2.5085 & -0.5320 & 0.2388 \end{bmatrix}; \\ K_3 &= \begin{bmatrix} -6.7700 & -0.8506 & 0.6457; & -5.2956 & -0.6654 & 0.5051 \end{bmatrix}; \\ K_4 &= \begin{bmatrix} -6.8463 & -0.7672 & 0.6440; & -5.3553 & -0.6001 & 0.5038 \end{bmatrix}. \end{aligned} \tag{B.1}$$

B.2 TS FUZZY VIRTUAL SENSOR GAINS

$$\begin{aligned} L_1 &= \begin{bmatrix} 0.7317 & 0.2683; & 0 & 0 \end{bmatrix}; \\ L_2 &= \begin{bmatrix} 0.8471 & 0.1529; & 0 & 0 \end{bmatrix}; \\ L_3 &= \begin{bmatrix} 0.9642 & 0.0358; & 0 & 0 \end{bmatrix}; \\ L_4 &= \begin{bmatrix} 0.9796 & 0.0204; & 0 & 0 \end{bmatrix}. \end{aligned} \tag{B.2}$$

B.3 TS FUZZY VIRTUAL ACTUATOR GAINS

$$\begin{aligned} M_1 &= \begin{bmatrix} -3.8575 & -1.4147; & -3.0175 & -1.1066 \end{bmatrix}; \\ M_2 &= \begin{bmatrix} -4.4660 & -0.8062; & -3.4935 & -0.6306 \end{bmatrix}; \\ M_3 &= \begin{bmatrix} -11.3758 & -0.4223; & -8.8988 & -0.3303 \end{bmatrix}; \\ M_4 &= \begin{bmatrix} -11.5575 & -0.2406; & -9.0409 & -0.1883 \end{bmatrix}. \end{aligned} \tag{B.3}$$

BIBLIOGRAPHY

- [1] J. D. Stefanovski. “Fault Tolerant Control of Descriptor Systems With Disturbances.” In: *IEEE Transactions on Automatic Control* 64.3 (2019), pp. 976–988. ISSN: 0018-9286. DOI: 10.1109/TAC.2018.2827702.
- [2] G. Yang and D. Ye. “Reliable H_∞ Control of Linear Systems With Adaptive Mechanism.” In: *IEEE Transactions on Automatic Control* 55.1 (2009), pp. 242–247. DOI: 10.1109/TAC.2009.2036293.
- [3] S. Sun, H. Zhang, Y. Wang, and Y. Cai. “Dynamic output feedback-based fault-tolerant control design for T–S fuzzy systems with model uncertainties.” In: *ISA Transactions* 81 (2018), pp. 32–45. DOI: 10.1016/j.isatra.2018.07.022.
- [4] J. Lunze and J. Richter. “Reconfigurable Fault-tolerant Control: A Tutorial Introduction.” In: *European Journal of Control* 14.5 (2008), pp. 359–386. ISSN: 0947-3580. DOI: 10.3166/ejc.14.359–386.
- [5] M. Fleps-Dezasse, F. Svaricek, and J. Brembeck. “Design and Experimental Assessment of an Active Fault-Tolerant LPV Vertical Dynamics Controller.” In: *IEEE Transactions on Control Systems Technology* 27.3 (2019), pp. 1267–1274. ISSN: 1063-6536. DOI: 10.1109/TCST.2018.2796066.
- [6] J. Lunze and T. Steffen. “Control reconfiguration after actuator failures using disturbance decoupling methods.” In: *IEEE Transactions on Automatic Control* 51.10 (2006), pp. 1590–1601. DOI: 10.1109/TAC.2006.882938.
- [7] A. Bounemeur, M. Chemachema, and N. Essounbouli. “Indirect adaptive fuzzy fault-tolerant tracking control for MIMO nonlinear systems with actuator and sensor failures.” In: *ISA Transactions* 79 (2018), pp. 45–61. DOI: 10.1016/j.isatra.2018.04.014.
- [8] N. Pizzi, E. Kofman, J. A. De Doná, and M. M. Seron. “Actuator fault tolerant control based on probabilistic ultimate bounds.” In: *ISA Transactions* 84 (2019), pp. 20–30. DOI: 10.1016/j.isatra.2018.08.021.

- [9] L. B. Cosme, W. M. Caminhas, M. F. S. V. D'Angelo, and R. M. Palhares. "A novel fault-prognostic approach based on interacting multiple model filters and fuzzy systems." In: *IEEE Transactions on Industrial Electronics* 66.1 (2019), pp. 519–528.
- [10] L. B. Cosme, M. F. D'Angelo, W. M. Caminhas, S. Yin, and R. M. Palhares. "A novel fault prognostic approach based on particle filters and differential evolution." In: *Applied Intelligence* 48.4 (2018), pp. 834–853.
- [11] T. A. Nakamura, R. M. Palhares, W. M. Caminhas, B. R. Menezes, M. C. M. de Campos, U. Fumega, C. H. Bomfim, and A. P. Lemos. "Adaptive fault detection and diagnosis using parsimonious Gaussian mixture models trained with distributed computing techniques." In: *Journal of the Franklin Institute* 354.6 (2017), pp. 2543–2572.
- [12] T. Steffen. *Control reconfiguration of dynamical systems: Linear approaches and structural tests*. Springer Berlin Heidelberg, 2005.
- [13] D. Rotondo, A. Cristofaro, and T. Johansen. "Fault tolerant control of uncertain dynamical systems using interval virtual actuators." In: *International Journal of Robust and Nonlinear Control* 28.2 (2018), pp. 611–624. ISSN: 1099-1239. DOI: 10.1002/rnc.3888.
- [14] J. Richter. *Reconfigurable control of nonlinear dynamical systems: A fault-hiding approach*. Lecture Notes in Control and Information Sciences. Springer Berlin Heidelberg, 2011. ISBN: 9783642176272.
- [15] I. Bessa, V. Puig, and R. M. Palhares. "TS fuzzy reconfiguration blocks for fault tolerant control of nonlinear systems." In: *Journal of the Franklin Institute* 357.8 (2020), pp. 4592–4623. DOI: 10.1016/j.jfranklin.2020.02.002.
- [16] I. Bessa, V. Puig, and R. M. Palhares. "Passivation blocks for fault tolerant control of nonlinear systems." In: *Automatica* 125 (2021), p. 109450. DOI: 10.1016/j.automatica.2020.109450.
- [17] J. Richter and J. Lunze. "Reconfigurable control of Hammerstein systems after actuator failures: Stability, tracking, and performance." In: *International Journal of Control* 83.8 (2010), pp. 1612–1630. ISSN: 0020-7179. DOI: 10.1080/00207179.2010.484072.

- [18] J. Richter, W. Heemels, N. Wouw, and J. Lunze. “Reconfigurable control of piecewise affine systems with actuator and sensor faults: Stability and tracking.” In: *Automatica* 47.4 (2011), pp. 678–691. ISSN: 0005-1098. DOI: 10.1016/j.automatica.2011.01.048.
- [19] A. Pedersen, J. Richter, M. Tabatabaeipour, H. Jóhannsson, and M. Blanke. “Fault tolerant emergency control to preserve power system stability.” In: *Control Engineering Practice* 53 (2016), pp. 151–159. ISSN: 0967-0661. DOI: 10.1016/j.conengprac.2015.11.004.
- [20] D. Rotondo, F. Nejjari, and V. Puig. “Fault tolerant control of a proton exchange membrane fuel cell using Takagi–Sugeno virtual actuators.” In: *Journal of Process Control* 45 (2016), pp. 12–29. ISSN: 0959-1524. DOI: 10.1016/j.jprocont.2016.06.001.
- [21] S. M. Tabatabaeipour, J. Stoustrup, and T. Bak. “Fault-tolerant control of discrete-time LPV systems using virtual actuators and sensors.” In: *International Journal of Robust and Nonlinear Control* 25.5 (2015), pp. 707–734. DOI: 10.1002/rnc.3194.
- [22] D. Rotondo, V. Puig, F. Nejjari, and J. Romera. “A fault-hiding approach for the switching quasi-LPV fault-tolerant control of a four-wheeled omnidirectional mobile robot.” In: *IEEE Transactions on Industrial Electronics* 62.6 (2015), pp. 3932–3944. ISSN: 0278-0046. DOI: 10.1109/TIE.2014.2367002.
- [23] D. Rotondo, F. Nejjari, and V. Puig. “A virtual actuator and sensor approach for fault tolerant control of LPV systems.” In: *Journal of Process Control* 24.3 (2014), pp. 203–222. DOI: 10.1016/j.jprocont.2013.12.016.
- [24] D. Rotondo, F. Nejjari, V. Puig, and J. Blesa. “Model reference FTC for LPV systems using virtual actuators and set-membership fault estimation.” In: *International Journal of Robust and Nonlinear Control* 25.5 (2015), pp. 735–760. ISSN: 1099-1239. DOI: 10.1002/rnc.3258.
- [25] J. Blesa, D. Rotondo, V. Puig, and F. Nejjari. “FDI and FTC of wind turbines using the interval observer approach and virtual actuators/sensors.” In: *Control Engineering Practice* 24 (2014), pp. 138–155. ISSN: 0967-0661. DOI: 10.1016/j.conengprac.2013.11.018.

- [26] D. Wu, J. Song, Y. Shen, and Z. Ji. “Active fault-tolerant linear parameter varying control for the pitch actuator of wind turbines.” In: *Nonlinear Dynamics* 87.1 (2017), pp. 475–487. ISSN: 1573-269X. DOI: 10.1007/s11071-016-3054-0.
- [27] R. Nazari, M. M. Seron, and J. A. D. Doná. “Actuator fault tolerant control of systems with polytopic uncertainties using set-based diagnosis and virtual-actuator-based reconfiguration.” In: *Automatica* 75 (2017), pp. 182–190. ISSN: 0005-1098. DOI: 10.1016/j.automatica.2016.09.012.
- [28] D. Rotondo, H. S. Sánchez, V. Puig, T. Escobet, and J. Quevedo. “A virtual actuator approach for the secure control of networked LPV systems under pulse-width modulated DoS attacks.” In: *Neurocomputing* 365 (2019), pp. 21–30. ISSN: 0925-2312. DOI: 10.1016/j.neucom.2019.06.050.
- [29] H. Behzad, A. Casavola, F. Tedesco, and M. A. Sadrnia. “Fault-tolerant sensor reconciliation schemes based on unknown input observers.” In: *International Journal of Control* 93.3 (2020), pp. 669–679.
- [30] A. Filasová, D. Krokavec, and P. Liščinský. “Relaxed formulation of the design conditions for Takagi–Sugeno fuzzy virtual actuators.” In: *Archives of Control Sciences* 26.2 (2016), pp. 199–221. DOI: 10.1515/acsc-2016-0012.
- [31] D. Ichalal, B. Marx, J. Ragot, and D. Maquin. “State estimation of Takagi–Sugeno systems with unmeasurable premise variables.” In: *IET Control Theory & Applications* 4.5 (2010), pp. 897–908.
- [32] T. M. Guerra, R. Márquez, A. Kruszewski, and M. Bernal. “ \mathcal{H}_∞ LMI-based observer design for nonlinear systems via Takagi–Sugeno models with unmeasured premise variables.” In: *IEEE Transactions on Fuzzy Systems* 26.3 (2017), pp. 1498–1509.
- [33] A.-T. Nguyen, J. Pan, T.-M. Guerra, and Z. Wang. “Avoiding Unmeasured Premise Variables in Designing Unknown Input Observers for Takagi–Sugeno Fuzzy Systems.” In: *IEEE Control Systems Letters* 5.1 (2020), pp. 79–84.
- [34] D. Quintana, V. Estrada-Manzo, and M. Bernal. “An exact handling of the gradient for overcoming persistent problems in nonlinear observer design via convex optimization techniques.” In: *Fuzzy Sets and Systems* 416.30 (2021), pp. 125–140.

- [35] J. Pan, A.-T. Nguyen, T.-M. Guerra, and D. Ichalal. “A unified framework for asymptotic observer design of fuzzy systems with unmeasurable premise variables.” In: *IEEE Transactions on Fuzzy Systems* (2020).
- [36] X.-K. Du, H. Zhao, and X.-H. Chang. “Unknown input observer design for fuzzy systems with uncertainties.” In: *Applied Mathematics and Computation* 266 (2015), pp. 108–118.
- [37] J. Li, Z. Wang, Y. Shen, and Y. Liu. “Unknown input observer design for Takagi-Sugeno systems with fuzzy output equation.” In: *International Journal of Control, Automation and Systems* 17.1 (2019), pp. 267–272.
- [38] M. M. Quadros, I. V. Bessa, V. J. S. Leite, and R. M. Palhares. “Fault tolerant control for linear parameter varying systems: An improved robust virtual actuator and sensor approach.” In: *ISA Transactions* 104 (2020), pp. 356–369. DOI: 10.1016/j.isatra.2020.05.010.
- [39] J. S. Shamma. “An overview of LPV systems.” In: *Control of linear parameter varying systems with applications*. Ed. by J. Mohammadpour and C. W. Scherer. Springer, 2012, pp. 3–26.
- [40] M. Lovera, M. Bergamasco, and F. Casella. “LPV modelling and identification: An overview.” In: *Robust Control and Linear Parameter Varying Approaches*. Ed. by O. Sename, G. Péter, and J. Bokor. Springer, 2013, pp. 3–24.
- [41] C. Briat. *Linear Parameter-Varying and Time-Delay Systems: Analysis, Observation, Filtering & Control*. Springer-Verlag Berlin Heidelberg, 2015.
- [42] J. S. Shamma. “Analysis and design of gain scheduled control systems.” PhD thesis. Massachusetts Institute of Technology, 1988.
- [43] M. B. A. Jabali and M. H. Kazemi. “Uncertain polytopic LPV modelling of robot manipulators and trajectory tracking.” In: *International Journal of Control, Automation and Systems* 15.2 (2017), pp. 883–891.
- [44] A. Kwiatkowski and H. Werner. “LPV Control of a 2-DOF Robot Using Parameter Reduction.” In: *Proceedings of the 44th IEEE Conference on Decision and Control*. 2005, pp. 3369–3374.
- [45] F. D. Adegas, C. Sloth, and J. Stoustrup. “Structured linear parameter varying control of wind turbines.” In: *Control of Linear Parameter Varying Systems with Applications*. Springer, 2012, pp. 303–337.

- [46] F. Bianchi, R. Mantz, and C. Christiansen. “Gain scheduling control of variable-speed wind energy conversion systems using quasi-LPV models.” In: *Control Engineering Practice* 13.2 (2005), pp. 247–255. ISSN: 0967-0661. DOI: <https://doi.org/10.1016/j.conengprac.2004.03.006>.
- [47] M. Pakmehr, N. Fitzgerald, E. M. Feron, J. S. Shamma, and A. Behbahani. “Gain scheduled control of gas turbine engines: Stability and verification.” In: *Journal of engineering for Gas turbines and power* 136.3 (2014).
- [48] B. Lu, F. Wu, and S. Kim. “Switching LPV control of an F-16 aircraft via controller state reset.” In: *IEEE Transactions on Control Systems Technology* 14.2 (2006), pp. 267–277.
- [49] B. White, L. Bruyere, and A. Tsourdos. “Missile autopilot design using quasi-LPV polynomial eigenstructure assignment.” In: *IEEE Transactions on Aerospace and Electronic Systems* 43.4 (2007), pp. 1470–1483.
- [50] L. C. A. Souza and R. M. Palhares. “Parameter estimation on linear time-varying systems.” In: *Journal of the Franklin Institute* 348.4 (2011), pp. 777–789.
- [51] L. A. Mozelli and R. M. Palhares. “Stability analysis of linear time-varying systems: improving conditions by adding more information about parameter variation.” In: *Systems & Control Letters* 60.5 (2011), pp. 338–343.
- [52] M. L. C. Peixoto, P. S. P. Pessim, M. J. Lacerda, and R. M. Palhares. “Stability and Stabilization for LPV systems based on Lyapunov functions with non-monotonic terms.” In: *Journal of the Franklin Institute* (2021), (To appear). DOI: [10.1016/j.jfranklin.2020.04.019](https://doi.org/10.1016/j.jfranklin.2020.04.019).
- [53] M. L. C. Peixoto, M. J. Lacerda, and R. M. Palhares. “On Discrete-Time LPV Control Using Delayed Lyapunov Functions.” In: *Asian Journal of Control* (2021), (To appear). DOI: [10.1002/asjc.2362](https://doi.org/10.1002/asjc.2362).
- [54] J. M. Gomes da Silva Jr., A. H. K. Palmeira, V. M. Moraes, and J. V. Flores. “ \mathcal{L}_2 -disturbance attenuation for LPV systems under sampled-data control.” In: *International Journal of Robust and Nonlinear Control* 28.16 (2018), pp. 5019–5032.
- [55] J. C. Geromel and P. Colaneri. “Robust stability of time varying polytopic systems.” In: *Systems & Control Letters* 55.1 (2006), pp. 81–85.

- [56] G. Chesi, A. Garulli, A. Tesi, and A. Vicino. “Robust stability of time-varying polytopic systems via parameter-dependent homogeneous Lyapunov functions.” In: *Automatica* 43.2 (2007), pp. 309–316.
- [57] W. J. Rugh and J. S. Shamma. “Research on gain scheduling.” In: *Automatica* 36.10 (2000), pp. 1401–1425.
- [58] T. Takagi and M. Sugeno. “Fuzzy identification of systems and its applications to modeling and control.” In: *IEEE Transactions on Systems, Man, and Cybernetics* 1 (1985), pp. 116–132.
- [59] M. Sugeno and G. Kang. “Structure identification of fuzzy model.” In: *Fuzzy sets and systems* 28.1 (1988), pp. 15–33.
- [60] H. O. Wang, K. Tanaka, and M. F. Griffin. “An approach to fuzzy control of nonlinear systems: Stability and design issues.” In: *IEEE Transactions on Fuzzy Systems* 4.1 (1996), pp. 14–23.
- [61] T. Taniguchi, K. Tanaka, H. Ohtake, and H. O. Wang. “Model construction, rule reduction, and robust compensation for generalized form of Takagi-Sugeno fuzzy systems.” In: *IEEE Transactions on Fuzzy Systems* 9.4 (2001), pp. 525–538.
- [62] T. M. Guerra, A. Sala, and K. Tanaka. “Fuzzy control turns 50: 10 years later.” In: *Fuzzy sets and systems* 281 (2015), pp. 168–182.
- [63] A.-T. Nguyen, T. Taniguchi, L. Eciolaza, V. Campos, R. Palhares, and M. Sugeno. “Fuzzy control systems: Past, present and future.” In: *IEEE Computational Intelligence Magazine* 14.1 (2019), pp. 56–68.
- [64] K. Tanaka and H. O. Wang. *Fuzzy control systems design and analysis: a linear matrix inequality approach*. John Wiley & Sons, 2004.
- [65] M. C. M. Teixeira, E. Assunção, and R. G. Avellar. “On relaxed LMI-based designs for fuzzy regulators and fuzzy observers.” In: *IEEE Transactions on Fuzzy Systems* 11.5 (2003), pp. 613–623.
- [66] M. Johansson, A. Rantzer, and K.-E. Arzen. “Piecewise quadratic stability of fuzzy systems.” In: *IEEE Transactions on Fuzzy Systems* 7.6 (1999), pp. 713–722.
- [67] K. Tanaka, T. Kosaki, and H. O. Wang. “Backing control problem of a mobile robot with multiple trailers: fuzzy modeling and LMI-based design.” In: *IEEE Transactions on Systems, Man, and Cybernetics, Part C (Applications and Reviews)* 28.3 (1998), pp. 329–337.

- [68] F. Sun, L. Li, H.-X. Li, and H. Liu. “Neuro-fuzzy dynamic-inversion-based adaptive control for robotic manipulators—Discrete time case.” In: *IEEE Transactions on Industrial Electronics* 54.3 (2007), pp. 1342–1351.
- [69] Y.-W. Liang, S.-D. Xu, D.-C. Liaw, and C.-C. Chen. “A study of T–S model-based SMC scheme with application to robot control.” In: *IEEE Transactions on Industrial Electronics* 55.11 (2008), pp. 3964–3971.
- [70] A. N. D. Lopes, V. J. S. Leite, L. F. P. Silva, and K. Guelton. “Anti-windup TS Fuzzy PI-like Control for Discrete-Time Nonlinear Systems with Saturated Actuators.” In: *International Journal of Fuzzy Systems* (2020), pp. 46–61. DOI: 10.1007/s40815-019-00781-0.
- [71] R.-E. Precup, M. L. Tomescu, M.-B. Rădac, E. M. Petriu, S. Preitl, and C.-A. Dragoş. “Iterative performance improvement of fuzzy control systems for three tank systems.” In: *Expert Systems with Applications* 39.9 (2012), pp. 8288–8299.
- [72] S. Bououden, M. Chadli, S. Filali, and A. El Hajjaji. “Fuzzy model based multivariable predictive control of a variable speed wind turbine: LMI approach.” In: *Renewable Energy* 37.1 (2012), pp. 434–439.
- [73] S. Mishra, Y. Mishra, F. Li, and Z. Y. Dong. “TS-fuzzy controlled DFIG based wind energy conversion systems.” In: *2009 IEEE Power & Energy Society General Meeting*. IEEE. 2009, pp. 1–7.
- [74] P. Hušek and K. Narenathreyas. “Aircraft longitudinal motion control based on Takagi–Sugeno fuzzy model.” In: *Applied Soft Computing* 49 (2016), pp. 269–278.
- [75] S. Behzadimanesh, A. Fatehi, and S. Fakhimi Derakhshan. “Optimal fuzzy controller based on non-monotonic Lyapunov function with a case study on laboratory helicopter.” In: *International Journal of Systems Science* 50.3 (2019), pp. 652–667.
- [76] R. F. Araújo, L. A. Torres, and R. M. Palhares. “Distributed control of networked nonlinear systems via interconnected Takagi-Sugeno fuzzy systems with nonlinear consequent.” In: *IEEE Transactions on Systems, Man, and Cybernetics: Systems* 51.8 (2021), pp. 4858–4867. DOI: 10.1109/TSMC.2019.2945500.

- [77] P. H. Coutinho, R. F. Araújo, A.-T. Nguyen, and R. M. Palhares. “A Multiple-parameterization approach for local stabilization of constrained Takagi-Sugeno fuzzy systems with nonlinear consequents.” In: *Information Sciences* 506 (2020), pp. 295–307.
- [78] R. F. Araújo, P. H. S. Coutinho, A.-T. Nguyen, and R. M. Palhares. “Delayed nonquadratic \mathcal{L}_2 -stabilization of continuous-time nonlinear Takagi–Sugeno fuzzy models.” In: *Information Sciences* 563 (2021), pp. 59–69. DOI: 10.1016/j.ins.2021.01.007.
- [79] P. H. S. Coutinho, J. Lauber, M. Bernal, and R. M. Palhares. “Efficient LMI conditions for enhanced stabilization of discrete-time Takagi–Sugeno models via delayed nonquadratic Lyapunov functions.” In: *IEEE Transactions on Fuzzy Systems* 27.9 (2019), pp. 1833–1843.
- [80] V. C. Campos, F. O. Souza, L. A. Torres, and R. M. Palhares. “New stability conditions based on piecewise fuzzy Lyapunov functions and tensor product transformations.” In: *IEEE Transactions on Fuzzy Systems* 21.4 (2012), pp. 748–760.
- [81] L. A. Mozelli, R. M. Palhares, F. Souza, and E. M. Mendes. “Reducing conservativeness in recent stability conditions of TS fuzzy systems.” In: *Automatica* 45.6 (2009), pp. 1580–1583.
- [82] L. A. Mozelli, R. M. Palhares, and G. S. Avellar. “A systematic approach to improve multiple Lyapunov function stability and stabilization conditions for fuzzy systems.” In: *Information Sciences* 179.8 (2009), pp. 1149–1162.
- [83] L. F. P. Silva, V. J. S. Leite, E. B. Castelan, and C. de Souza. “Regional input-to-state stabilization of fuzzy state-delayed discrete-time systems with saturating actuators.” In: *Information Sciences* 557 (2021), pp. 250–267.
- [84] A. Z. N. Lazarini, M. C. M. Teixeira, J. M. De S. Ribeiro, E. Assunção, R. Cardim, and A. S. Buzetti. “Relaxed Stabilization Conditions for TS Fuzzy Systems With Optimal Upper Bounds for the Time Derivative of Fuzzy Lyapunov Functions.” In: *IEEE Access* 9 (2021), pp. 64945–64957. DOI: 10.1109/ACCESS.2021.3076030.

- [85] E. D. Sontag. “Input to state stability: Basic concepts and results.” In: *Nonlinear and optimal control theory*. Ed. by P. Nistri and G. Stefani. Vol. 1932. Berlin: Springer, 2008, pp. 163–220. DOI: 10.1007/978-3-540-77653-6_3.
- [86] Z. Jiang and Y. Wang. “Input-to-state stability for discrete-time nonlinear systems.” In: *Automatica* 37.6 (2001), pp. 857–869. DOI: 10.1016/S0005-1098(01)00028-0.
- [87] H. K. Khalil. *Nonlinear systems*. 3rd. Prentice Hall, 2002.
- [88] Z.-P. Jiang and I. Marcell. “A small-gain control method for nonlinear cascaded systems with dynamic uncertainties.” In: *IEEE Transactions on Automatic Control* 42.3 (1997), pp. 292–308.
- [89] Z.-P. Jiang and Y. Wang. “Small gain theorems on input-to-output stability.” In: *Dynamics of Continuous, Discrete and Impulsive Systems Series B: Applications and Algorithms* (Jan. 2003).
- [90] Jiang Zhongping, Lin Yuandan, and Wang Yuan. “Nonlinear small-gain theorems for discrete-time large-scale systems.” In: *Proceedings of 2008 27th Chinese Control Conference*. 2008, pp. 704–708.
- [91] R. M. Palhares, R. H. C. Takahashi, and P. L. D. Peres. “ \mathcal{H}_∞ and \mathcal{H}_2 guaranteed costs computation for uncertain linear systems.” In: *International Journal of Systems Science* 28.2 (1997), pp. 183–188.
- [92] J. Daafouz and J. Bernussou. “Poly-quadratic stability and \mathcal{H}_∞ performance for discrete systems with time varying uncertainties.” In: *Proceedings of the 40th IEEE Conference on Decision and Control*. Vol. 1. IEEE, 2001, pp. 267–272.
- [93] J. H. Richter. *Reconfigurable Control of Nonlinear Dynamical Systems: A Fault-Hiding Approach*. Vol. 408. Springer, 2011.
- [94] G. C. Silva, W. M. Caminhas, and R. M. Palhares. “Artificial immune systems applied to fault detection and isolation: A brief review of immune response-based approaches and a case study.” In: *Applied Soft Computing* 57 (2017), pp. 118–131.
- [95] I. V. Bessa, R. M. Palhares, M. F. S. V. D’Angelo, and J. E. Chaves Filho. “Data-driven fault detection and isolation scheme for a wind turbine benchmark.” In: *Renewable Energy* 87 (2016), pp. 634–645.

- [96] M. F. D'Angelo, R. M. Palhares, M. C. Camargos Filho, R. D. Maia, J. B. Mendes, and P. Y. Ekel. "A new fault classification approach applied to Tennessee Eastman benchmark process." In: *Applied Soft Computing* 49 (2016), pp. 676–686.
- [97] M. F. D'Angelo, R. M. Palhares, L. B. Cosme, L. A. Aguiar, F. S. Fonseca, and W. M. Caminhas. "Fault detection in dynamic systems by a Fuzzy/Bayesian network formulation." In: *Applied Soft Computing* 21 (2014), pp. 647–653.
- [98] H. Niemann and J. Stoustrup. "Controller reconfiguration based on LTR design." In: *Proceedings of 42nd IEEE International Conference on Decision and Control*. 2003, pp. 2453–2458. DOI: 10.1109/CDC.2003.1272988.
- [99] A. O. Farias, G. A. C. Queiroz, I. V. Bessa, R. L. P. Medeiros, L. C. Cordeiro, and R. M. Palhares. "Sim3tanks: A benchmark model simulator for process control and monitoring." In: *IEEE Access* 6 (2018), pp. 62234–62254.
- [100] M. G. Na. "Auto-tuned PID controller using a model predictive control method for the steam generator water level." In: *IEEE Transactions on Nuclear Science* 48.5 (2001), pp. 1664–1671.
- [101] B. Stenlund and A. Medvedev. "Level control of cascade coupled flotation tanks." In: *Control engineering practice* 10.4 (2002), pp. 443–448.
- [102] R. Zhang, A. Xue, and S. Wang. "Modeling and nonlinear predictive functional control of liquid level in a coke fractionation tower." In: *Chemical engineering science* 66.23 (2011), pp. 6002–6013.
- [103] T. Tani, S. Murakoshi, and M. Umamo. "Neuro-fuzzy hybrid control system of tank level in petroleum plant." In: *IEEE transactions on Fuzzy Systems* 4.3 (1996), pp. 360–368.
- [104] R. Lakerveld, B. Benyahia, P. L. Heider, H. Zhang, A. Wolfe, C. J. Testa, S. Ogden, D. R. Hersey, S. Mascia, J. M. Evans, et al. "The application of an automated control strategy for an integrated continuous pharmaceutical pilot plant." In: *Organic Process Research & Development* 19.9 (2015), pp. 1088–1100.
- [105] A. J. Gaikwad, P. Vijayan, S. Bhartiya, R. Kumar, H. Lele, and K. Vaze. "Selection of steam drum level control method for multiple drum interacting loops pressure tube-type BWR." In: *IEEE Transactions on Nuclear Science* 58.2 (2011), pp. 479–489.

- [106] P. P. Biswas, R. Srivastava, S. Ray, and A. N. Samanta. “Sliding mode control of quadruple tank process.” In: *Mechatronics* 19.4 (2009), pp. 548–561.
- [107] H. Gouta, S. H. Said, and F. M’sahli. “Model-based predictive and backstepping controllers for a state coupled four-tank system with bounded control inputs: A comparative study.” In: *Journal of the Franklin Institute* 352.11 (2015), pp. 4864–4889.
- [108] H. Gouta, S. H. Saïd, A. Turki, and F. M’Sahli. “Experimental sensorless control for a coupled two-tank system using high gain adaptive observer and nonlinear generalized predictive strategy.” In: *ISA transactions* 87 (2019), pp. 187–199.
- [109] I. Rubio-Scola, M. M. Quadros, and V. J. S. Leite. “Robust hybrid PI controller with a simple adaptation in the integrator reset state.” In: *IFAC-PapersOnLine* 50.1 (2017), pp. 1457–1462.
- [110] K. H. Johansson. “The quadruple-tank process: A multivariable laboratory process with an adjustable zero.” In: *IEEE Transactions on Control Systems Technology* 8.3 (2000), pp. 456–465. DOI: 10.1109/87.845876.
- [111] A. E. O. Franco, L. S. Oliveira, and V. J. S. Leite. “Síntese de ganhos para compensação robusta de sistema linearizados por realimentação.” In: *Proceeding of the Congresso Brasileiro de Automática*. 2016, pp. 2695–2700.
- [112] A. C. de Sousa, V. J. S. Leite, and I. Rubio-Scola. “Affordable control platform with MPC application.” In: *Studies in Informatics and Control* 27.3 (2018), pp. 265–274. DOI: 10.24846/v27i3y201802.
- [113] A. P. Pandey and M. C. de Oliveira. “A new discrete-time stabilizability condition for linear parameter-varying systems.” In: *Automatica* 79 (2017), pp. 214–217. DOI: 10.1016/j.automatica.2017.02.006.
- [114] K. J. Åström and T. Hägglund. *PID Controllers: Theory, Design and Tuning*. Instrument Society of America, 1995.
- [115] J. C. Butcher. *Numerical methods for ordinary differential equations*. John Wiley & Sons, 2016.
- [116] MOSEK ApS. *The MOSEK optimization toolbox for MATLAB. Version 9.0*. Version, 2019. URL: <http://docs.mosek.com/9.0/toolbox/index.html>.

- [117] S. X. Ding. *Model-based fault diagnosis techniques: design schemes, algorithms, and tools*. Springer, 2008.
- [118] H. Behzad, M. A. Sadrnia, A. Casavola, A. Ramezani, and A. Darabi. “Multiplicative fault estimation based on the energetic approach for linear discrete-time systems.” In: *International Journal of Control* (2020), pp. 1–13. DOI: 10.1080/00207179.2020.1815857.